



Universidad Autónoma de San Luis Potosí
Facultad de Ciencias



Coupled quantum wells as a novel source of optical anisotropies in nanostructured systems

Doctoral Thesis in Applied Sciences
submitted by:

Oscar Ruiz Cigarrillo

Supervisors:

Dr. Luis Felipe Lastras Martínez

Dr. Raul Eduardo Balderas Navarro

Dr. Edgar Armando Cerda Méndez

SAN LUIS POTOSÍ, S.L.P. MÉXICO

AUGUST 2022

Statement of authorship

I, Oscar Ruiz Cigarrillo, student of the Graduate Program in Applied Sciences of the School of Sciences of the Universidad Autónoma de San Luis Potosí, as the author of the thesis “Coupled quantum wells as a novel source of optical anisotropies in nanostructured systems”, declare that the thesis is an original, unpublished, authentic, personal work, that the corresponding sources have been cited and in its execution the legal provisions in force that protect the copyright and intellectual and industrial property rights were respected. The ideas, doctrines, results, and conclusions I have reached are my absolute responsibility.

Abstract

In the present work, it is proposed a new source of IOAs occurring in asymmetric coupled quantum wells ACQWs, namely a reduction of the symmetry from D_{2d} to C_{2v} as imposed by asymmetry along the growth direction. We report on reflectance anisotropy spectroscopy (RAS) of double GaAs quantum wells structures coupled by a thin (< 2 nm) tunneling barrier (CQWs). Two groups of DQWs systems were studied: one where both QWs have the same thickness (SCQWs) and another one where they have different thicknesses (ACQWs). RAS measures the in-plane optical anisotropies (IOAs) arising from the intermixing of the heavy- and light- holes in the valence band when the symmetry of the DQW system is lowered from D_{2d} to C_{2v} . If the CQWS are symmetric, residual IOAs stem from the asymmetry of the QW interfaces; for instance, associated to Ga segregation into the AlGaAs layer during the epitaxial growth process. In the case of an ACQWs with QWs with different thicknesses, the AlGaAs layers (that are sources of anisotropies) are not distributed symmetrically at both sides of the tunneling barrier. Thus, the system losses its inversion symmetry yielding an increase of the RAS strength. The RAS line shapes were compared with reflectance spectra in order to assess the heavy- and light- hole mixing induced by the symmetry breakdown. The energies of the optical transitions were calculated by numerically solving the one-dimensional Schrödinger equation using a finite-differences method. Our results are useful for interpretation of the transitions occurring in both, symmetric and asymmetric CQWs.

*A mi Mámá Rosalba (Muñeco), a mi Pápa Alberto
(Lobo) y a mi mejor amigo, mi carnal Angel Alberto*

CONTENTS

Abbreviations	III
List of codes and packages	IV
Symbols	V
List of Figures	VI
List of Tables	XII
1 Physical Background	1
1.1 Semiconductor Band Structure	2
1.1.1 Valence and Conduction Bands	3
1.1.2 Excitons	7
1.2 Low Dimensional Semiconductor Structures	8
1.2.1 Quantum Wells	9
1.2.2 Preliminary Approach of Quantum Confinement Effect in QWs	11
1.3 Summary	13
2 Physical model	14
2.1 The Context of Symmetry	15
2.1.1 The Symmetry and the Band Structure	17
2.2 Symmetry breaking in CQWs	19
2.2.1 Coupled Quantum Wells	21
2.2.2 Special Symmetry Reduction From $D_{2d} \rightarrow C_{2v}$	23
2.3 Numerical Calculations	26
2.3.1 Envelope Function and Effective Mass Approximation Methods	28
2.3.2 Finite Difference Method	31
2.4 Numerical Results	34
2.5 Anisotropy Model in CQWs	36
2.6 Summary	41
3 Experimental Details and Results	42
3.1 Samples Description	43
3.2 Spectroscopy: Experimental Setups and Results	46
3.2.1 Photoluminescence Spectroscopy (PL)	48

3.2.2	Photoreflectance spectroscopy (PR)	55
3.2.2.1	Excitonic Effects	61
3.2.2.2	The PR Summary	70
3.2.3	Reflectance Anisotropy Spectroscopy (RAS)	70
3.2.3.1	RAS Strength Discussion and the Physical Model Justification	73
3.2.3.2	The RAS summary	78
4	Conclusions and Future Work	79
Bibliography		83

ABBREVIATIONS

BS	Band structure
BZ	<i>Brillouin zone</i>
QS	Quantum Structures
QW	Quantum Well
SQW	Single Quantum Well
CQWs	Coupled Quantum Wells
VB	Valence Band
CB	Conduction Band
SCQWs	Symmetric coupled quantum wells
ACQWs	Asymmetric coupled quantum wells
RAS	Reflectance Anisotropy Spectroscopy
PL	Photoluminescence spectroscopy
PR	Photoreflectance spectroscopy
R	Reflectance spectroscopy
PRD	Photo-Reflectance Differential Spectroscopy
FDM	Finite difference method
CCD	Charge coupled device
0D	Zero-dimensional
1D	One-dimensional
2D	Two-dimensional
3D	Three-dimensional
fcc	Face-centered cubic
2DEG	Two-dimensional electron gas
BL	Beer-Lambert-Law
PD	Photo-Detector
PEM	Photo-Elastic Modulator
QM	Quantum Mechanics
$k \cdot p$	Semiempirical theoretical tool to calculate band-structure
TB	Semiempirical Tight-Binding Method
DFT	Density Functional Theory
SOC	Spin-Orbit Coupling, also called Spin-Orbit interaction
NanophotonIICOs	Nanophotonics IICO group.
EFA	Envelope function Approximation
EMA	Effective Mass Approximation
FKOs	Franz Keldysh oscillations
IOA	In-plane Optical Anisotropy
MBE	Molecular Beam Epitaxy

LIST OF CODES AND PACKAGES

This list denote the *Open-Source* packages, codes, tools, and repositories for the development of this work. All inside of this work as images or numerical calculations are subject to the *Open-Source* ideology. Our codes are housed in our own GitHub repository, both personal and laboratory repository. It is important to say that without the development of the *Open-Source* codes like contents in this list, our codes, they could not have been enhanced.

cqws-codes Repository of our codes implemented in this work. [1]

kp-nanoiico-group $k \cdot p$ julia [2] package developed by our group research [3]

ASE The Atomic Simulation Environment (ASE) is a set of tools and Python modules for setting up, manipulating, running, visualizing and analyzing atomistic simulations. [4]

Spglib Software library for crystal symmetry search [5]

SOLCORE A multi-scale, Python-based library for modelling solar cells and semiconductor materials [6]

Aestimo One-dimensional (1D) self-consistent Schrödinger-Poisson solver for semiconductor heterostructures [7]

VESTA 3D visualization program for structural models, volumetric data such as electron/nuclear densities, and crystal morphologies. [8]

PGF/TikZ PGF is a macro package for creating graphics. It is platform- and format-independent and works together with the most important TeXbackend drivers, including pdfTeX and dvips. It comes with a user-friendly syntax layer called TikZ. [9]

pst-optexp PStricks package to drawing optical experimental setups. [10]

SYMBOLS

X⁻ Negative Trion Transition

X⁺ Positive Trion Transition

X Direct Exciton Transition

IX Indirect Exciton Transition

$\text{Al}_x\text{Ga}_{1-x}\text{As}$ AlGaAs semiconductor as a function of Al concentration x

\hbar Planck's constant (eV)

m_0 electron effective mass

(hkl) Family of lattice planes with Miller indices h , k and l

E_g Energy bandgap

e electron

hh heavy-hole

lh light-hole

$e_n - hh_n$ or $e_n - lh_n$ Electronic transitions

LIST OF FIGURES

1.1 Band energy diagram for insulators (left), semiconductors (center) and metals (right). The principal difference is the gap energy: for insulators this is bigger than semiconductors, although in semiconductors gap energy depends on materials. Metals do not exhibit gap energy, instead exist overlapping bands. Dashed line determines the Fermi level.	4
1.2 GaAs crystal structure, where each sublattice corresponds to Ga and As atoms respectively.	5
1.3 Band structure of GaAs, (a) shows the zoom around of Γ to denote the direct band gap and the electrons energy needed to jump from valence to conduction band. (b) denotes the two directions to dispersion of the bands corresponds to Brillouin zone: $\Gamma \rightarrow X$ and $\Gamma \rightarrow L$. [11]	6
1.4 Two typical transitions for GaAs near $\mathbf{k} = 0$. The first one correspond to the heavy-hole and second one to the light-hole.	7
1.5 Qualitative scheme of exciton creation in GaAs as direct gap.	8
1.6 General scheme of GaAs/ $Al_xGa_{1-x}As$ heterostructure. Scheme of atomic arranged of this heterojunction, the dashed lines are the matched between two dissimilar materials (top). Band-edge profile (bottom).	9
1.7 Heterostructures from bulk (3D), to Quantum Wells (2D), Quantum Wires (1D) and Quantum Dots (0D).	10
1.8 Single GaAs/ $Al_xGa_{1-x}As$ Quantum Well	11
1.9 General scheme of typical Schrödinger's equation solutions to one-dimensional potential as (a) where the eigenenergies of both electron and holes are denoted with same color depending on n value.(b) it is plot, of the subbands in the same case of (a) to both particles.	12
2.1 (a) GaAs crystal structure in “real space” known as unit cell, into which with dashed line is denoted the primitive cell. This lattice is well-defined by the vectors \mathbf{a} , \mathbf{b} and \mathbf{c} , these vectors are defined as the basis vectors. In (b) is schematized the GaAs crystal structure in k -space, also known as reciprocal space.	16
2.2 Atomic arrangement of a $Al_xGa_{1-x}As /GaAs/Al_xGa_{1-x}As$ single QW. At bottom we can appreciate the atom structure assuming an Al concentration in the barriers. Middle: the conduction band edge as a potential profile; at the interfaces in between it changes from barrier to well and vice versa. Top: the atoms' basis are added where it has taken the Arsenic as the central atom, and scheme keeps rotating along the y -axis.	20

2.3	General scheme to describe a SCQWs structure. In this case, the barriers are composed by $\text{Al}_x\text{Ga}_{1-x}\text{As}$ and the wells are made of GaAs with the same width ($d_1 = d_2$) and the coupling barrier also composed by $\text{Al}_x\text{Ga}_{1-x}\text{As}$. In top, (a) denotes both CB and VB edges profiles over z -axis (Real-space) direction, whereas in bottom (b) the atomic structure of CQWs is depicted.	22
2.4	General scheme depicting an ACQWs structure. As in Figure 2.3(b), the structure is basically the same both in both barriers height, composition and dimensions as well as the coupling barrier, only the relative position of these are varied. Then, as a result is that one of the QWs is wider than the other ($d_1 < d_2$). Thus, this is the reason causing the asymmetry in structure. Also, at top (a) draws the potential profile along z direction, and bottom (b) schemes the atoms structure where is clear that only shows changes in the coupling barrier relative position with respect to Figure 2.3(b)	23
2.5	Roadmap developed around of QWs with possible potential profiles, each one possessing a desired C_{2v} symmetry. It starts with an asymmetric QW (a) [12, 13] in the potential profile due to the semiconductor difference in adjacent barriers to the well. At the center-left (b) and bottom left (c) are asymmetric QWs: in the first case the asymmetry [14, 15] is caused by a graded concentration in a barrier and bottom, whereas in the other case the asymmetry is originated by inserting an atomic specie different that of the barrier [16]. At the top center (d), it is shown a QW under strain [17–19] causing symmetry breakdown, while the bottom center (e), shows the CQWs under applying electric field [20], the relation of both, it is the external perturbation which causes the breaking symmetry. Finally, right (f) is an ACQWs which have a symmetry breaking due to the relative width of the constituents QWs [21].	25
2.6	(a) The GaAs band structure calculated with 8-band Khane Hamiltonian [22, 23]	28
2.7	(a) it is the focus over $\Gamma = 0$ and inside is the SQW VB $\mathbf{k} \cdot \mathbf{p}$ results, while (b) is the potential profile considered due to the VB splitting. This VB splitting, it is the cause that of 1D potential profile, can be implemented	29
2.8	Sketch of discrete potential band-edge profile which depends on spacial displacement δz . HJ denotes the Heterojunction boundary junction.	31
2.9	Doble Quantum Wells structure reproduce from Harrison et al. [24], (a) shows the plot to each energy calculate e_1 and e_2 , while in (b) the table exposes the comparison of numerical results from Harrison et. al. , Nextnano software [25] and our results. The difference taken into account the Harrison's results practically are the same, but around of meV orders our results are precisely.	34
2.10	From (a) a to (d) shcemes the numerical results obtained to solved 1D-Schrödinger equation in both SQWs and ACQWs.	36

2.11	Diagram of three principal structures studied in this work, starting with CQWs with the same width (bottom, $d_1 = d_2$), this sample structure is called as SCQWs, the second one the first asymmetric structure (top, $d_1 \sim d_2$), this means that one of the wells is slightly width than the other. Finally the third sample (right middle) it is more asymmetric, which means that one of the wells is double wider than the other.	37
2.12	Wave functions and confined energies calculated for (a) sample S1 (SCQWs sample) and (b) sample A2(ACQWs sample 2)	40
3.1	GaAs substrate growth direction	43
3.2	AlGaAs superlattice	44
3.3	Processes that occur inside a solid in the light-matter interaction phenomena.	47
3.4	PL Scheme	48
3.5	(a) shows PL experiments of the samples M4_3171 , M4_3172 and M4_3226 at 14K. Plots in how the comparison between these samples, where clearly can see the relative intensity among in each experiment. In (b) it can be seen each PL spectra with the respective direct transitions, numerically calculated, hh ₁ and lh ₁ indicates the first energy level that corresponds to heavy- and light-holes respectively.	50
3.6	Absorption calculated as a function of sample depth. Dashed lines closed the CQWs region, left: Figures 3.6(a) to 3.6(c). Here the samples have Al _x Ga _{1-x} As layers with different compositions $x = 0.15$, $x = 0.2$ and $x = 0.3$; this results in a change of refractive index then also in the absorption. Right: Figures 3.6(d) to 3.6(f)these samples are equal in structure but different on their width of one of the QWs, therefore the absorption manifests strongly homogenous than the first three samples.	52
3.7	(a) Shows the PL spectra of samples M4_3140, M4_3521 and M4_3523, in this comparison is clear the shift between these in respect to first transitions. The relative change in width of one of the QW modifies the energy transitions being the sample 3521 the lowest energy. (b) It is plotted each PL spectra result with the correspondent e ₁ -hh ₁ and e ₁ -lh ₁ transitions energies.	54
3.8	Scheme of the PR effect showing the carrier dynamics involved in the mechanism. Right and Left: the corresponding photoinduced changes when the laser is off and on, respectively.	56
3.9	PR Scheme	57
3.10	PR experiments of samples M4_3171, M4_3172, and M4_3226 at 30K. Arrows point the calculated transitions for each sample. As pump probe a laser with a wavelength similar to the PL experiments was used, with an average power of 5mW. Dashed line indicated the GaAs substrate fundamental transition.	59

3.11 PR experiments of samples: M4_3140, M4_3141, M4_3521, M4_3522 and M4_3523 at 30K. Arrows point to calculated transitions for each sample, the used laser wavelength was the same, which in PL experiments and the previous PR experiments. Dashed line indicate the GaAs substrate, in these samples this transition is well located. The PR spectra of sample M4_3522 p-type doped (orange) is five times smaller than their corresponding n-type, the sample M4_3521. The experiments in sample M4_3140 was performed at 2.5mW, then was multiply it by four in according to samples M4_3521 and M4_3523, in case of the sampleM4_3141 even if, was performed at a power = 5mW the result was 5 times smaller than sample M4_3521. The discussion concerning this is explained in the text.	60
3.12 Comparison of : (a) PR spectra of the 3521 (n-type) and 3522 (p-type) samples, the p-type sample is 5 times smaller than n-type sample. (b) R spectra obtained at same time in each experiment, the arrows point to each direct transitions for two first confined energies. The line shape is practically the same in both spectra.	61
3.13 The PR comparison between samples M4_3521 (ACQWs-2) and M4_3523 (SCQWs), the electron wave function are plotted for each sample where, the SCQWs sample at top left and at top right to ACQWs sample. The top arrows pointed to forbidden transitions in ASQWs-1 sample, while the bottom arrows pointed to the direct transitions in both samples.	63
3.14 PR spectra of the ACQWs-1 sample designed as a function of slits aperture, where it can see the increase of peak resolution as decrease the aperture of slits.	64
3.15 The peak tends to height as increase the laser power, which also is very observable as a redshift.	65
3.16 Trions formation scheme in terms of band structure (a) in this case, the exciton is bound to an electron in the conduction band leading to a three-body system knew as negative trion X^- . On the other hand, in (b) it presents the possible formation of X^- due to a slight width of one in the CQWS, consequently, the narrow well transfers electrons through tunneling to a wide well, if it is calculated the wave functions of this structure, the wave functions have the characteristic of to be distributed asymmetrically as in the case of the applied electric field along z [26,27].	66
3.17 Results to self-consistently Schrödinger-Poisson equation, in order with down to top the n-type layer $\text{Al}_{0.15}\text{Ga}_{0.85}\text{As}$ doped ($6 \times 10^{18}\text{cm}^{-3}$) is increasing in width from 15nm, 75nm, 150nm to 300nm. The goal of this is to calculate in a general way the effects of the dopped layer, specifically due to the electric field induced by this. The strength of the field is expressed in kV/cm units, although this magnitude is great, we assume that does not significantly, latter we explained this.	68

3.18 Band conduction profile $V(z)$ calculated by numerical solution of self-consistent Schrödinger-Poisson equation. The calculations were performed considering the width of the doped n-type 6×10^{18} layer with 600nm. The zoom inset shows the comparison between total potential calculated (blue) and when applied field $F \approx 1.2 \text{ kVcm}^{-1}$ (dotted magenta), where at around of CQWs zone are similar.	69
3.19 RAS Scheme	71
3.20 Experimental results from samples: M4_3171, M4_3172 and M4_3226, from top to bottom respectively. In left, shows the RAS result where with a dashed line it is denote the substrate transition, in each sample denotes the direct transitions with arrows. The right side, show the plots of R spectra, which is the average result of all experiments carried in each correspond sample.	72
3.21 Experimental results of samples: M4_3140, M4_3141, M4_3521, M4_3522 and M4_3523, from top to bottom, respectively. In left, shows the RAS result where a dashed line denotes the substrate transition. In each spectrum the direct transitions with arrows are remarked. The right side show the plots of the R spectra, which is the average result of all experiments carried out. The direct transitions are located by two peaks with opposite concavity where we can attest that the larger one transition is $e_1\text{-hh}_1$ and a smaller, one associated with the $e_1\text{-lh}_1$	74
3.22 RAS spectra for the (a), (b), asymmetric and (c) symmetric CQWs. The dashed vertical line indicates the expected energy of the excitonic transition of the GaAs substrate. Above this energy, the optical transitions come from the CQWs. The inset shows the PL spectra measured for each sample. Two peaks can be identified in each spectrum, a larger one associated with the transition $e_1\text{-hh}_1$ and a much smaller one associated with the $e_1\text{-lh}_1$ (for spectrum (b) this peak is observed as a shoulder). The energies obtained from the PL spectra are indicated by the arrows in the RAS spectra. Note that the structures associated with $e_1\text{-hh}_1$ and $e_1\text{-lh}_1$ increase their strength when the CQWs become more asymmetric. The RAS spectra were measured at 30 K.	75
3.24 Reflection anisotropy (RAS, (a), (b)) and differential reflection (DR, solid line) spectra for ACCQWs-2 and ACQWs-3, grown on an AlGaAs n-type and p-type layer respectively. Note that while for the heavy hole transitions ($e_1\text{-hh}_1$ and $e_2\text{-hh}_2$) in the RAS and DR spectra have the same concavity, for light holes transitions ($e_1\text{-lh}_1$ and $e_2\text{-lh}_2$) the concavities are opposite and DR spectra shows the highest level transitions. The bottom arrows point to the experimental transitions for the two first levels, whereas the top arrows show the calculated energies to three energy levels. The RAS and DR spectra were measured at 30K.	76

3.26 RAS experiment designed to demonstrate the non-existence of built-in electric field trough sequential measured along the preferential direction, in this case, it was chosen along the pits $[1\bar{1}0]$ [28]. The signal result in both samples practically is the same, the sign is conserving. At top left and right located the images recorded with a microscope of back substrate which shows typical and well known etch pits elongated [29] along of $[1\bar{1}0]$ direction.	77
4.1 Spin resolve RAS experiments worked on ACQWs-2 sample, this experiments carried out in sequential way, firstly measured with one polarization state and then the second state. The sample it was placed along preferential direction ($[1\bar{1}0]$), maybe this be a reason can observer a structural signal of RAS, this means, the line shape of anisotropy due to the asymmetry structure. Although, it's notable the difference between mutual polarization states.	81

LIST OF TABLES

2.1	Direct transitions (X) calculated for two ACQWs and one SCQW detailed in Section 3.1 and Table 3.1. From up to down shows the numerical (<i>E</i>) and experimental results, the experimental results was obtained from RAS experiments which are performed at 30K.	35
3.1	Table of samples description	45
3.2	Photo-cathodes,usually implemented in PD to the spectroscopy of semiconductors [30].	47
3.3	Table of PL experimental parameters	49
3.4	Comparison table between experimental transitions obtained trough PL measures and numerical transitions calculated as explained in Section 2.3 .	55
3.5	Comparative of experimental (E) and numerical calculations (N) of first level transition energies (in eV). δE_e , δE_{hh} and δE_{lh} corresponds to the difference between electrons, heavy- light holes states, respectively. ΔE_n is the numerical calculation of energy splitting for transitions 1 and 2 (n = 1, 2). .	76

1

PHYSICAL BACKGROUND

This chapter bears the basis of fundamental physics in compound semiconductors and quantum structures that were implemented to understand the results in this work.

Contents

1.1 Semiconductor Band Structure	2
1.1.1 Valence and Conduction Bands	3
1.1.2 Excitons	7
1.2 Low Dimensional Semiconductor Structures	8
1.2.1 Quantum Wells	9
1.2.2 Preliminary Approach of Quantum Confinement Effect in QWs	11
1.3 Summary	13

QUANTUM MECHANICS concerns electronic behavior that manifest many phenomena not explained by the classical regime. In semiconducting condensate matter, Quantum structures (QS) are artificially systems conformed by semiconductors where both electrons and holes exhibit quantum nature and are great platforms to propose novel devices. Nowadays, the progress in creation of QS consist in precisely synthetizing conglomerates, in which electrons and holes show remarkable electrical and optical properties [31, 32]. Most of these properties arise due energy confinement, which is the principal interest in the study of electrons and their consequent magnetic, optical and electrical interactions. Therefore, their study is still an ongoing emerging topic [33]. In this chapter, fundamental concepts to describe the physical phenomena inherent to this work, without the intention to replicate concepts and models already explained in publications with major impact, are presented. Therefore, the aim of this chapter is to highlight the subtle concepts behind the results of this thesis.

1.1 Semiconductor Band Structure

We start describing the band structure (BS) of zincblende semiconductors. The BS dictates the electron behavior in a solid; therefore, we can invoke the Schrödinger equation. Inside a solid, around 10^{23} valence electrons contribute to the bonding in each cubic centimeter, which results in a many-body complex problem [34], with a general Hamiltonian [35, 36]:

$$H = \frac{1}{2M} \sum_{i=1}^{N_n} \mathbf{P}_j^2 + \frac{1}{2m_0} \sum_{j=1}^{N_e} \mathbf{p}_j^2 + \frac{Z^2}{2} \sum_{i,j=1, i \neq j}^{N_n} V_c(\mathbf{R}_i - \mathbf{R}_j) - Z \sum_{i=1}^{N_n} \sum_{j=1}^{N_e} V_c(\mathbf{r}_j - \mathbf{R}_i) + \frac{1}{2} \sum_{i,j=1, i \neq j}^{N_e} V_c(\mathbf{r}_i - \mathbf{r}_j), \quad (1.1)$$

where N_n is the number of atomic nuclei, N_e is the number of electrons with mass m_0 , assuming that each nuclei has mass M , and charge Z_e . As a result, this Hamiltonian is too complicated as the sum comprises five terms which consists in: kinetic energies of electrons and nuclei, the nucleus-nucleus interactions, the nucleus-electron and electron-electron Coulomb interactions $V_c(\vec{x})$; \mathbf{R}_i are the positions of the nuclei and \mathbf{r}_j are the position of the electrons; the operators \mathbf{P} and \mathbf{p} are momentum operators to nuclei and electrons respectively [35]. Fortunately, because the QS are formed by crystalline materials, the Bloch theorem provides us with a most important tool to handle the required equations. The Bloch theorem establishes a periodic potential $U(\mathbf{r})$ for electrons, accounting for the material's periodicity (definition of crystal structure) and the Schrödinger equation can thus be described in terms of single electron picture as:

$$\left[-\frac{\hbar^2}{2m_0} \nabla^2 + U(\mathbf{r}) \right] \psi(r) = \mathbf{E} \psi(\mathbf{r}). \quad (1.2)$$

The key reason that the periodic potential in a crystal structure is highly important relies on both the translational invariance concept and the consequent symmetry operations that are inherent in a crystalline solid. The symmetry concept, as a tool to further understand solids, is discussed in detail in the next chapter. In accordance to Bloch theorem, we can associate a wave vector \mathbf{k} with each energy state, $E_n(\mathbf{k})$. Thus, it is useful to display the energies $E_n(\mathbf{k})$ as a function of the wave vector \mathbf{k} . This result is known as dispersion relation, but in general terms, is the electron band structure of the given solid, and the QS stemming from it [34].

Even if the calculation of electron band structure in solids is further complicated by the inclusion of the distance between atoms, and because the Bloch theorem provides the most important tool to reduce the problem to crystalline structures, there exist several methods to calculate the realistic BS for semiconductors that can be categorized into two groups: Atomistic methods* (Tight-binding, orthogonalized plane wave methods) and Perturbative methods $(\mathbf{k} \cdot \mathbf{p})^\dagger$. These two main categories with theirs respective methodologies, have special characteristics which become in the decision to choose them. The reasons have to do on how to describe BS which means, in case of Atomistic methods, the entire bands (both valence and conduction) can be well described; whereas perturbative methods are focused to near band edge BS. Hence, each of these methods can be chosen and enhanced as the system to study requires. We will not enter in details regarding which of these methods are the best for our case and the reasons are simple: each method is very powerful, and we must bear in mind that the complexity of solutions requires that these are solved by numerical techniques, each giving very good approximations. Thus, we basically conclude that the (effective) electron behavior inside a semiconductor consist in solutions of the Schrödinger equation [37].

1.1.1 Valence and Conduction Bands

In general, the bands of semiconductors are composed by valence and conduction bands separated by a region known as bandgap. The bandgap, which is proportional to separation energy of valence and conduction bands is also called as forbidden region; this is because electron states are nominally forbidden. Therefore, this gap energy determines the electron conduction in a semiconductor and the difference they have with the insulators and metals, as shown in Figure 1.1.

*In this category can include the ab initio methods, these are the most complex methods due to propose solutions of the many-body problem

[†]In fact, both TB and $\mathbf{k} \cdot \mathbf{p}$ also consider in same kind, because both are *semi-empirical* methods due to they consider experimental parameters.

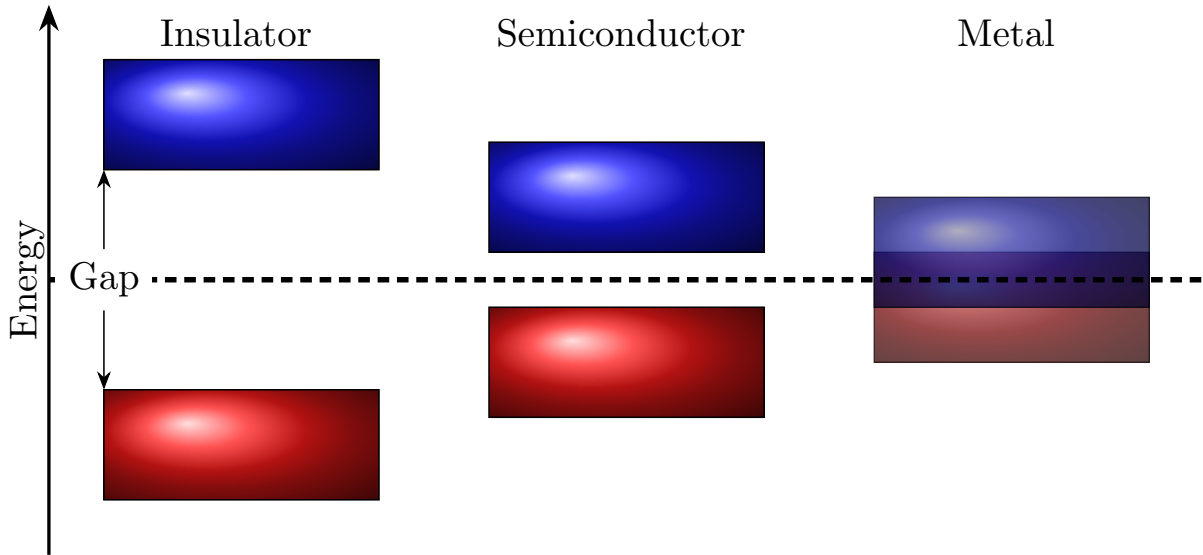


Figure 1.1: Band energy diagram for insulators (left), semiconductors (center) and metals (right). The principal difference is the gap energy: for insulators this is bigger than semiconductors, although in semiconductors gap energy depends on materials. Metals do not exhibit gap energy, instead exist overlapping bands. Dashed line determines the Fermi level.

The bandgap determines many characteristics and functionalities in semiconductors. In addition, the bandgap energy is classified in direct and indirect, but they do not only depend on this energy but the BS is the liable signature for this difference. As pointed out before, it is so difficult to describe electron behavior in solids due to the many body interactions that exists rendering the Schrödinger equation very hard to solve. Starting by describing bulk semiconductors, for example GaAs, that belongs to the family III-V cubic semiconductor with a lattice composed by two sublattices with a single atom each (Figure 1.2). For this case when the atoms in two sublattice are different the crystal structure is called *zinc-blende* [38].

To calculate BS of bulk semiconductors it is important to define specific symmetry directions. For each three-dimensional wave vector \mathbf{k} , then the plot energy as a function of \mathbf{k} is along of different high-symmetry directions [34]. GaAs is a direct semiconductor for which the [001] direction is of high-symmetry denoted by Γ point ($\mathbf{k} = 0$)

The most “exact” computation is carried out by DFT theory. These calculations are commonly called atomistic even some semiempirical models can be regarded as atomistic, but the semiempirical models are also good approximations in comparison with the DFT approach. Then, which is the reason to call “exact” solutions to the DFT results? The answer leads us to big discussion, and it is not intended to get into controversy, but in general the DFT calculations have the capacity to calculate several properties in terms of electrons interaction and the empirical methods are based in the electrical potential choice.

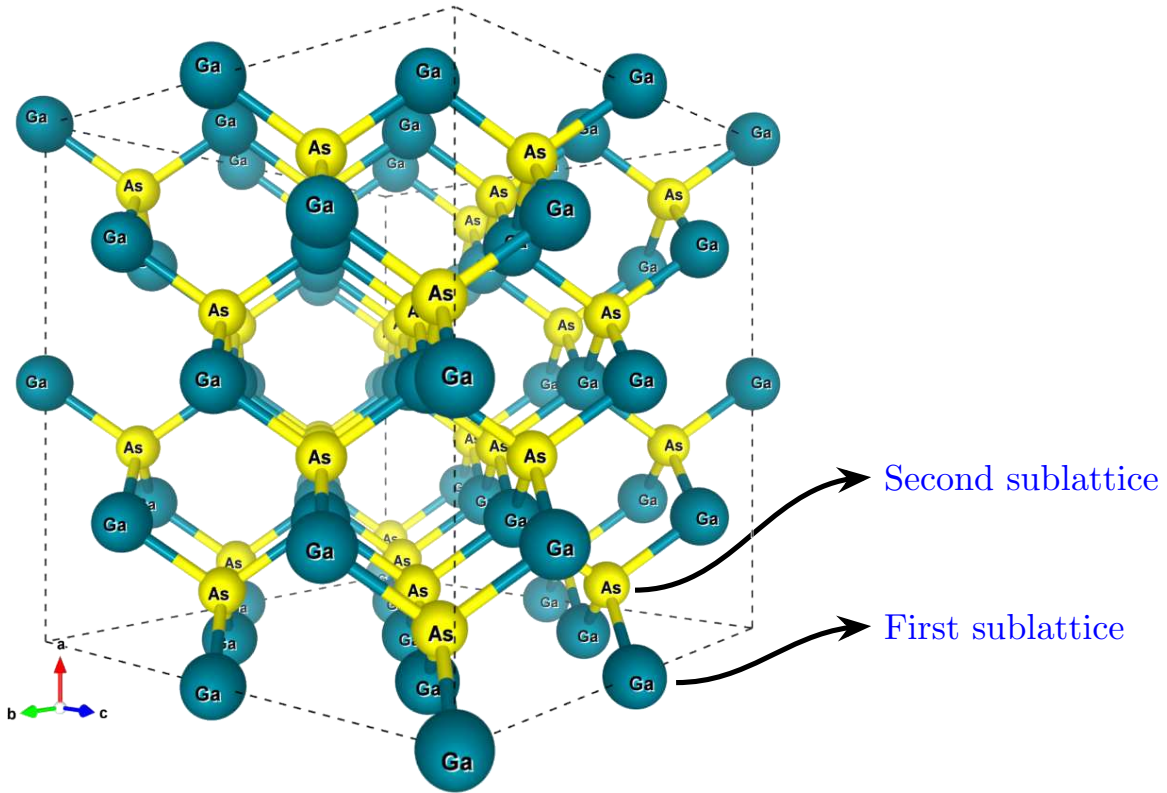


Figure 1.2: GaAs crystal structure, where each sublattice corresponds to Ga and As atoms respectively.

We will not get into details regarding BS theories and models, but will give a brief reference and the importance to this work. The models much preferred in semiconductor heterostructures such as $\text{GaAs}/\text{Al}_x\text{Ga}_{1-x}\text{As}$ are semiempirical, this is because DFT theory and their derived models are very limited to carry out into large structures, and their electron interaction nature need high computational performance. Therefore, in comparison with empirical models where the main role is the potential of semiconductor structures, it reduces computational effort. Then, most models used in semiconductor BS are empirical, and thus these models are distinguished by low computational requirements for this reason are considered as approximated. The importance in discussing these concepts will take relevance when considering physical model proposed in this work.

Section 1.1.1 shows the results of calculations of TB model as discussed in [39] and the code was implemented by R. Muller [40]. The model proposed by Vogl *et al.*, takes into account a small number of localized pseudo-orbitals based on the empirical parameters to be substituted in a TB Hamiltonian. The importance to calculate the BS is to predict reliable and detailed optical properties of solid structures that can be compared with the experimental data.

Figure 1.3(a) shows that the GaAs BS. Figure 1.3(b) depicted, the band dispersion around Γ point, which exhibits the highest symmetry. It is well-known that the band dispersion

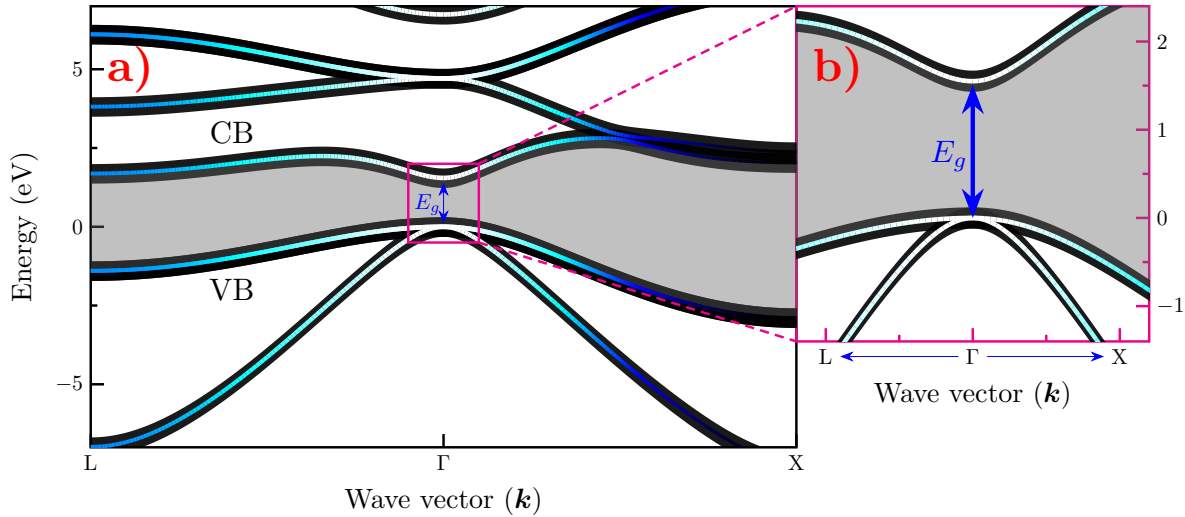


Figure 1.3: Band structure of GaAs, (a) shows the zoom around of Γ to denote the direct band gap and the electrons energy needed to jump from valence to conduction band. (b) denotes the two directions to dispersion of the bands corresponds to Brillouin zone: $\Gamma \rightarrow X$ and $\Gamma \rightarrow L$. [11]

increasing \mathbf{k} along two different directions of the Brillouin zone, from $\mathbf{k} = (0, 0, 0)$ to X point $\mathbf{k} = (2\pi a_L)(1, 0, 0)$ and L point $\mathbf{k} = (2\pi a_L)(1, 1, 1)$. These figures are the typical representation of a direct gap III-V semiconductors around $\mathbf{k} = 0$ and the shape of the dispersion is parabolic.

The BS of GaAs shown in Section 1.1.1 does not take into account the contribution of the spin*. It is important to mention that the characteristic curvature $E-\mathbf{k}$ of the dispersion bands correspond to an electron (e) in case of positive curvature, while the negative curvature corresponds to hole states; heavy (hh) and light hole (lh) bands, denoting that the transitions, are of dipole nature [11, 36].

All the above discussion refers to a basic quantum mechanism in solids. The electron absorption, specifically interband absorption, offers a way to a fundamental physical process involving the principle of many basic studies of semiconductors, applications, and the importance to understand the electron behavior in a semiconductor structures disputed in this work. Then Figure 1.4 schematizes the two typical transitions in GaAs bulk, these transitions are near $k = 0$, so that is called interband absorption. It is important to remark that the interband transitions are observed in all solids, but the mechanisms are different depending on their BS, for which, the BS is the key to study solids through the very well-known Fermi's golden rule. The excitation of electron in the CB creates a hole VB, then the final quasiparticle is called **electron-hole pair**, which is the main subject of the following sections.

*This spin contribution is called as split-off (so) hole band.

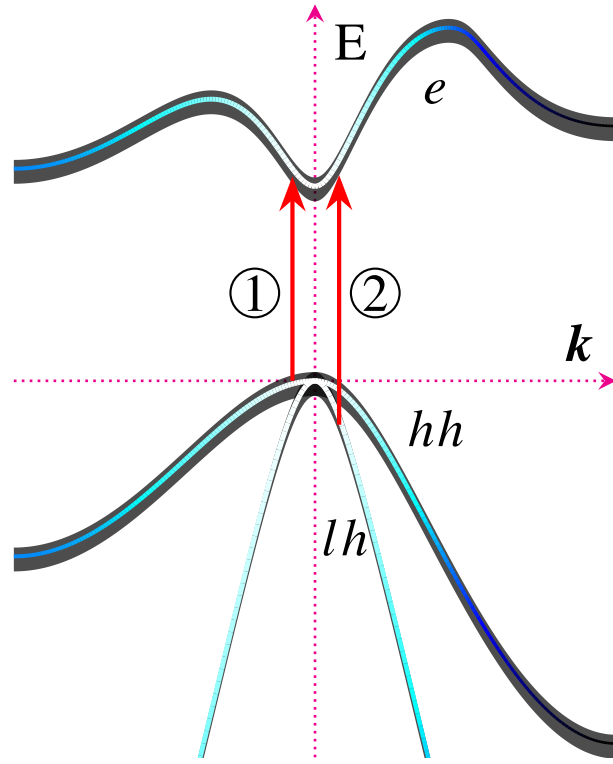


Figure 1.4: Two typical transitions for GaAs near $k = 0$. The first one correspond to the heavy-hole and second one to the light-hole.

1.1.2 Excitons

The importance to study BS of semiconductors is very clear so far, so it could be stated that the absorption process is the source of optical properties of solids, and is because of this that the importance to study of semiconductors for optoelectronics applications. In addition, this process gives rise to the formation of one of the most important excitations in crystal structures. The photon absorption process promotes an electron to be excited from the CB to VB, generating an empty location in VB which has a net positive charge. This positive empty location is called a hole, thereby the electron and hole have opposite charges then it is to be expected that they are attracted by Coulomb force, thus creating bound state called an exciton [41, 42].

From Figure 1.4 and Figure 1.5 it is clear that excitons are commonly present indirect band gap semiconductors such as GaAs, denoted by absorption experiments. This is mentioned in Section 3.2.1 as the cause of the photoluminescence mechanism.

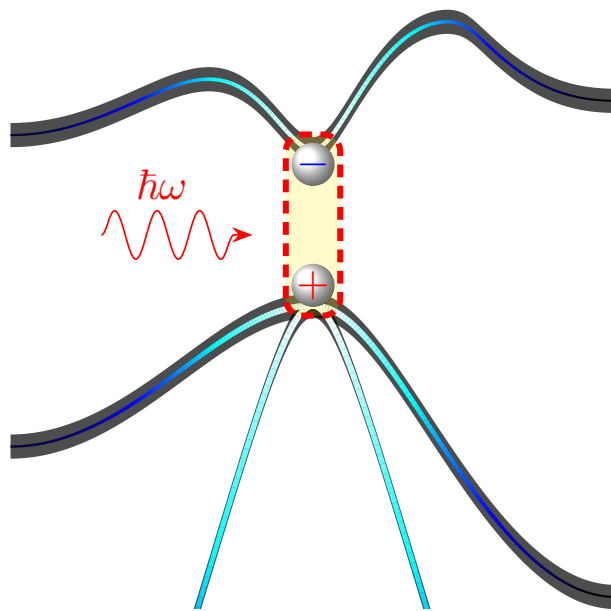


Figure 1.5: Qualitative scheme of exciton creation in GaAs as direct gap.

1.2

Low Dimensional Semiconductor Structures

The previous section considered the principles of semiconductors; in particular throughout the existence of their BS. The first approximations were done for bulk GaAs, for which its symmetry practically defines their nature and consequently the physical effects as excitons existence. But, what happens if several semiconductors with the same symmetry and similar structural parameters are joined together?. Do the bulk properties and physical properties are the same?. The answers are well-known: when two materials with relatively same structural parameters, as lattice constant can create a matched heterojunction, the union of several heterojunction make up a heterostructure with a profound impact on the overall optoelectronics properties.

Figure 1.6 shows a general scheme for a heterostructure. In this case it is presented three species of atoms Al, As and Ga. These atoms are located in the III-V columns in periodic table, hence they are called III-V semiconductors. The principal characteristic of these atoms is that they can create matched structures such as GaAs, AlAs and ternary alloys as $\text{Al}_x\text{Ga}_{1-x}\text{As}$ with specific Al concentration. The matched semiconductors produce a material with new properties based principally in the difference of bandgap which involves the alloys. As can see in Figure 1.6 it is consisting a GaAs/ $\text{Al}_x\text{Ga}_{1-x}\text{As}$ heterostructure, these interface is well-matched due to the lattice parameters is relatively equals, therefore and thanks to powerful growth technics as MBE it is possible to get high-quality quantum structures.

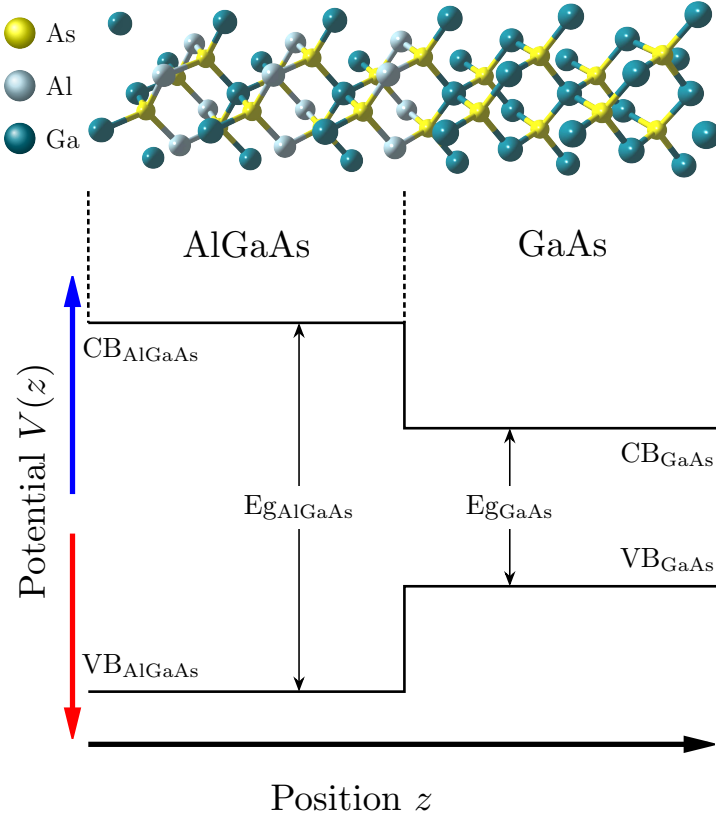


Figure 1.6: General scheme of $\text{GaAs}/\text{Al}_x\text{Ga}_{1-x}\text{As}$ heterostructure. Scheme of atomic arrangement of this heterojunction, the dashed lines are the matched between two dissimilar materials (top). Band-edge profile (bottom).

Also, the heterostructure composed by two semiconductors with different band gaps generate a discontinuity in either the conduction or the valence band can be represented by a constant potential term [43]. The theory for treatment of the electron behavior in these structures is relatively simple if we consider the above. Although this chapter has not the intention to explore the theory of electron behavior, it is worth noting that in order to get the one-dimensional potential $V(z)$ for both bands, the Schrödinger equation can be solved accurately.

1.2.1 Quantum Wells

The major relevance in nanostructured systems lies in the quantum confinement, and the junction of semiconductors results in an interesting quantum structures with specific dimensions. From 3D bulk, the dimensions reduce to 2D, 1D and 0D dimensional structures. Therefore, each of that has interesting properties and their corresponding applications. Figure 1.7 shows the low dimensional heterostructures from 3D bulk, the first low dimensional from 3D to 2D is the Quantum Wells, then from 2D to 1D it has the

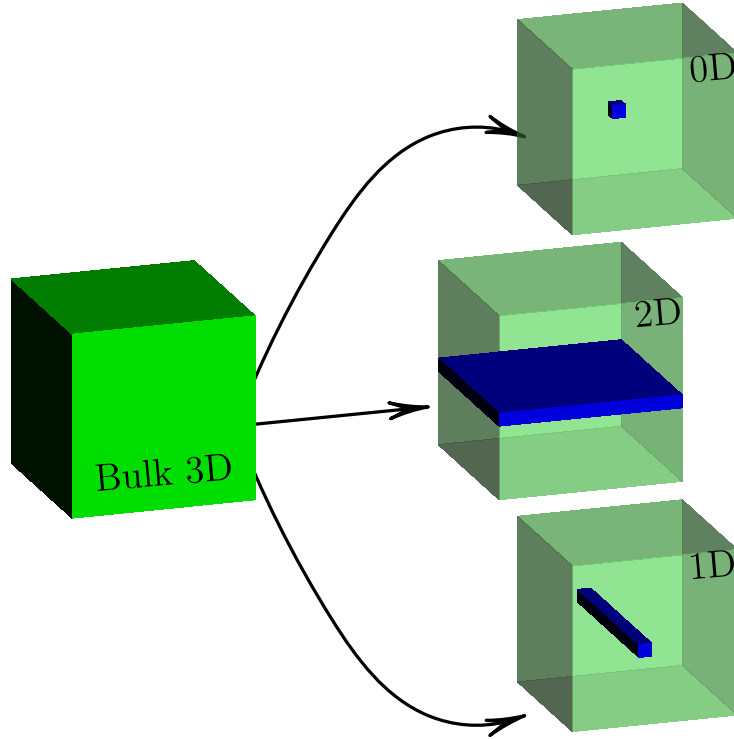


Figure 1.7: Heterostructures from bulk (3D), to Quantum Wells (2D), Quantum Wires (1D) and Quantum Dots (0D).

Quantum Wires finally with 0D have the Quantum Dots. Quantum confinement is the principal reason to study those structures. The electron behavior exhibited in it should help to understand a gamut of quantum mechanical phenomena as electron interaction in a crystal. Suppose a heterostructure composed with a two semiconductor alloys, this 2D quantum structure is called a Single Quantum Well (SQW).

These dissimilar semiconductors in terms of their potential energy ($V(z)$) can be schematized in Figure 1.8. The Gap difference of $\text{Al}_x\text{Ga}_{1-x}\text{As}$ and GaAs is due to x (Al concentration) in $\text{Al}_x\text{Ga}_{1-x}\text{As}$; a one dimensional potential profile is obtained, with the possibility to confinement electrons in a 2D plane perpendicular to the z direction (growth direction). If we consider an electron captured by two potential barriers separated a distance L , the wavefunction describing such an electron will be spatially confined. So if we confine many electrons in that potential, we have two important physical aspects: the first one is known as Pauli exclusion principle, which give Fermion nature and prevents carriers with the same spin occupying the same region in space [43, 44]. The second concerns the Heisenberg's uncertainty principle. The latter, is the consequence of quantum confinement due to the space reduction of the electrons, which brings that momentum to be increased by an amount of the order \hbar/L . Therefore, the energy of that confined particles increases, and it is referred to as confinement energy [36].

Then the quantum confinement is our starting point to understand the optical properties in QWs. As is referred in the figure, the uni-dimensional potential profile can well describe

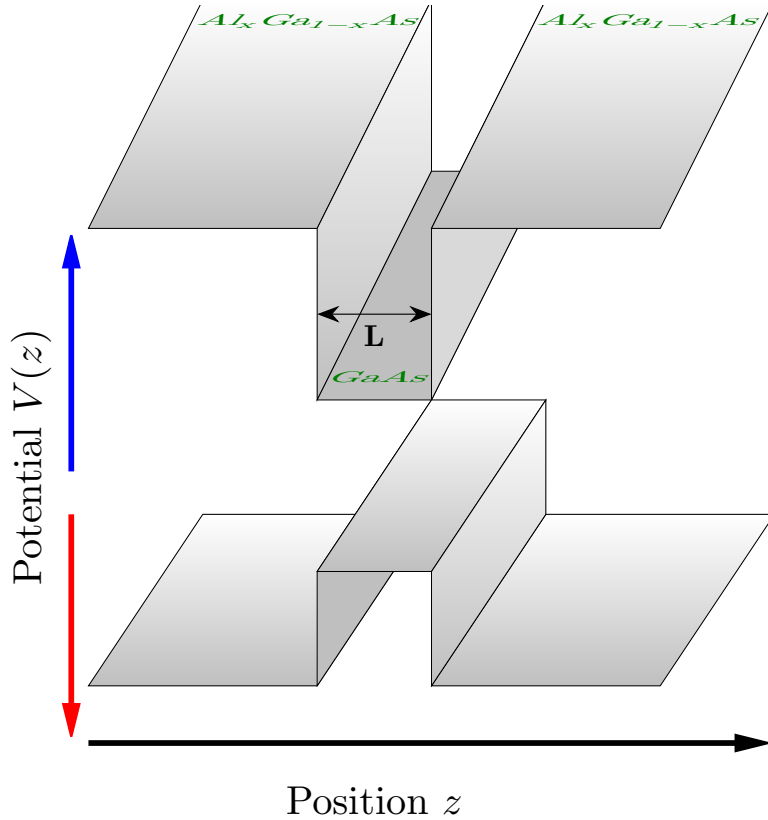


Figure 1.8: Single $GaAs/Al_xGa_{1-x}As$ Quantum Well

by top conduction- and bottom valence-bands, where band offset in these two correspond gap energy between that, while Al concentration increases their bandgap and the band offset (Q_c to CB and Q_v to VB) also to.

It is now clear that QWs have the potential to exhibit amazing quantum properties, even if all of these are very important, we focus on the optical properties and basically our interest is the light-matter interaction process.

1.2.2 Preliminary Approach of Quantum Confinement Effect in QWs

We describe the reciprocal space by having two components, k_x and k_y . In the case of $GaAs/Al_xGa_{1-x}As$ QWs it is Γ point, as long as $x < 0.4$, that the BS depends on confinement energy *. In this case, the electronic properties in comparison with a bulk semiconductor properties can be solved through particle-in-a-box as textbook problem as a first approximation. Nevertheless, even if it can be solved without a much mathematical formalism, it is very essential to discuss it here. Here we exploit the symmetry properties to understand the corresponding Hamiltonian describing the QW. The model which give the

*It will be explained in the next section, although it is due to the Gap go from direct to indirect, shortly the symmetry $\Gamma \rightarrow X$.

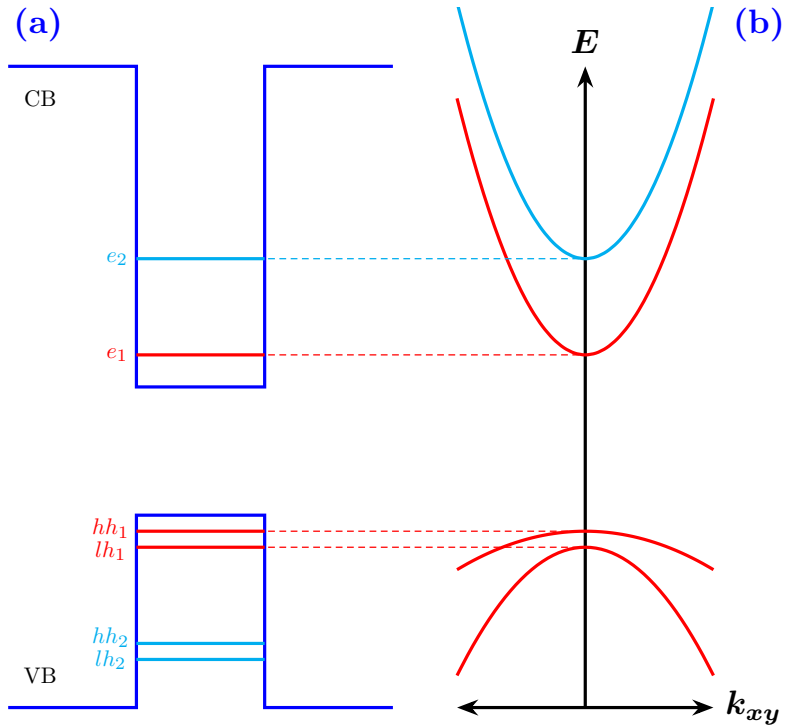


Figure 1.9: General scheme of typical Schrödinger's equation solutions to one-dimensional potential as (a) where the eigenenergies of both electron and holes are denoted with same color depending on n value.(b) it is plot, of the subbands in the same case of (a) to both particles.

tools to get the solutions is called as Effective Mass Approximation, thus their correspond Schrödinger equation is [11, 43, 45–48]:

$$-\frac{\hbar^2}{2m^*} \frac{\partial^2}{\partial z^2} \psi(z) + V(z)\psi(z) = E\psi(z), \quad (1.3)$$

where the m^* is the effective mass in each material, and $V(z)$ is the potential profile deduced from heterostructure materials properties. Therefore, that differential equation can be solved as in textbooks [11, 43, 45, 47, 49–52]. The idea is to think as a one particle in a finite potential well with definite and established boundary conditions and solving the Schrödinger equation in each part of single QW, this means that we need to create a potential function. Thus the Eigenfunctions and their corresponding Eigenenergies are computed.

The principal idea is not reproducing something which is very well known, the objective of this part is to established the scope of the next chapter. Therefore, before to continue, we will finish explaining the dispersion in-plane of single QW. As in the QW the one-dimensional potential set up the 1D confinement, is important do not confuse which the QW is a 2D structure, but their confinement is along of z direction, this means a 1D. Then, the particle can motion in the $x - y$ plane. By this reason, even if consider 3D

Schrödinger equation and the above is considered it obtain Equation (1.3) therefore, the solutions in the one-dimensional potential produce discrete states of energy $E_z = E_n$ [43], where n is the energy level it which produce subbands as shows in Figure 1.9. In contrast, before it called as “energy bands” in the bulk case, now due to the quantum confinement gets subbands to both conduction- and valence bands.

These subbands are the result of the sum of E_z and $E_{x,y}$, which are the 1D confinement energy and the in-plane momentum $k_{x,y}$ then [43]:

$$E = E_n + \frac{\hbar^2 |\mathbf{k}_{x,y}|^2}{2m^*}. \quad (1.4)$$

From this equation the effective mass m^* depends on particle, i.e the effective mass to electrons in CB and the holes in VB. Hence, the most relevant parameter in the solution is the energy E_n (Figure 1.9(b)) which discrete, thus yielding the quantum confinement in the low-dimensional heterostructures.

1.3

Summary

This chapter exposed the generalities of semiconductor band structure and low-dimensional heterostructures, highlighting GaAs/Al_xGa_{1-x}As , which is of uttermost importance in this work. The band structure interpretation is usually hard to tackle analytically, the impact and relevance in optical properties of semiconductors starts from that interpretation. Another significant concept which was treated as first approach, is the effective mass concept, even if solved, the bulk Hamiltonian it considers the mass as constant parameter or depending on semiconductor material, contrary in low-dimensional structures have an important role.

In general, the band structure of semiconductors is key to understand quantum properties of solids, and for this work the relevant issued is the *light-matter* interaction within the linear regime. Remember that *light-matter* interaction in solids can be studied by process resulting in it, as absorption, reflection, transmission, diffraction, scattering, and others [53]. Although, the light-matter interactions are fundamentally quantum electrodynamical, also, it can be studied in quantum way through aforementioned process. Firstly, is the photon absorption process can help to understand or calculate the fundamental parameter in semiconductors as is bandgap energy. This parameter is the started point in the study of semiconductors, this is the start point in the map called BS, if it ignores the gap value in the semiconductor to study it couldn't possibly get the principal optical properties of that. Then, the BS of semiconductors is the map to understand them and without these routes to assess fundamental parameters, we could not have quantum devices at hand.



PHYSICAL MODEL

The fundamental physics concepts to understand the experimental results through physical model, both numerical and phenomenological, are presented. The symmetry properties of semiconductors which is the basis of our model, is also emphasized

Contents

2.1	The Context of Symmetry	15
2.1.1	The Symmetry and the Band Structure	17
2.2	Symmetry breaking in CQWs	19
2.2.1	Coupled Quantum Wells	21
2.2.2	Special Symmetry Reduction From $D_{2d} \rightarrow C_{2v}$	23
2.3	Numerical Calculations	26
2.3.1	Envelope Function and Effective Mass Approximation Methods	28
2.3.2	Finite Difference Method	31
2.4	Numerical Results	34
2.5	Anisotropy Model in CQWs	36
2.6	Summary	41

III-V semiconductors are binary materials with either zincblende or hexagonal structure and can be engineered to exhibit quantum confinement. From now on, we will focus on the study Coupled Quantum Wells (CQWs).

The CQWs are heterostructures grown from a semiconductor substrate as GaAs as previous treated SQW (see Figure 1.8) but coupled by a thin (tunneling) barrier which poses a very significant role. But before mentioning the objective of study of these structures and the physical model to explain the experimental results, it is important to treat symmetry arguments inherent to such CQW [54] and their relevance to understand the physics supporting the optical study tackled in this work.

Owing to *symmetry* it is possible to understand the existence of conservation laws in nature, and it is pretty clear that when talking about symmetry is inevitable to think in geometry or nature patterns in an inherently way. In the next sections it is established the symmetry role arising from the band structure calculations with the importance of the electron behavior in CQWs structures.

2.1 The Context of Symmetry

Symmetry is change without change [55,56]. The reason the symmetry is crucial in physics has to do with transformations, this mean that if a physical system is affected or perturbed and this appears to be exactly the same before and after that transformation, it is said to be invariant. The symmetry of the system is made up of all the transformation operations that render the system invariant [55].

To formally study symmetries, we resort on Group Theory, which describes a geometric object by all the transformations under which the object is rendered invariant. In general, a group is a set or collection of elements that obey certain criteria and are related to each other through a specific rule of interaction and obey four group axioms [55, 57, 58]. It is important to remark that the heterostructures considered in this thesis are composed by GaAs/ $\text{Al}_x\text{Ga}_{1-x}\text{As}$. Then we started with the GaAs crystal to understand its symmetry role in the CQWs. As pointed out before, a crystalline solid can be defined as an arrangement of atoms in strictly periodic arrays [59, 60] raising two concepts: basis and lattice, where the later the set of mathematical points to which the basis is attached [59]. These crystal concepts give place of crystal primitive cell in three dimensions also considered as the seed to reproduce a crystal. One can classify fundamental types of lattices defined by a collection of symmetry operations (rotation, translation etc.). Also, there exists a lattice point group. In the three-dimensional case, the point symmetry groups require 14 different lattices types*, where are classified into seven systems. Into these systems it is

*This lattices are known as Bravais Lattices

found the cubic system, which posses three number of lattices. Remember that the GaAs crystal is cubic, specifically, is the type FCC lattice. The FCC lattice is easy to imagine, if place an atom in each corner of a cube and in a center of each face of it. Therefore, it is easier to define the planes and crystal directions if we take the cube faces as a reference (hkl) plane and the directions [hkl], which must be perpendicular to a plane (hkl) [59].

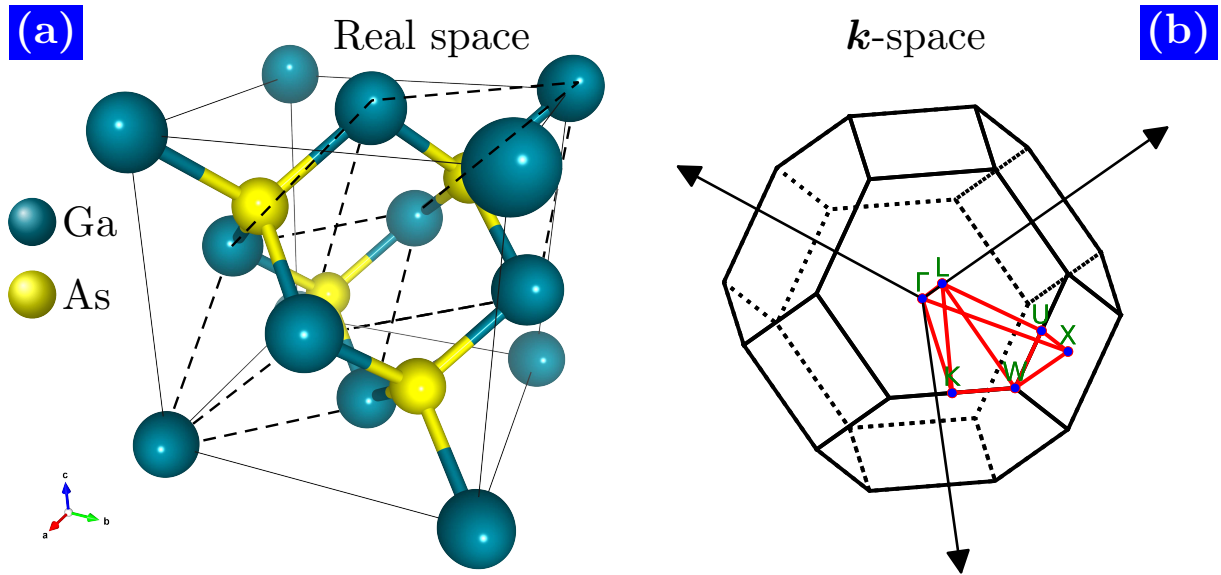


Figure 2.1: (a) GaAs crystal structure in “real space” known as unit cell, into which with dashed line is denoted the primitive cell. This lattice is well-defined by the vectors \mathbf{a} , \mathbf{b} and \mathbf{c} , these vectors are defined as the basis vectors. In (b) is schematized the GaAs crystal structure in k -space, also known as reciprocal space.

The lattice is an array of points which make the space lattice of a *crystal* and the repetitions or disposition of these points is controlled by “*symmetry operations*” [61]. The crystal is composed by a space lattice this is a plane lattice* which have three *symmetry* operations: *Rotation axes*, *Mirror plane* and *Centre of Symmetry*. If add a one dimension to plane lattice it gets a space lattice, which define the unit cell of a *crystal*, so this adds one more *symmetry* operation which is *Rotation Inversion* or *Roto-Inversion*. Then, can get *symmetry* elements of a *crystal* if apply the four *symmetry* operations and their possible combinations. If collect that *symmetry* elements obtains the *point symmetry* or the *point group of symmetry* of a *crystal*. The GaAs crystal as before mentioned is a *cubic* system, but have a defined *cubic* structure called as *cubic zinc sulfide* or simply *zincblende*.

This specific *cubic* structure is characterized by arrangement of two type atoms with places coordinates: 000 , $0\frac{1}{2}\frac{1}{2}$, $\frac{1}{2}0\frac{1}{2}$, $\frac{1}{2}\frac{1}{2}0$ for one type of these as Zn in ZnS or Ga in GaAs structure. In case of the second one atom, it has coordinates : $\frac{1}{4}, \frac{1}{4}, \frac{1}{4}, \frac{1}{4}, \frac{3}{4}, \frac{3}{4}, \frac{3}{4}, \frac{1}{4}, \frac{3}{4}, \frac{3}{4}, \frac{1}{4}$ for S in ZnS or As in GaAs [59, 62].

*2D point pattern array

The Figure 2.1(a) shows the unit cell of GaAs structure and into them, it dashed the primitive cell for the FCC lattice, also denoted the basis vectors \mathbf{a} , \mathbf{b} and \mathbf{c} .

In the case of the symmetry of GaAs, is important to remark that this symmetry can also denote in Hermann-Maguin notation $F\bar{4}3m$ which corresponds to three fourfold rotary inversion parallel to the edges of a cube, with four threefold rotation axes parallel to the body diagonal and six mirror planes, each containing a face diagonal [61]. The F label corresponds to cubic system FCC, following by the corresponds operations.

The symmetry context before exposed can view as a macroscopic symmetry about a crystal system which means, is very interactive to think as a pattern well-ordered can conform a plane lattice and is intuitively work the symmetry operations. But it is not the only symmetry concept in crystal systems, if we enter into crystal it found atoms or molecules which conforms it. So, the internal study of a crystal add two symmetries to the actual worked before. These “microscopic symmetry” [61] the make reference to \mathbf{k} -space or reciprocal space. So, the previous concept of lattice it is also known as direct space lattice. Thanks to X-Ray, Electron or Neutron diffraction techniques, it was possible to study the internal structure o crystal symmetries in the reciprocal space, this trough diffraction phenomena, the propagation of waves into crystal can to form well-defined pattern they which are explained by the wave-vector concept [55, 63]. Therefore, is expected that the electron wave function can be denoted with a lattice periodic part $u(\mathbf{r})$ and wavelike part $e^{i\mathbf{k}\cdot\mathbf{r}}$ so, the set of all wave vectors \mathbf{k} corresponds to plane waves due the lattice, this is known as reciprocal lattice [64]. Then taken into account this, and the vectors \mathbf{a} , \mathbf{b} and \mathbf{c} in reciprocal space can describe the total unit cell [55, 64].

Finally, as a result to get the unit cell in reciprocal space and known which this is composed by lattices, these lattices are called as *Brillouin zones*. Practically the *Brillouin zones* are constructed by drawing the vectors \mathbf{K} defining the reciprocal lattice and then bisecting each of these with planes perpendicular to \mathbf{K} [55]*. In Figure 2.1(b) it is schematized the *Brillouin zone* to GaAs crystal structure, specifically this representation is called as *first Brillouin zone*. To GaAs crystal it was defined the symmetry operations which compose the symmetry elements in Hermann-Maguin notation as the point group $F\bar{4}3m$, it is important to consider the Schoenflies notation also, this due people often speak in terms of both, although the Hermann-Maguin notation is considered as the international notation. In Schoenflies notation, GaAs corresponds T_d point group.

2.1.1 The Symmetry and the Band Structure

Looking back to Figure 2.1(b), the BZ is labeled denoting a point group symmetry. These points are: Γ , X , L , W , U , K . In Schoenflies notation these correspond to: $\Gamma \rightarrow O_h$, $X \rightarrow C_{4v}$, $L \rightarrow D_{3d}$, $W \rightarrow C_{4v}$, $U \rightarrow C_{2v}$, being Γ the high symmetry point. Then, why is

*The wave vector \mathbf{K} is defined in [65] equation (1.5)

the importance of the BZ role in semiconductor band structure?; the answer is the aim of this subsection. We started with the first section of this work, in it refer the importance of solution of Schrödinger equation, specifically at crystal structures as semiconductors. Here, the most important tool is the Bloch theorem, developed to account periodicity-related properties in crystals, either single or artificially produced.

The symmetry of system define the basis function to get the electron band structure [36, 66–68]. Remember that the concept of *basis function* is a mathematical concept, which in quantum mechanics it is known as *Wave functions*. The BZ is the result of Group theory applied in crystal structures, then the BZ is the map to understand the electron behavior in crystal structures, this defined the \mathbf{k} points through high symmetry paths, where this starts at Γ point or $\mathbf{k} = 0$. If observe the Section 1.1.1 the horizontal axis correspond to \mathbf{k} points and labeled the high-symmetry directions from Γ , then this is the \mathbf{k} paths in BZ as can see in Figure 2.1(b).

By aided form symmetry, the well-known analytical models to calculate BS can be exploited. Here, highlights the invariants concept, which is the connection of symmetry and Quantum Mechanics. The Hamiltonian of the crystal bears this symmetry which depends on their potential, then the crystal potential posses a point group, which is invariant under any transformation. Therefore, the solution of the Schrödinger equation contains all the information of the system. From these tools, we can elucidate the physics of electrons or another quasi-particle inside a semiconductor, for example in perturbation theory, starts from Hamiltonian \mathcal{H}_0 with its specific space group, but under perturbation the Hamiltonian of the system should be the sum of $\mathcal{H} = \mathcal{H}_0 + \mathcal{H}'$, where this last has the symmetry correspond to a subgroup of the \mathcal{H}_0 group. This is, the principle of this work which after will be discussed with detail. While the solution of Schrödinger equation with the total Hamiltonian \mathcal{H} will result in the energy spectrum $E(\mathbf{k})$ along of the BZ. Being a crystal system and the potential is the periodic, it is to hope which a multiband spectrum. Although here does not consider the degeneracy* term, it is evident which the Group Theory has the solution, in general words, are the irreducible representations of the symmetry group which determine the dimension of degeneracy [69].

Thus the band structure as a whole exhibits the symmetry characterized by the crystal [69]. All previous it is about of an ideal crystal, then it is possible to get exact solutions of Schrödinger equation. But, to determine in detail the spectrum $E(\mathbf{k})$ throughout the BZ, one needs a numerical solution of the Schrödinger equation. In previous sections, it shows the results of apply TB method to GaAs bulk, this method parts from Bond Orbital Model [39, 70, 71], in this case, the basis functions it is forming linear combinations of atomic orbitals (LCAO) to specific symmetry group [66].

In this method, the importance is the arrangement of atoms and their orbitals considered, for Figure 1.2 these are sp^3 . In another way, in the case of $\mathbf{k} \cdot \mathbf{p}$ method, apart from perturbed model, but in both the main idea it is found the \mathbf{k} -points correspond to the

*This is due to the linear independent solutions, which corresponds to one energy, this mean m -fold band degeneracy at the point \mathbf{k} [69]

symmetry of the system. In another way, in the case of $\mathbf{k} \cdot \mathbf{p}$ method, apart from disturbance model, but in both the main idea it is found the \mathbf{k} -points correspond to the symmetry of the system. The difference apart from their basis is the efficiency in their applied over semiconductor structures, this means that the $\mathbf{k} \cdot \mathbf{p}$ -method is appropriate in a small region of BZ to describe $E(\mathbf{k})$, therefor is the preferred option to describe semiconductor bands around of Γ , while if the idea is describing $E(\mathbf{k})$ in an extended region of the BZ the TB-method is the correct [66, 69]. In any way, the symmetry establishes the basis to envisage semiconductor band structure, no matter the method this, includes the first principle methods as DFT, which requires the symmetry information of the system to get the pseudopotentials and the geometric optimization to enhance calculations.

When we applied a perturbation to a crystal, as an electromagnetic perturbation, the principal symmetry group reduces to a subgroup of itself, which is also invariant. This conception is also knew or called *symmetry breaking*, was first introduced by Pierre Curie at ended of nineteenth century [72, 73], But, what is the importance to focussing on that?. The importance of symmetry breaking is the physical effects that are present: the properties of semiconductors changes under reduce symmetry and this can observe in band structure. Next section will discuss the importance of symmetry breaking in semiconductors and above all over QWs.

2.2

Symmetry breaking in CQWs

The symmetry breaking, it is the basis for the physical model in this work. Starting from the general and brief concept of the symmetry importance in the Solid State viewed in the past section will arise the symmetry role and the reduced symmetry in CQWs. Before starting the history, it is important to clarify that the SOC is not considered in this work, although in the future works of the NanophotonIICOs are considered, and they study spin phenomena in CQWs. In the superlattice case the symmetry reduces at interfaces due to the change of atom species, that is to say, if it parts from GaAs and added an AlAs or $\text{Al}_x\text{Ga}_{1-x}\text{As}$ lattice the new atom structure reduce symmetry elements that can be done then the point group T_d it is reduce. Let's discuss first the simple QW GaAs/ $\text{Al}_x\text{Ga}_{1-x}\text{As}$ structure grown over [001] direction, if suppose that the $\text{Al}_x\text{Ga}_{1-x}\text{As}$ /GaAs and GaAs/ $\text{Al}_x\text{Ga}_{1-x}\text{As}$ interfaces* are “perfect”, this mean the QWs structurally are perfect, the symmetry of system it is reduced to from $T_d \rightarrow D_{2d}$ [74, 75].

If taken into account a common atom as in this case the As atom as can see in Figure 2.2 and consider that structures growth (001)-oriented lack of translational symmetry [75], then in a single QW, the translational invariance along z axis is lost [76] as can see in Section 2.2. Is so fact which the visualization of symmetry operations isn't trivial, it can

*Another nomenclature usually used is A/B interfaces, being reference to two dissimilar atoms.

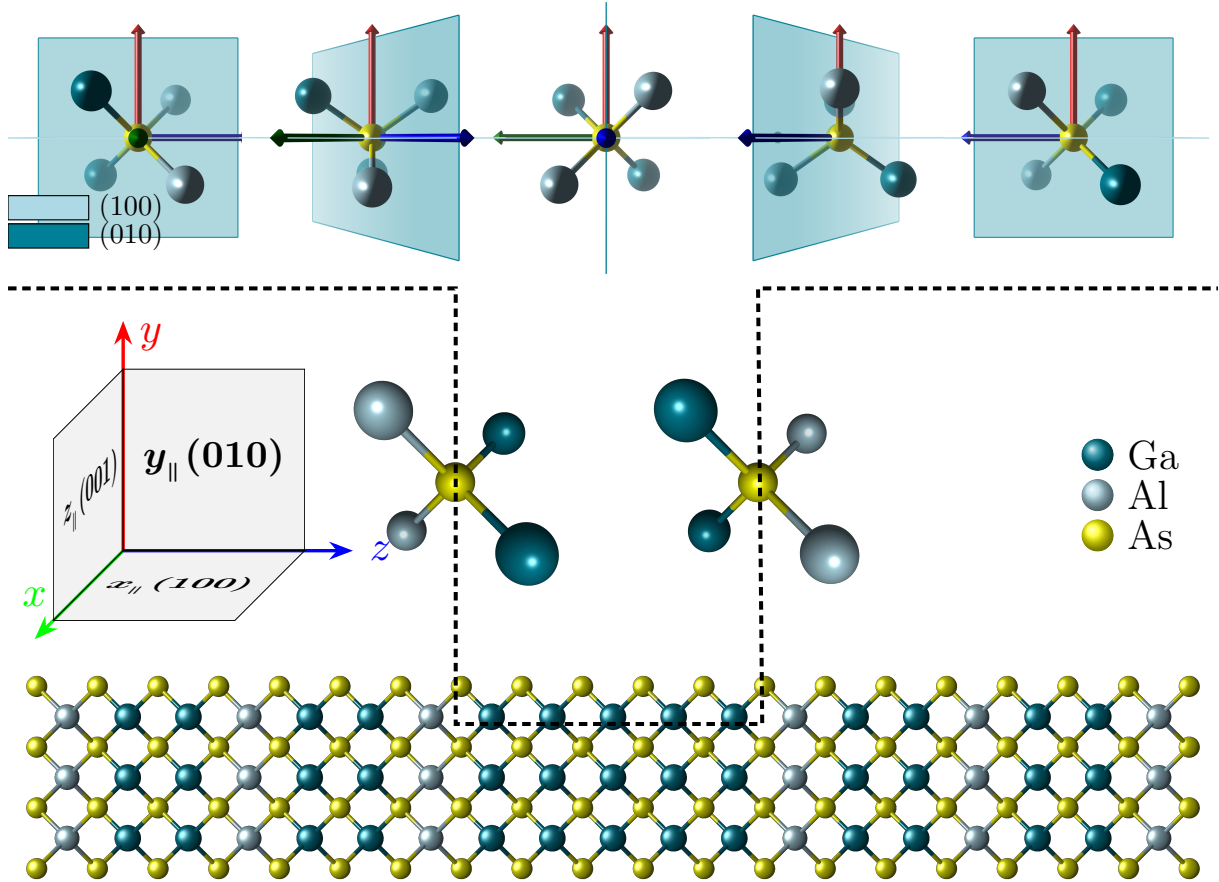


Figure 2.2: Atomic arrangement of a $\text{Al}_x\text{Ga}_{1-x}\text{As}/\text{GaAs}/\text{Al}_x\text{Ga}_{1-x}\text{As}$ single QW. At bottom we can appreciate the atom structure assuming an Al concentration in the barriers. Middle: the conduction band edge as a potential profile; at the interfaces in between it changes from barrier to well and vice versa. Top: the atoms' basis are added where it has taken the Arsenic as the central atom, and scheme keeps rotating along the y -axis.

support each other with open software library as Spglib or ASE symmetry functions, these are great tool which has an iterative algorithm under applied recursive operations. If set the arrangement of atoms as the bottom of Figure 2.2, sorting the atoms positions as As-Al-Ga-Ga-As-Al super lattice then at the center of heterostructure the GaAs atoms to finally complement with the heterostructure composed by the first super lattice. Then, it is applies over these the continuous operations under ASE package the result is the $P\bar{4}m2$ symmetry in terms of international notation, therefore the D_{2d} point symmetry group. Although that is well-known and described in [74–80], the use of package software will be got a powerful tool to developed future works. So, in order to understand reducing symmetry from $T_d \rightarrow D_{2D}$ of QW grown on the (001), the $z_{\parallel}(001)$ direction becomes inequivalent to both $x_{\parallel}(100)$ and $y_{\parallel}(010)$ directions, hence the symmetry is reducing.

In terms of band structure the symmetry breaking, or symmetry reducing, generate changes, above all over the VB of QWs. This was expected, the reason is the due to the BZ zone is reduce to Γ point. From here starts the relevance of Γ and the events which occurs

are the next: the first one event which occurs is over VB, due to the BZ is reduces to Γ the VB it splits for heavy- and light-holes. This is, from bulk as show the band structure in Section 1.1.1 the VB is four-fold degenerate, then in QWs the heavy- and light- holes bands splits, so, it gets two-fold degeneracy as shows in Figure 1.9. In fact, when refer to Γ in really it is refer to near band extrema, in case of GaAs and $\text{Al}_x\text{Ga}_{1-x}\text{As}$ being direct band gap semiconductors this really clearly. The consequences of bands split it is the reason which the effective mass approximation (EFA) can works, thanks to that the Schrödinger's equation can solve as one dimensional equation over both CB and VB band under structure material parameters. Then, the facility of solve Schrödinger's equation it is limited to only getting information about transitions, it is important to remember which this solution is over real-space, for this reason, it says that the potential profile is called a band edge profile and can't confuse with the band structure. So, this is the principle of symmetry reduction in QWs structures, in the next section will be addressed the symmetry in CQWs structures and the mechanisms to reduce it.

2.2.1 Coupled Quantum Wells

In therm to study changes in physical properties in this work it is focus on optical properties, the light matter interaction gets information about the symmetry breaking through transitions. The GaAs QWs as a direct band gap semiconductor are excellent platform to study light-matter interaction and the effects on symmetry. It is important to remark that from here the excitons played it an important role, in fact, over them falls the physical interpretation of optical properties.

Then, in the case, of Coupled Quantum Wells (CQWs) through excitons get optical properties really it is interesting, although, to get that properties the CQWs should get a double reduce symmetry from T_d , even if that's not obtained it is important to anisotropy spectroscopy get it as a basis. Then, firstly, it is start with the symmetric coupled quantum wells (SCQWs), these are QWs with same width and coupled with a thin barrier, this barrier must be enough thinner so that electron wave function can be overlapping along potential of the two wells. For these structures the symmetry is also D_{2d} as in single QW, it is important to say which, if they are not consider the interface defects as roughness it is possible to consider ideal interfaces, then the same symmetry operations works in both single QW like a SCQWs.

From Figure 2.3 it is possible to compare which in contrast with the SQW (Figure 1.8) is the same case with exception to the two QWs, although it is true that the technology of growth it is really accurate, the interfaces are not be exempt free of them. Even, the rough by possible of Al impurity can cause the possible segregation of this, then it is important the Al concentration x [81, 82]. Even tought, an interface grown over (001) is

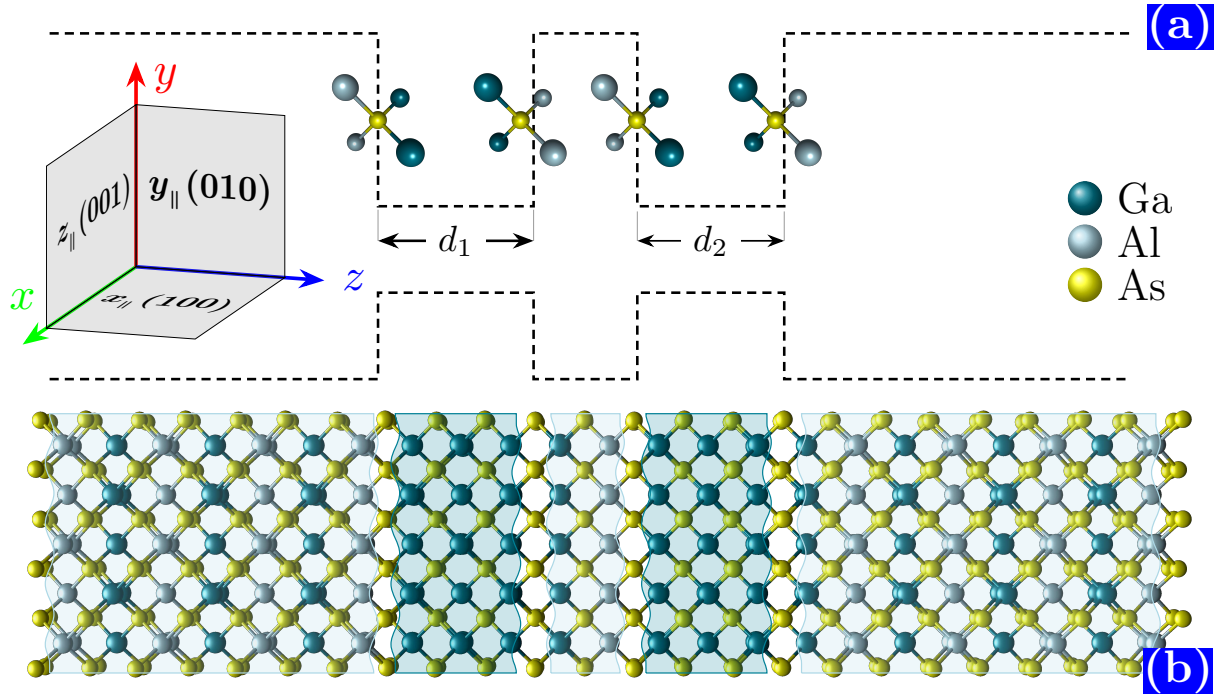


Figure 2.3: General scheme to describe a SCQWs structure. In this case, the barriers are composed by $\text{Al}_x\text{Ga}_{1-x}\text{As}$ and the wells are made of GaAs with the same width ($d_1 = d_2$) and the coupling barrier also composed by $\text{Al}_x\text{Ga}_{1-x}\text{As}$. In top, (a) denotes both CB and VB edges profiles over z -axis (Real-space) direction, whereas in bottom (b) the atomic structure of CQWs is depicted.

C_{2v} , if consider structurally perfect as SQW or SCQWs, the overall symmetry of both interfaces is D_{2d} [74].

As Pierre Courie mentioned [72,73,83]: a system under perturbation reduces their symmetry to a subgroup of original symmetry group, then, if now starts with D_2 symmetry this subgroup can only reduce to a subgroup of six possibles, into them is C_{2v} subgroup. Previously it mentioned which, exist several mechanisms can reduce the symmetry, these are usually called perturbations. These perturbations can be nature by different sources, *in this work has been it found a novel source which reduces the symmetry, in other words, broken symmetry without needed external source as applied electric or magnetic fields.* In the next section, it details the reason which it is called a novel source of reduce symmetry, therefore, before continue it is important to mentioned that the simple reason of modify the one well width in CQWs structures makes the system loses fourfold rotations over $z_{\parallel}(001)$ then, the symmetry it reduces.

If compares Figures 2.3 and 2.4 it is clearly that the representative part of the coupling barrier only shift over z , this allows to simulate a ACQWs heterostructure, this mean which QW is wider than the other, so, it gets an asymmetric structure which along z losses the rotation symmetry. Also, if it is uses symmetry code packages as ASE or Spglib

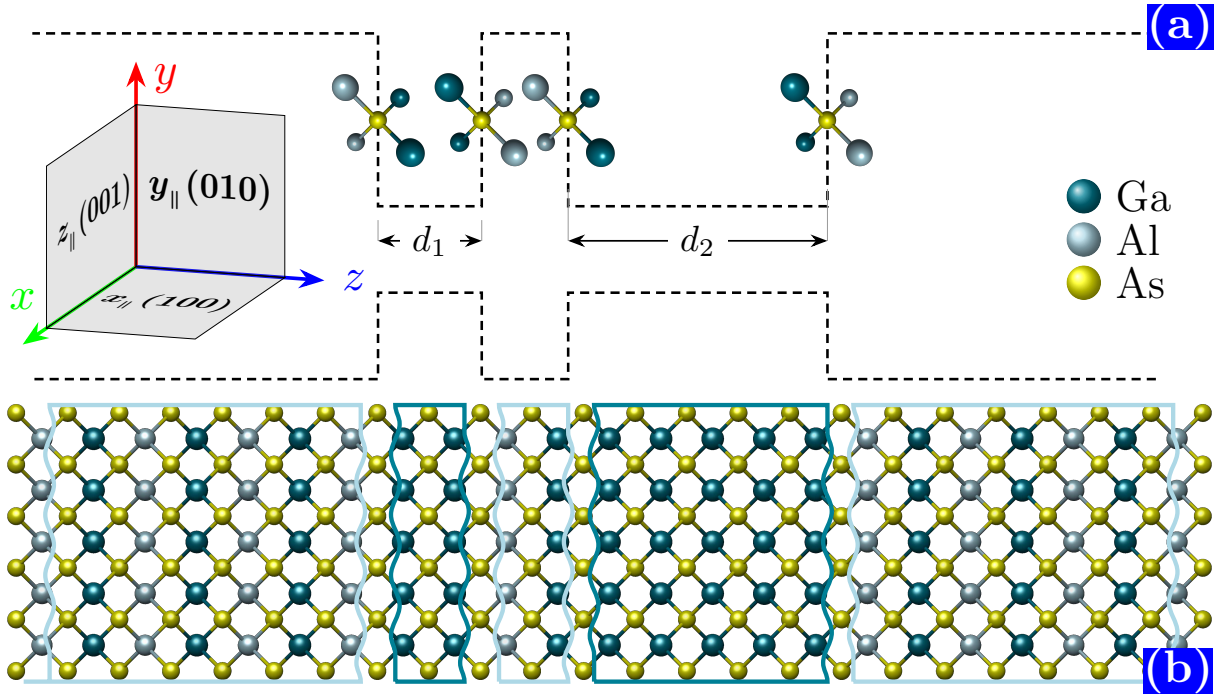


Figure 2.4: General scheme depicting an ACQWs structure. As in Figure 2.3(b), the structure is basically the same both in both barriers height, composition and dimensions as well as the coupling barrier, only the relative position of these are varied. Then, as a result is that one of the QWs is wider than the other ($d_1 < d_2$). Thus, this is the reason causing the asymmetry in structure. Also, at top (a) draws the potential profile along z direction, and bottom (b) schemes the atoms structure where is clear that only shows changes in the coupling barrier relative position with respect to Figure 2.3(b)

which applies consecutively symmetry operations to both CQWs structures, it results in a D_{2d} and C_{2v} for SCQWs and ACQWs respectively.

2.2.2 Special Symmetry Reduction From $D_{2d} \rightarrow C_{2v}$

The importance of C_{2v} point group inherent to QWs system is attractively to study properties of them, over all quantum properties as “spin” [13, 77, 80, 84–86]. Also, it is very important the quantum mixing which exhibits as a result of symmetry breaking, in fact, in Section 3.2.3 it presents the result of RAS experiments, which are the result of hole mixing.

The detected anisotropy is caused due to the mixing at VB. Figure 2.5 shows a scheme of the roadmap to get a QWs structures with a C_{2v} symmetry. This starts at the left side with asymmetrical structures Figures 2.5(a) and Figures 2.5(a) and 2.5(b), this asymmetry is related with the potential, exists a variety of them but the objective it is practically the same, the asymmetric potential profile can be obtained by: asymmetric

barrier, this can be due to the change of semiconductor type between adjacent barriers, *i.e.*, AlAs/GaAs/Al_xGa_{1-x}As structure, this can interpret as high barrier/well/low barrier [12]. Another way of them, is caused of a barrier it is under gradient composition [14, 15]. The end case under asymmetric potential consideration shows in Figures 2.5(a) and 2.5(c), this case is due in one of the barriers which is intentionally “inserted” as an atom from other specie [16], this causes an asymmetric potential profile. Continuing with the map: at top center, Figure 2.5(d) a QW structure under applied strain, whereas at bottom center Figure 2.5(e) a QW structure under electric field applied, are outlined. In these both there is an external perturbation which causes a lost of symmetry. Finally, the CQWs structure studied in this work is presented in Figure 2.5(f), which in comparison with the rest, it has two wells. It is notably that this kind of structure has two wells which are coupled by a thin tunneling barrier and by this reason is regarded as Coupled Quantum Wells. Then, which is the reason by these structures are novel?. To discuss this answer, it is important to mention the relevance of CQWs being that these structures are recurrent studied to observe quantum phenomena as exciton (**X**) condensation [87–89].

It is to be expected that in CQWs can measure indirect transitions, this means that in comparison with a single QWs whereby exists direct transitions (band to band) hardly can measure these. But, the reality of the importance of CQWs being that excitons are very interested to apply in semiconductor devices, the properties of excitons and their interactions really exhibit quantum attractive properties. So, unlike with single QW in CQWs the life of excitons increases [90, 91], in fact, this is one of the principal reasons which that are attractive structures [87, 92, 93]. Also, in terms of spin properties, the CQWs exhibit great potential [94]. In comparison between CQWs, the symmetric structures need it perturbed to them exhibit these properties, while asymmetric structures are an excellent platform to study quantum properties such as holes mixing, spin, etc. It is then *ACQWs interesting structures, which besides from being artificial, they are naturally perturbed**, even though, as can see does not are the unique structures with “natural perturbation” which generates a symmetry breaking, all above mentioned it is reduced to confinement way. This, is the reason to call special symmetry reduction in a structure hardly studied in several sub-areas of solid state.

*Thanks Dr. Raul for magnificent description.

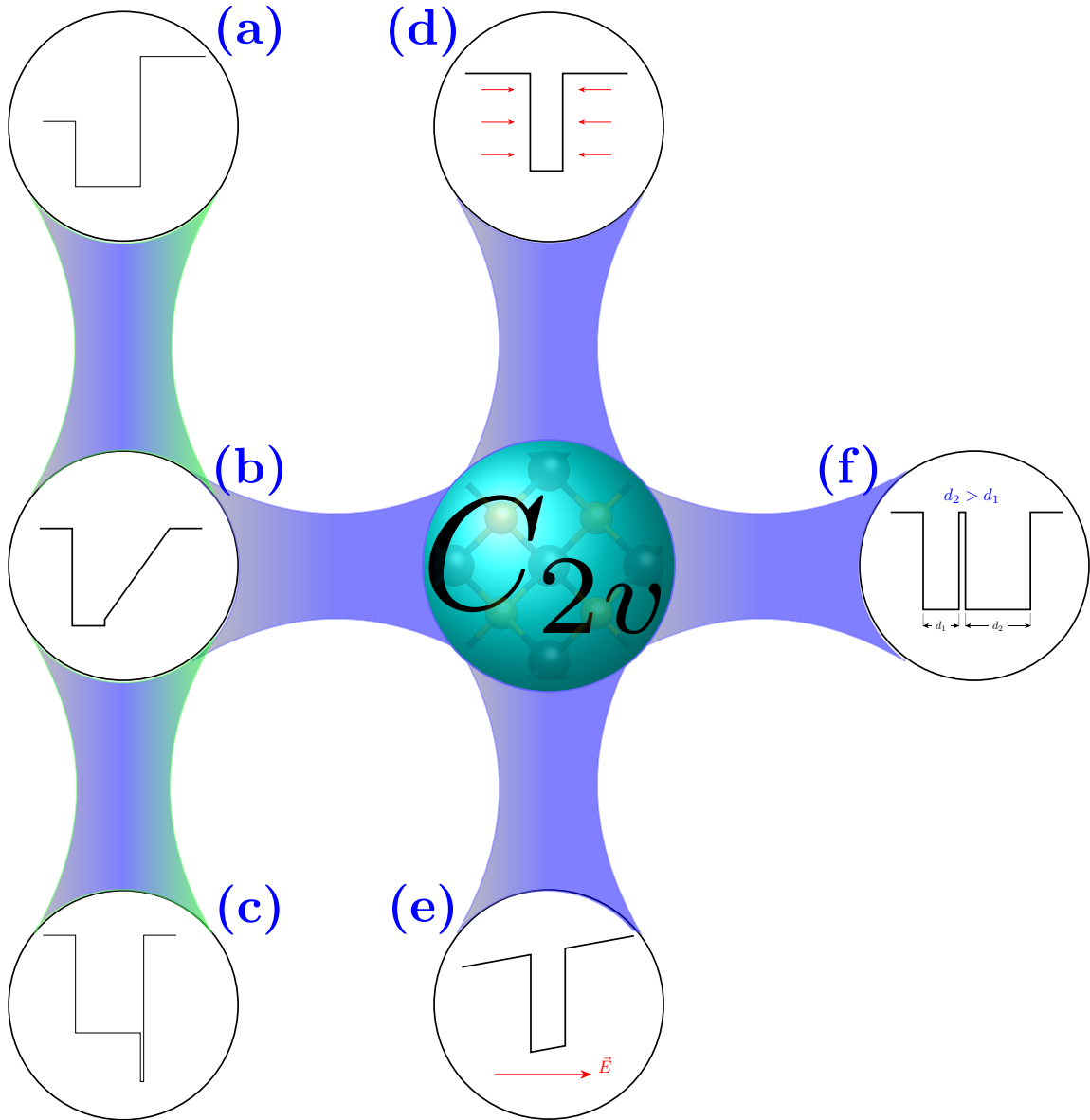


Figure 2.5: Roadmap developed around of QWs with possible potential profiles, each one possessing a desired C_{2v} symmetry. It starts with an asymmetric QW (a) [12,13] in the potential profile due to the semiconductor difference in adjacent barriers to the well. At the center-left (b) and bottom left (c) are asymmetric QWs: in the first case the asymmetry [14,15] is caused by a graded concentration in a barrier and bottom, whereas in the other case the asymmetry is originated by inserting an atomic specie different that of the barrier [16]. At the top center (d), it is shown a QW under strain [17–19] causing symmetry breakdown, while the bottom center (e), shows the CQWs under applying electric field [20], the relation of both, it is the external perturbation which causes the breaking symmetry. Finally, right (f) is an ACQWs which have a symmetry breaking due to the relative width of the constituents QWs [21].

2.3 Numerical Calculations

All the properties mentioned above, could not have been predicted or observed without their knowing their electronic properties. For this, we implemented a *simple* model-based in EFA method to calculate the confined energies in CQWs structures. Before explaining the numerical method to obtain these solutions, it is important to discuss the reason why this method can be applied. Section 1.1.1 discussed the concept of VB and CB, the significant methods to calculate them, in case of a CQWs. In bulk, the case is well-known several methods to calculate BS, where all of them are developed by the symmetry properties of the system at stake. In the case of the heterostructure, the symmetry is also important, the problem is to develop a Hamiltonian capable to describe all of the system, this means, building a Hamiltonian which considers all properties as symmetry, perturbations, and in this case the potential. The history and development of methods and techniques to calculate electronic properties is an area in constant evolution, from the fifties with Kane [22], Luttinger and Kohn [95] in perturbed methods as $\mathbf{k} \cdot \mathbf{p}$ to Slater and Koster [71] which proposed an atomistic method based on a linear combination of atomic orbitals called as TB, all of this already discussed and mentioned. So, we developed a model to calculate the confined energies in coupled structures. Even though there exist analytical methods to calculate confined energies, for the case of CQWs is more difficult to get an exact analytical approach; but in this case, there exist some analytical approximate methods as described in [96–98]. In the Section 1.2.2 it is developed the analytical solution of a simple quantum well taken into account the EFA method. It is possible to use this type of methods due to the symmetry reduction from bulk to QW, this due to the split in VB which passes from being a fourfold degenerate to be a twofold degenerate. It is precisely in VB where is it complicated to solved it.

The Figure 2.6 it is the result of apply $\mathbf{k} \cdot \mathbf{p}$ method, specifically taken into account 8-band model Hamiltonian [22, 38, 99] which is an extension of four band model [99] and even, this model is raised to bulk semiconductors, but in Figure 2.6(b) shows the results applied in a GaAs SQW heterostructure. To give support to these calculations is important to invoke EMA, this method is an efficient method to computational calculations [43, 100] and their basis allows developed electron solutions. In general, exist a variety of Hamiltonian intending to calculate the BS of heterostructures. From conventional Luttinger-Kohn model, [95] to relatively recent models by Burt and Foreman [101–103], which they consider the basis functions depends on symmetry, this is the reason which Hamiltonian is associated to the bulk structure as in this case is Zinc-Blende type. Although it has been discussed applying this method over heterostructures as the QWs, this work considers it as an “exploratory” tool. The reason for taking it into account in that way is basically their difficult and tedious way to get a correct Hamiltonian that describes our structures, in fact, $\mathbf{k} \cdot \mathbf{p}$ is not the unique difficult method, also TB and others, have laboriousness way

to build their Hamiltonians. So, we take the technic and equations from Vurgaftman [38] and solve it numerically to gets the GaAs bulk as shown in Figure 2.6(a) and in the same route, we take the Hamiltonian from Marchewka [23, 104] and solve under FDM, without major preamble the idea is to denote the split between heavy- and light-hole bands which is the justification to our numerical calculations proposed. In Equation (2.1) it is presents the 8×8 Hamiltonian solved to get BS to GaAs SQW.

$$H_0 = \begin{bmatrix} T & 0 & -\frac{1}{\sqrt{2}}Pk_+ & \sqrt{\frac{2}{3}}Pk_z & \frac{1}{\sqrt{6}}Pk_- & 0 & -\frac{1}{\sqrt{3}}Pk_z & -\frac{1}{\sqrt{3}}Pk_- \\ 0 & T & 0 & -\frac{1}{\sqrt{6}}Pk_+ & \sqrt{\frac{2}{3}}Pk_z & \frac{1}{\sqrt{2}}Pk_- & -\frac{1}{\sqrt{3}}Pk_+ & \frac{1}{\sqrt{3}}Pk_z \\ -\frac{1}{\sqrt{2}}k_-P & 0 & U + V & -\bar{S}_- & R & 0 & \frac{1}{\sqrt{2}}\bar{S}_- & -\sqrt{2}R \\ \sqrt{\frac{2}{3}}k_zP & -\frac{1}{\sqrt{6}}k_-P & -\bar{S}_-^\dagger & U - V & C & R & \sqrt{2}V & -\sqrt{\frac{3}{2}}\tilde{S}_- \\ \frac{1}{\sqrt{6}}k_+P & \sqrt{\frac{2}{3}}k_zP & R^\dagger & C^\dagger & U - V & \bar{S}_+^\dagger & -\sqrt{\frac{3}{2}}\bar{S}_+ & -\sqrt{2}V \\ 0 & \frac{1}{\sqrt{2}}k_+P & 0 & R^\dagger & \bar{S}_+ & U + V & \sqrt{2}R^\dagger & \frac{1}{\sqrt{2}}\bar{S}_+ \\ -\frac{1}{\sqrt{3}}k_zP & -\frac{1}{\sqrt{3}}k_-P & \frac{1}{\sqrt{2}}\bar{S}_-^\dagger & \sqrt{2}V & -\sqrt{\frac{3}{2}}\bar{S}_+^\dagger & \sqrt{2}R & U - \Delta & C \\ -\frac{1}{\sqrt{3}}k_+P & \frac{1}{\sqrt{3}}k_zP & -\sqrt{2}R^\dagger & -\sqrt{\frac{3}{2}}\bar{S}_-^\dagger & -\sqrt{2}V & \frac{1}{\sqrt{2}}\bar{S}_+^\dagger & C^\dagger & U - \Delta \end{bmatrix} \quad (2.1)$$

where

$$\begin{aligned} k_{\parallel}^2 &= k_x^2 + k_y^2, k_{\pm} = k_x \pm ik_y, k_z = i\partial/\partial z, \\ T &= E_c(z) + \frac{\hbar^2}{2m_0} [(2F+1)k_{\parallel}^2 + k_z(2F+1)k_z], \\ U &= E_v(z) - \frac{\hbar^2}{2m_0} (\gamma_1 k_{\parallel}^2 + k_z \gamma_1 k_z), \\ V &= -\frac{\hbar^2}{2m_0} (\gamma_2 k_{\parallel}^2 - 2k_z \gamma_2 k_z), \\ R &= -\frac{\hbar^2}{2m_0} \sqrt{3} (\mu k_+^2 - \bar{\gamma} k_-^2), \\ \bar{S}_{\pm} &= -\frac{\hbar^2}{2m_0} \sqrt{3} k_{\pm} (\{\gamma_3, k_z\} + [\kappa, k_z]), \\ \tilde{S}_{\pm} &= -\frac{\hbar^2}{2m_0} \sqrt{3} k_{\pm} \left(\{\gamma_3, k_z\}, \frac{1}{3} [\kappa, k_z] \right), \\ C &= \frac{\hbar^2}{2m_0} k_- [\kappa, k_z] \end{aligned}$$

and each of these parameters taken from [38]. The Hamiltonian H_0 is defined for [001], and the principal idea is evaluating it in a “discrete” SQW structure, the “discrete” term refers to a numerical technique for solving it. The results are shown in fig. 2.6(b), this approximation is enough to evince the VB split, even, the results also CB information the

importance falls on VB, this is due that difficult to solve there. Then, the VB split allows applying “simple” numerical methods without needing to define complex Hamiltonian and many parameters. Next section discusses the physical and mathematical formulation to calculate the electron energy confined, beginning with the symmetry reduction causing the VB splitting around of $\Gamma = 0$.

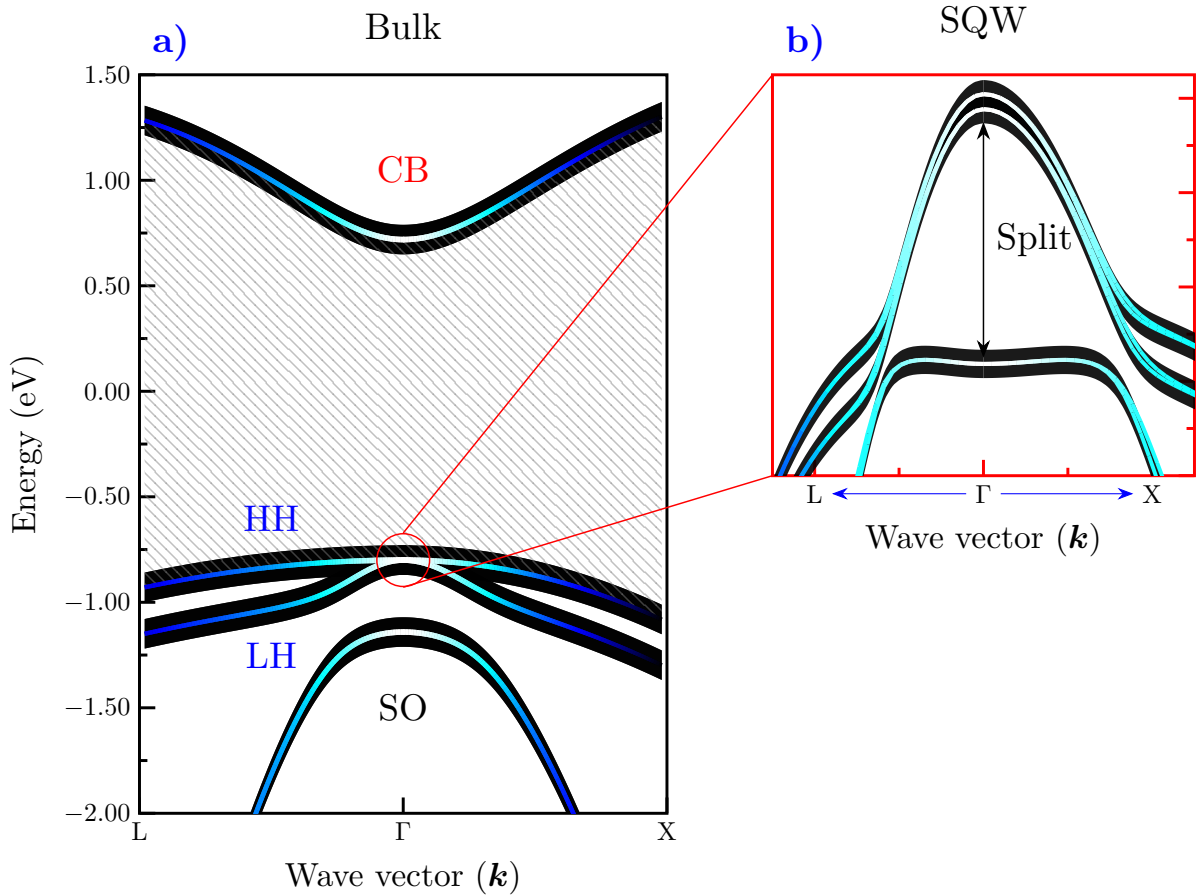


Figure 2.6: (a) The GaAs band structure calculated with 8-band Khane Hamiltonian [22, 23], with the SOC considered. At $\Gamma = 0$ in Bulk VB is enclosed by a circle pointing the degeneracy, while in (b) it is denoted the split (Δ) between heavy- and light hole bands. Also, due to SOC consideration, it displays the spin up and down, bands.

2.3.1 Envelope Function and Effective Mass Approximation Methods

Furthermore, to obtain a numerical method and robust solution, we can take into account the effect of asymmetric in the width well of the CQWs which causes the symmetry breaking and its role on the increase of the optical anisotropy, depending on their relative width. The EFA is the mathematical justification to model electron behavior under periodic potential, and the EMA is the physical model to describe electronic behavior inside a

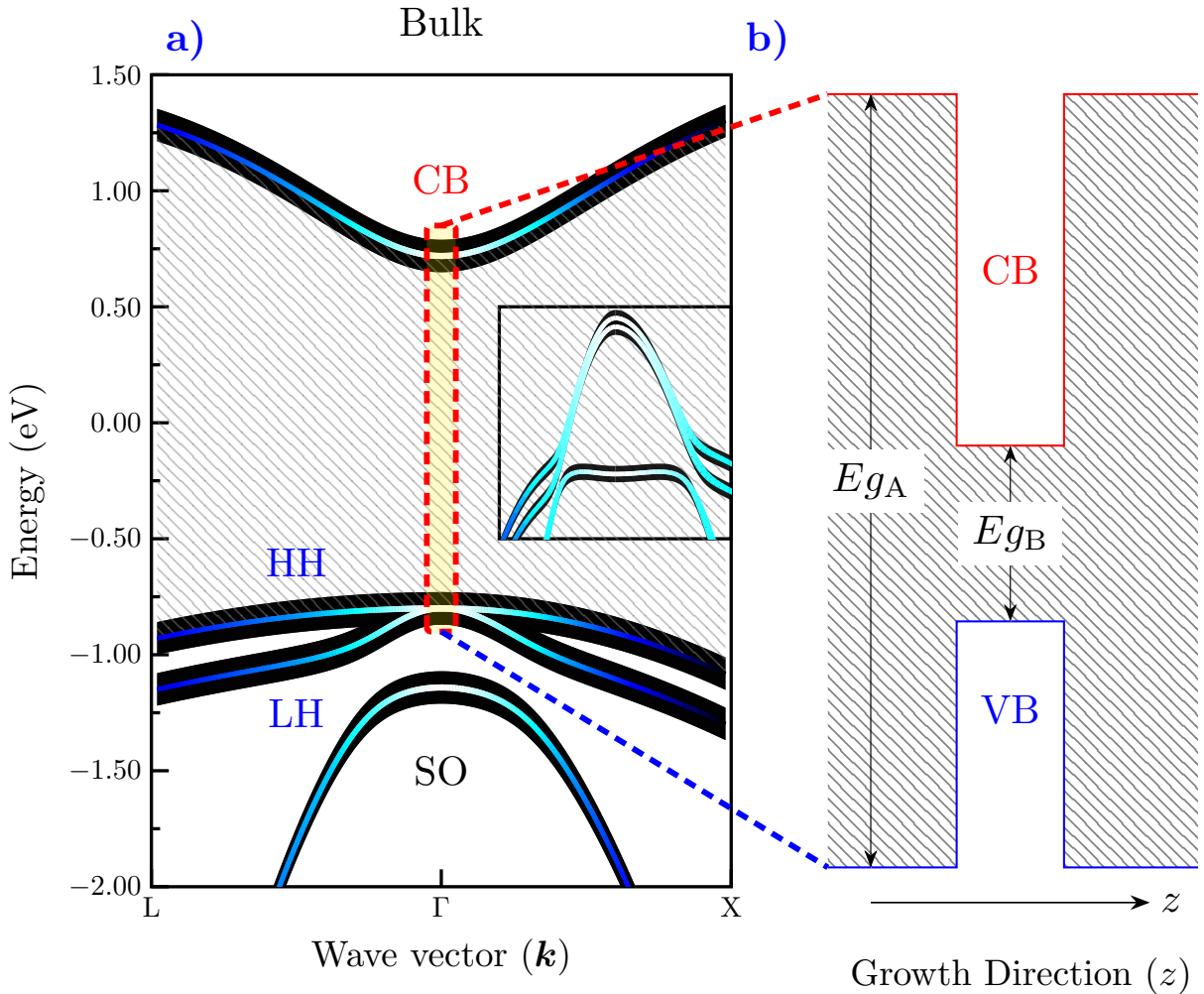


Figure 2.7: (a) it is the focus over $\Gamma = 0$ and inside is the SQW VB $\mathbf{k} \cdot \mathbf{p}$ results, while (b) is the potential profile considered due to the VB splitting. This VB splitting, it is the cause that of 1D potential profile, can be implemented

periodic potential from a crystal [43]*. Under that assumptions, it is possible to review several considerations. Firstly, from here we can study the electron and holes behavior by separately, from basic assumption which $\Gamma = 0$ this enables to pass from electronic band to band edge (see Figure 2.7). So, it is important to define that tools previously mentioned. The EMA is a valid approximation in bulk materials, in fact this is an elemental model which due to the good results and simplicity it is can be applied over heterostructures. About of this last, the heterostructures are complex, the dissimilar matched semiconductors which conformed that it, posses does not only difference in band-gap energy but also the effective mass.

*Both EFA and EMA approximations are considered the same approach, but EMA depends on the formalism of EFA.

If join all of that parameters involved it, the model to solve should being proportional to the considers in it, by this reason models as TB are complex due to the difficult to define all that parameters, while in $\mathbf{k} \cdot \mathbf{p}$ are well-defined, but contrary, the method frequently is submitted to discussion due to the assumptions as the does not “see” the correct point-group symmetries, in fact, frequently assumes which the system already owns it. We can introduce ourselves in a heavy discussion about of BS calculations methods, but the reality is can not define a standard method, so that, doing reference to Harrison *et al.* [43], we can apply the simplicity method. Then, assuming the simplicity term, in which practically mentioned that, it is important to consider the simple way to get a result as a long as this works.

So, in this work, will discuss the increase of the IOA due to the relative width in the wells of the coupled system, then here only considers the potential profile as a really significant parameter, of course, the effective mass and the band-gap are also essential, but these are considers as a part of the model. Being this the basis of the model, this work will employ the formalism of EFA where in a general explain, this it gives the envelope functions to calculate the single electron behavior under periodic potential as a heterostructure, therefore, this can allow describing it through position-depend material properties [47, 105, 106], then it is also indispensable to declare the boundary conditions owned by the EFA. Therefore, with a mathematical formalism, then it is employed the EMA which parts of the fundamental parameter which is the effective-mass, then it can works with the 1D-Schrödinger’s equation as a function of effective-mass, as traditional eigen-value equation:

$$\mathbf{H}\psi(z) = E\psi(z), \quad (2.2)$$

Then, the Hamiltonian of EMA it is developed mainly by the effective-mass, this has the advantage of evaluated along of heterostructure, allowing the change of semiconductors which composed that, so, this makes it a great method. Therefore, the Hamiltonian for a particle is given by [47, 105, 107]:

$$H_z = \frac{p_z^2}{2m^*(z)} + V(z). \quad (2.3)$$

Equation (2.3) takes z -axis as a direction perpendicular to interface of QWs, or simply as the growth direction, consequently the potential $V(z)$ it is depend on, and the effective-mass $m^*(z)$ also depends on position z . As can see in Figure 2.7(b), it is showing the band-edge profile as a potential profile which depends on semiconductor band-gap along of heterostructure. Also in Equation (2.3), it considers the momentum as p_z^2 as a 1D, due to the before discussed. Then it is allow to developed a method to solution which depends of position z . Finally, it can denote a 1D Schrödinger equation under EMA to electron also heavy- and light-holes :

$$\left[-\frac{\hbar^2}{2m_{jz}^*} \frac{d^2}{dz^2} + V(z) \right] \psi_{nj}(z) = E_{nj} \psi_{nj}(z), \quad (2.4)$$

$j = e, hh, lh.$

The Equation (2.4) it is then the effective-mass equation implemented in this work. The solution of that, it is detailed in next section where explains the numerical method to solve it. Before to continue, it is important to discuss the 1D equation. This equation will be applied over each particle ($j = e, hh, lh$), this means, over electron, heavy- and light-holes, where only considers the effective-mass (m_{jz}^*) trough each semiconductor in heterostructure studied and the most important in this work, the potential profile $V(z)$ which depends on relative widths of coupled wells.

2.3.2 Finite Difference Method

In this section we discuss the numerical method to solve the 1D Schrödinger's equation. Starting from the fact that the Equation (2.4) can be discretized, and solved for electron and holes, with a spcial discretization depending on δz . Figure 2.8 schematizes the discrete

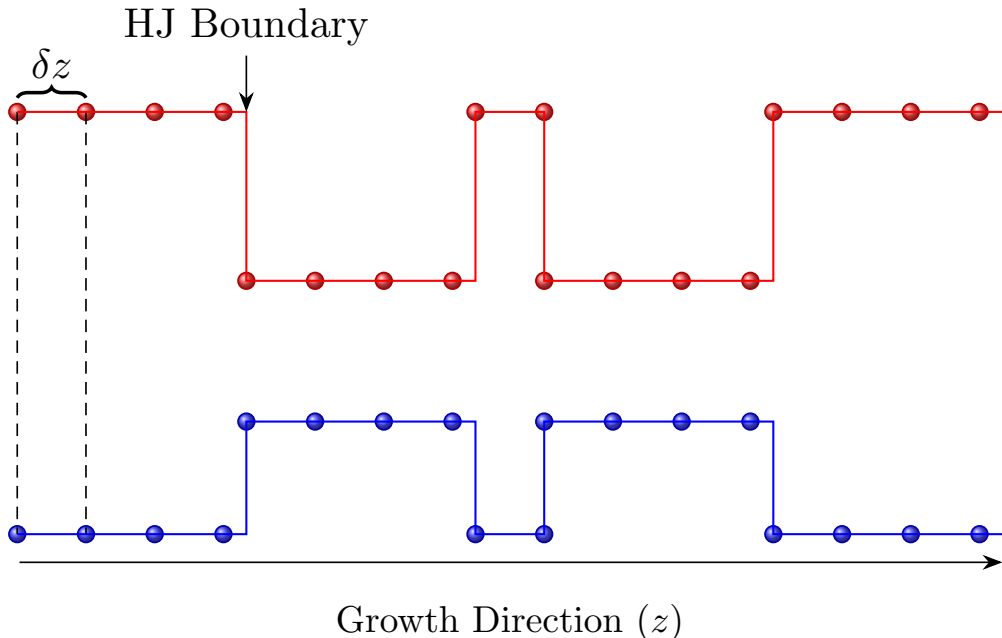


Figure 2.8: Sketch of discrete potential band-edge profile which depends on spacial displacement δz . HJ denotes the Heterojunction boundary junction.

potential corresponding to a SCQWs structure. Note that potential $V(z)$ arises from the bend-edge energy (E_{edge}), like in the CB and VB. Then, we can divide a heterostructure with coupled quantum wells basically into two parts, the adjacent barriers and the zone of wells which is considered the coupled barrier and their width as well as the relative widths

of each well. Hence, if we consider the discrete structure we can apply Equation (2.4) in each point which composes that.

The solution of Equation (2.4) it is the central discussion, although exist several numerical methods to solve it, this work employs the *Finite Difference Method*. Even if, this method does not unique in applied discretization in comparison with the other method as Shooting [43, 108], it reduces the computational time and assure the correct convergence as long as the boundary conditions are correct. In other words, the FDM is a non-sensible convergence method, being focused on matrix solution. Taking the Equation (2.4) and reformulated as a *difference equation* [43]:

$$-\frac{\hbar^2}{2m^*} \left[\frac{\psi(z + \delta z) - 2\psi(z) + \psi(z - \delta z)}{(\delta z)^2} \right] + V(z)\psi(z) = E\psi(z). \quad (2.5)$$

In Equation (2.5) the difference terms denote the numerical difference, thus, being a discrete equation. Something that it is important to consider is the boundary conditions which depend on the number of semiconductor layers involves in the structure and their dimensions, then it requires high precision important two factors: the total dimension of the structure, which contemplates each heterojunction boundary and the spatial step defined by δz . When considering a wide structure, as well as a very small step ($\delta z \approx 1\text{\AA}$), the computational effort is high and for this reason, the computation calls for a consider amount of memory. Thus, by taking into account these two factors, the best choice is a Matrix solution.

The Matricial solution allows solving the system of equations naturally as an eigenvalue problem, then it has several numerical alternatives* to solve the system. The reason to assert these have to do with the discrete solution as large as the ratio between structure width and spatial step. This means the matrix has dimensions as: $N = \text{total width}/\delta z$. Then, the way to get matrix (\mathbf{H}) , from Harrison et al. [43], consists in reformulate Equation (2.5) as function of spatial potential band edge taken into account the variable effective mass, then:

$$a_i\psi_{i-1} + b_i\psi_i + c_i\psi_{i+1} = E\psi_i \quad (2.6)$$

where the coefficients are:

$$a_{i+1} = c_i = -\frac{\hbar^2}{2m_{i+\frac{1}{2}}^*(\delta z)^2} \quad \text{and} \quad b_i = \frac{\hbar^2}{2(\delta z)^2} \left(\frac{1}{m_{i+\frac{1}{2}}^*} + \frac{1}{m_{i-\frac{1}{2}}^*} \right) + V_i. \quad (2.7)$$

From Equation (2.2), then the matrix \mathbf{H} is conformed by the system of equations which is

*This refers to linear algebra techniques [43, 109]

evaluated in each point os structure, then \mathbf{H} is:

$$\mathbf{H} = \begin{pmatrix} b_1 & c_1 & 0 & \cdots & 0 \\ a_2 & b_2 & c_2 & \cdots & 0 \\ 0 & \ddots & \ddots & \ddots & 0 \\ \vdots & \cdots & a_{N-1} & b_{N-1} & c_{N-1} \\ 0 & \cdots & 0 & a_N & b_N \end{pmatrix} \quad (2.8)$$

then ψ is in Equation (2.2) is a vector column which containing all the samples of the wave function.

For the solution of the $N \times N$ matrix we use algebraic algorithms [110, 111]. Therefore, this method simplifies the solution of any structure with arbitrary or in our case dependent on band-edge potential. The next task is to define the potential profiles and their dependence of effective-mass and band gap energy (E_g). Firstly, we take as reference the double quantum wells as proposed by Harrison *et al.* [24] and reproduce the eigenenergies and wave functions as shows in Figure 2.9. For this structure, it is taken into account symmetric double wells, that is to say, with same width $l_w = 6\text{nm}$, Al_{0.2}Ga_{0.8}As central barrier of $l_b = 4\text{nm}$. For the semiconductor parameters with compose that structure, as shown in Equation (2.4), it does not take into account the effective mass as energy function and not taken into account the nonparabolicity [112, 113]. Then, to define potential profile $V(z)$, it uses the Varshni's model [114] to calculate bandgap energy to GaAs/Al_xGa_{1-x}As [115–118]; finally it employs the Vegard's law to define the ternary semiconductors [119, 120]. It defines the potential profile as:

$$V(z), m^*(z) = \begin{cases} \text{Al}_{0.2}\text{Ga}_{0.8}\text{As} & 0 < z < 20 \text{ nm} \\ \text{GaAs} & 20 < z < 26 \text{ nm} \\ \text{Al}_{0.2}\text{Ga}_{0.8}\text{As} & 26 < z < 32 \text{ nm} \\ \text{GaAs} & 32 < z < 38 \text{ nm} \\ \text{Al}_{0.2}\text{Ga}_{0.8}\text{As} & 38 < z < 58 \text{ nm}, \end{cases} \quad (2.9)$$

where $V(z)$ depends on the correspond value of E_g and the effective-mass $m^*(z)$, both with the spatial z dependence. But, this work takes into account the model by **Harrison** et al. [43] as a reference, the **Nextnano** software [25, 121] also takes it, Figure 2.9 and Figure 2.9(b) shows the table of comparison results, taken as basis **Harrison** *et al.* and compare also with **Nextnano** software and the codes developed in this work [1]. As can be seen, the results in this work are precise with respect to Harrison, and it is important to remark this work does not intend to denote supremacy since that fall short of sense, the intent is only the comparison to demonstrate that our codes works. The table in Figure 2.9(b) denotes (with red) the precision around of meV, this is what we mean when say the major precision with respect to Harrison's results. Thus, we can trust the codes

and model presented here.

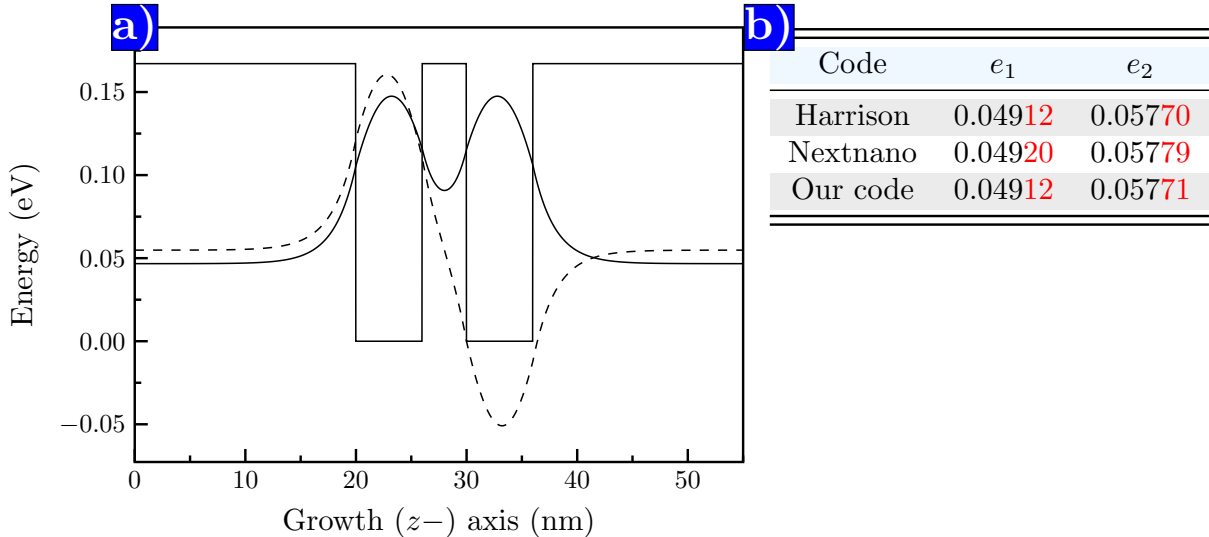


Figure 2.9: Double Quantum Wells structure reproduce from Harrison et al. [24], (a) shows the plot to each energy calculate e_1 and e_2 , while in (b) the table exposes the comparison of numerical results from **Harrison et. al.**, **Nextnano** software [25] and our results. The difference taken into account the Harrison's results practically are the same, but around of meV orders our results are precisely.

2.4

Numerical Results

Here, we introduce the results obtained in CQWs studied in this work. Section 3.1 details the structures' composition as well as their properties. Then, here we focus only on the numerical and computational results. Figure 2.10 shows the plot of wave functions for electrons, and both heavy- and light-holes resultant from numerical calculations taking into account only four samples detailed in Section 3.1 of Table 3.1. In the Figure 2.10 it is calculated ψ to denote more clarify the overlapping wave functions over two coupled wells, even though here does not show the total table of confinement energies results, later these will compare with the experimental transitions. Therefore, in this section, we limited to specify the numerical results in accordance with the published work [21]. In the Table 2.1 exposes and compares the numerical results obtained, it is importantly to remark that the calculations were performed at 30K, this due to the central experiments (RAS) are performed to that temperature, by this reason the parameters involved are well-defined as a function of temperature. These calculations taken into account the conduction and valence-band offsets of 65% and 35% respectively. Both electron and hole effective masses for GaAs and AlAs can be found in Refs. [115–117], whereas the ternary $\text{Al}_x\text{Ga}_{1-x}\text{As}$ we

used the Vegard's law [119]. For the numerical direct transitions (\mathbf{X}) calculated, it is consider the exciton binding energy as a function of well width [122, 123], as commonly only shows the direct transitions in a range of wells widths, we interpolate these energies to used in accordance with the structures used in this work.

The Figure 2.10 denotes some interesting physical issues, one of these with principal role in this work it is a linked between barrier width and the relative width of the coupled wells. The barrier width as can see plays an important role, because the width define tunneling of electrons and holes, for example Figure 2.10(b) and Figure 2.10(d) structures has the same wells widths with exception to barrier type, the first one is $\text{Al}_{0.15}\text{Ga}_{0.9}\text{As}$ and the width is $b_w = 1.98\text{nm}$ while the second one is AlAs type with a width of $b_w = 0.565\text{nm}$. It is known that the difference between these are the bandgap energy then, as is expected, the tunneling is less than the $\text{Al}_{0.15}\text{Ga}_{0.9}\text{As}$ barrier. Concerning tunneling, if compares the Figure 2.10(a) and Figure 2.10(c) structures, which basically are the same structures except for the width of the second well, the wave function in one of these, are symmetrically localized as a doublets states, while the other the wave function practically is well localized in one of the wells as single state energy of a single QW [26]. While if compares with Figure 2.10(b) where one of the coupled wells is slightly width than the other, the wave function distribution seems an SQCWs under applied external electric field [92], later in Section 3.2.2 this take a sense, in PR experiments appear transitions which we associated to three-body particles known as trions (\mathbf{X}^- or \mathbf{X}^+). Trions are particular particles that consist of the bound of two electrons and one hole (\mathbf{X}^-) or vice versa, two holes and one electron (\mathbf{X}^+). The fact of one of the wells is slightly width, entails quantum interactions measured experimentally. But, this does not only the unique, interesting phenomena observed in these structures. As before mentioned this work, focuses on the optical properties consequent of the structural asymmetry, this means, the relative width in double wells.

Sample	$e_1\text{-hh}_1$	$e_1\text{-lh}_1$	$e_2\text{-hh}_2$	$e_2\text{-lh}_2$	$e_3\text{-hh}_3$
SCQWs	(N)1.5328 (E)1.5297	(N)1.5380 (E)1.5341	(N)1.5394	(N)1.5499	(N)1.5948
ACQWs-1	(N)1.5265 (E)1.5273	(N)1.5296 (E)1.5314	(N)1.5368	(N)1.5460	(N)1.5837
ACQWs-2	(N)1.5181 (E)1.5190	(N)1.5206 (E)1.5210	(N)1.5330	(N)1.5394	(N)1.5460

Table 2.1: Direct transitions (\mathbf{X}) calculated for two ACQWs and one SCQW detailed in Section 3.1 and Table 3.1. From up to down shows the numerical (E) and experimental results, the experimental results was obtained from RAS experiments which are performed at 30K.

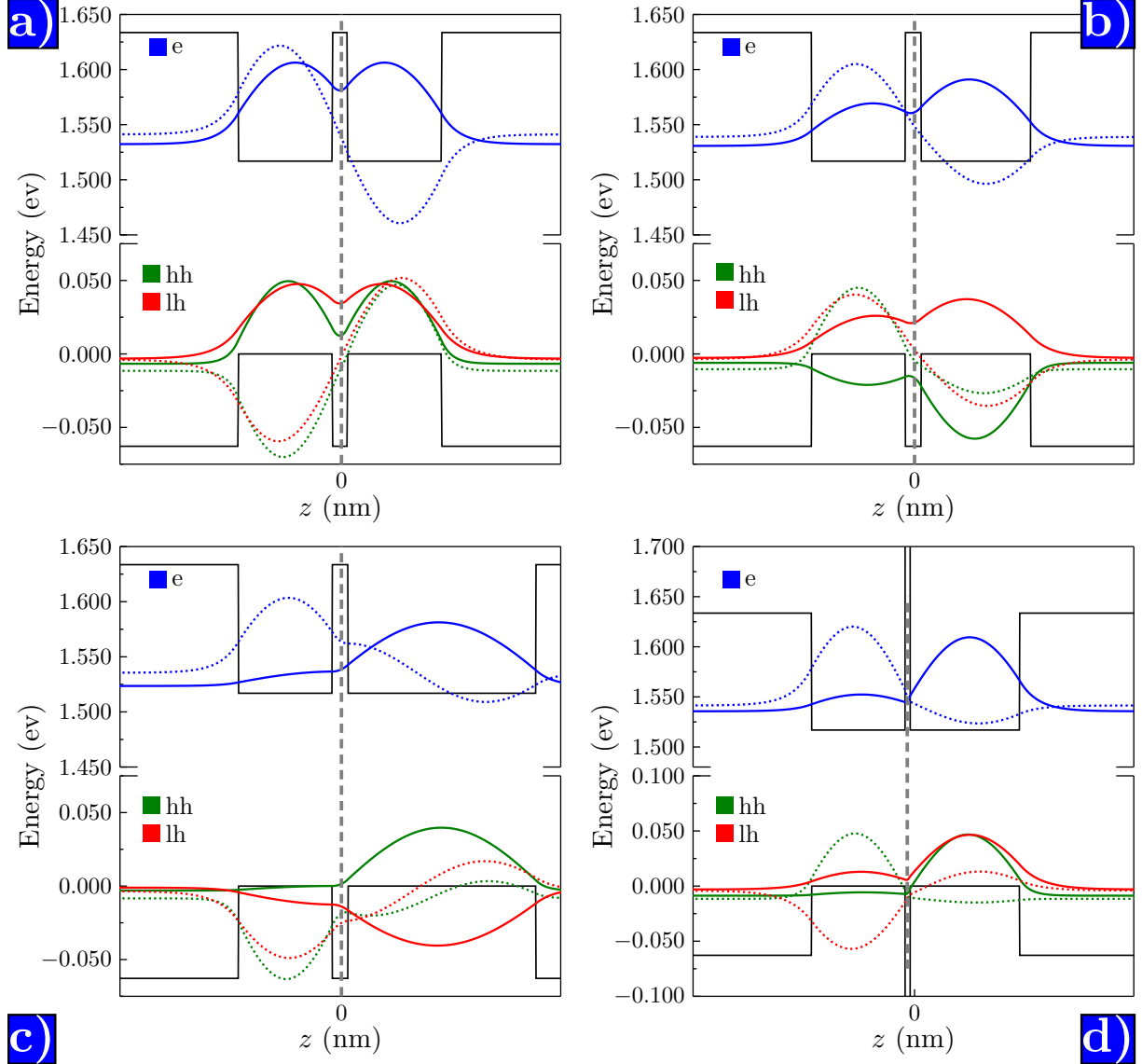


Figure 2.10: From (a) to (d) shcemes the numerical results obtained to solved 1D-Schrödinger equation in both SQWs and ACQWs.

2.5

Anisotropy Model in CQWs

Now, we focus on the central part either, the core of this work. The asymmetry in structure entails a very interesting quantum process in these semiconductor structures. The symmetry reduction is the basis of the model in this work, as explained before, symmetry is the cause of many quantum phenomena its exhibits in solids, and the fact, that symmetry breaking in CQWs increases the optical anisotropy, which among many properties this opens the field of spin properties [92, 124–127].

Generalizing the before discussed in the symmetry section exists several mechanisms to reduce symmetry in QWs structures, principally in the single QWs with external perturbations such as electric or magnetic field, mechanics perturbations as applied strain among others. But, the objective is the same, reduce the symmetry in these structures from T_d which is the symmetry group to cubic crystals to C_{2v} which in turn a subgroup of this. As the result of the symmetry breaking, it originates an OA which was measured through RAS experiments results in a peculiar way, this refers to the spectral results. In our case, it compares the experimental results of RAS experiments (later discussed) about three CQWs structures, in which the difference between these is only the width of one of the wells (as many times mentioned), the RAS spectra increase as the relative width also, this, come back to these structures very interesting. Therefore, it will discuss the Anisotropy Model which includes all of the previous contained and focused on the CQWs. The IOA was borns as of the Quantum-mechanically effect of mixing between holes states,

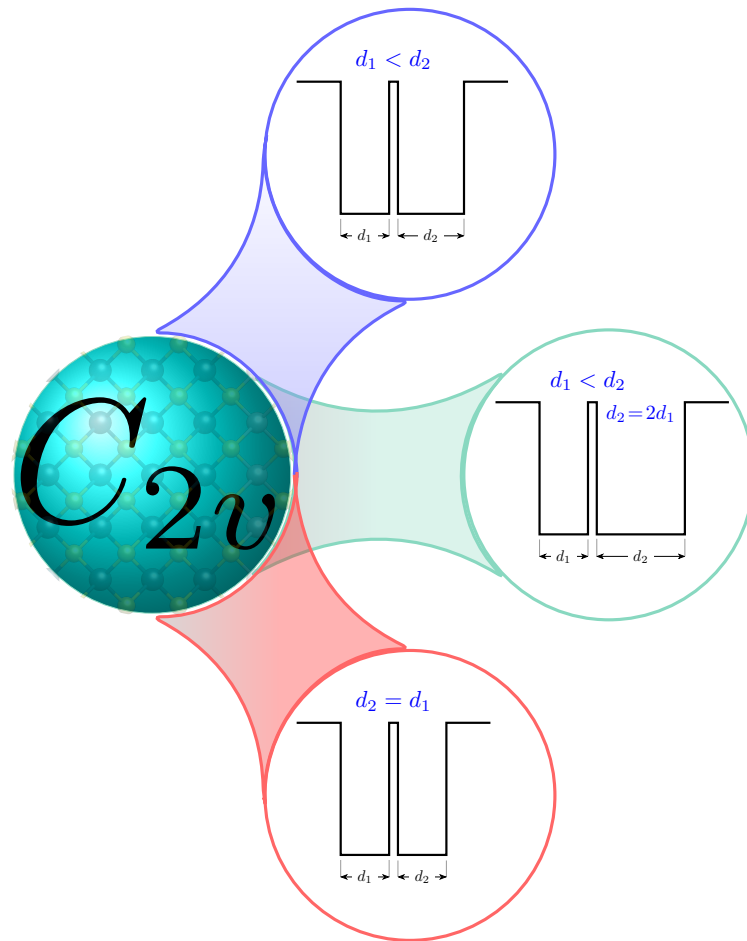


Figure 2.11: Diagram of three principal structures studied in this work, starting with CQWs with the same width (bottom, $d_1 = d_2$), this sample structure is called as SCQWs, the second one the first asymmetric structure (top, $d_1 \sim d_2$), this means that one of the wells is slightly width than the other. Finally the third sample (right middle) it is more asymmetric, which means that one of the wells is double wider than the other.

the theoretical formalism frequently is developed around effective mass but it is important to remember the difficulty of solid physics, now if it adds the physics of the interface this is so crazy. The role of interfaces is crucially in heterostructures in point of fact is the principal cause, then, having a standard model which explains it, is practically impossible. Therefore, the *simplicity method is ever the good choice*.

The EFA usually employs the analytical method to explain the heavy- and light- holes states lack of interface contribution [128]. In the fact, always it desires high-quality interfaces but even though the growth technologies are very precise and powerful this remains a natural atom process. It is important to say that the quality of structures studied it is amazing, even in the SCQWs were expected a non-observable anisotropy due to the conserve of D_{2d} symmetry, experimentally observes a remanent of anisotropy. As it is exposed in the Figure 2.11 the three CQWs structures studied, including the symmetric double wells sample which remarks in red because this is the basis to demonstrate the evolution of anisotropy as increases as the asymmetry in wells also to. If we inside into discussion we increase the uncertainty of who is the best method to explain the IOA increases, on the one hand, the perturbative methods like the $\mathbf{k} \cdot \mathbf{p}$ have a powerful several Hamiltonians while the “atomistic” as TB which advantage is the consideration symmetry intrinsically. Then as mentioned before we employs one method based on EFA, which consider each interface a scalar potential [75, 79, 128, 129]. Then, to deal measure the hole-mixing caused by interface anisotropy it is important that this be sensitive to changes in polarization, by this reason, the models by a QW’s consider a hole-mixing Hamiltonian H' as [79, 128, 130]:

$$H' = \{E_p + [P_0\delta(z - w/2) - P_0\delta(z + w/2)]\} \{\hat{J}_x \hat{J}_y\} \quad (2.10)$$

with

$$\{\hat{J}_x \hat{J}_y\} = \begin{pmatrix} 0 & i & 0 & 0 \\ -i & 0 & 0 & 0 \\ 0 & 0 & 0 & i \\ 0 & 0 & -i & 0 \end{pmatrix}. \quad (2.11)$$

The Equation (2.10) is employs in a SQW [79], here, we denoted E_p as the external perturbations parameter, this parameter usually involves the multiplication of electric field along z direction, D as deformation potential and other as the piezo-electric constant d_{14} . The δ is the “abrupt” interface as a function of position z and well width w and P_0 is the potential parameter, finally considers the angular momentum operators with basis [79]:

$$\left| \frac{3}{2}, \frac{3}{2} \right\rangle, \left| \frac{3}{2}, -\frac{1}{2} \right\rangle, \left| \frac{3}{2}, \frac{1}{2} \right\rangle, \text{ and } \left| \frac{3}{2}, -\frac{3}{2} \right\rangle \quad (2.12)$$

This Hamiltonian is usually implemented to explain the interface anisotropy, of course, does not only limit to SQW, also is implemented to superlattice structures [130], where is considered a summation of interfaces contribution. In our case, this Hamiltonian H' it is not enough to explain the hole mixing which origins the OA, the principal reason is that this H' considers the interface sign \pm refers to BA or AB interfaces, then the total mixing would be canceled by that reason. Also, this last is not necessarily true, remember that this would occur in an ideal interface where is expected a structure with D_{2d} symmetry then the IOA should be zero. Then, the non-abrupt interfaces should be generated a residual IOA [19, 79, 129]. RAS spectra of single QWs have been reported extensively in the literature [12, 16, 18, 19, 79].

The thickness of the QW plays a fundamental role in the amplitude of the RAS signal. For the anisotropies originating at the interfaces and the ones induced by the segregation of Ga or In (in the case of the inclusion of a thin InAs layer), the RAS amplitude decreases when the thickness of the QW increases [79]. Contrary to this behavior, for the IOA induced by strain, the RAS signal increases with the thickness of the QW [18]. In any case, the RAS signal is associated with the mixing between the heavy- and light-hole valence subbands of the QW [75]. In a perturbative approach, the IOA strength is proportional to

$$\frac{\langle \psi_{en} | \psi_{hhn} \rangle \langle \psi_{hhn} | \mathcal{H} | \psi_{lnh} \rangle \langle \psi_{lnh} | \psi_{en} \rangle}{\Delta E_n}, \quad (2.13)$$

where $\langle \psi_{en} | \psi_{hhn} \rangle$ and $\langle \psi_{lnh} | \psi_{en} \rangle$ are the overlap integrals between the $|\psi_{en}\rangle$ electron state in the conduction band and the $|\psi_{hhn}\rangle$ and $|\psi_{lnh}\rangle$ hole states in the valence band respectively. The mixing between heavy- and light-hole subbands is $\langle \psi_{hhn} | \mathcal{H} | \psi_{lnh} \rangle$, \mathcal{H} being the perturbative Hamiltonian. The difference in energy between the hole states before their mixing is $\Delta E_n = E_{hhn} - E_{lnh}$.

As previously mentioned, \mathcal{H} could account for a perturbation by applied uniaxial stresses, electric fields (built-in or external) and abrupt or smooth interfaces. In the case of CQWs system, \mathcal{H} is a measure of the asymmetry of the two QWs. In a CQWs, if both QWs have the same thickness, the electron and hole energy levels are brought into resonance and their probability density is distributed symmetrically at both sides of the barrier that connects both QW, as can be seen in Figure 2.10.

If the AlGaAs/GaAs interfaces of the DQW are equivalent the symmetry of the DQW structure belongs to the D_{2d} crystallographic point group. However, as we mentioned, if the GaAs/AlGaAs interfaces (sources of anisotropies) are non-equivalent, and a residual IOA is induced by the symmetry reduction from D_{2d} to C_{2v} of the whole CQWs structure. In this case the number of symmetry operations is reduced to four: the operations that inverts the z -axis, are excluded, thus leading to a mixing of heavy- and light- holes in the valence band, and hence an IOA. When the thickness of one QW is larger than the other QW (ACQWs), the energy of the electron and hole states of each QW become different and are no longer

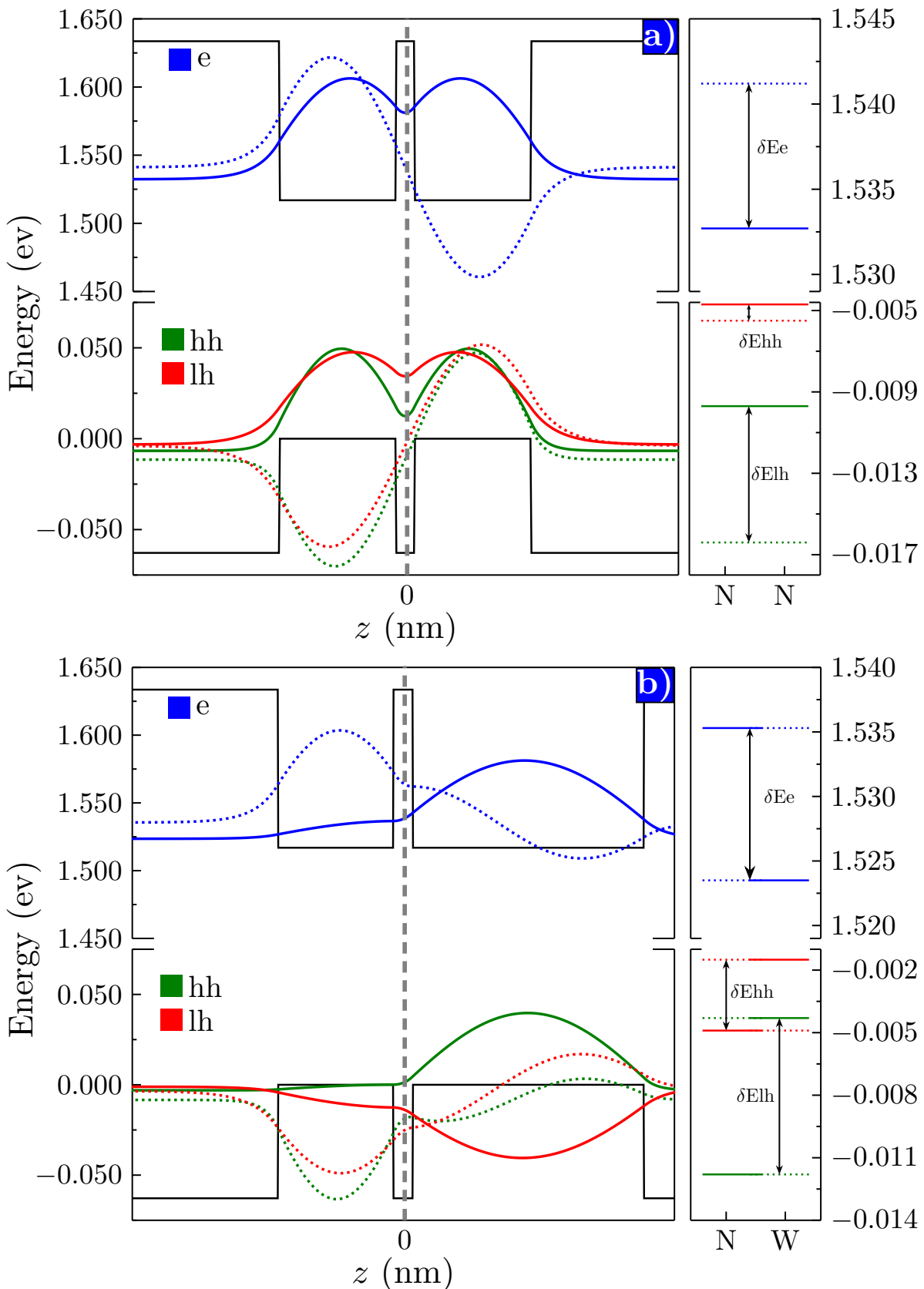


Figure 2.12: Wave functions and confined energies calculated for (a) sample S1 (SCQWs sample) and (b) sample A2(ACQWs sample 2)

in resonance. In this case, the probability density is distributed asymmetrically as can be seen in Figure 2.12(a). Besides of the anisotropic source induced by the GaAs/AlGaAs interfaces as in the symmetric case, for the asymmetric CQWs system another mechanism of IOA should be considered. Suppose that the AlGaAs/GaAs interfaces are equivalent. As we mentioned, in this case a symmetric CQWs system belongs to the D_{2d} symmetry. If the thickness of one QW is modified, the system changes symmetry from D_{2v} to C_{2v} . As can be seen in Figure 2.12(b), the symmetry operations that change the sign of the z -axis (i.e., a reflection on a plane perpendicular to z), are no longer possible because the AlGaAs/GaAs interfaces are located at different distances from the barrier. The number of symmetry operations of the ACQWs structure is reduced to the four operations of the symmetry group C_{2v} [77, 80]. In this case the IOA strength can be modulated by changing the relative thicknesses of the QWs in the CQWs system. This anisotropy is added to the residual IOA produced by the non-equivalence of the interfaces.

2.6

Summary

This chapter explains and discusses the physics required in this thesis, starting from the relation between symmetry and the BS in semiconductors to the importance in understanding its role on the “breaking” symmetry mechanism. We focus on enhancement of the particular symmetry “breaking” in CQWs which occurs naturally: the asymmetric coupled QWs.

3

EXPERIMENTAL DETAILS AND RESULTS

This chapter describes the experimental results and their interpretation by using a model based on the breakdown of T_d symmetry.

Contents

3.1 Samples Description	43
3.2 Spectroscopy: Experimental Setups and Results	46
3.2.1 Photoluminescence Spectroscopy (PL)	48
3.2.2 Photoreflectance spectroscopy (PR)	55
3.2.2.1 Excitonic Effects	61
3.2.2.2 The PR Summary	70
3.2.3 Reflectance Anisotropy Spectroscopy (RAS)	70
3.2.3.1 RAS Strength Discussion and the Physical Model Justification	73
3.2.3.2 The RAS summary	78

3.1 Samples Description

QUANTUM STRUCTURES studied in this work were fabricated by Molecular Beam Epitaxy (MBE) which consists in growing high quality thin films of semiconductor materials on a suitable crystalline substrate with great precision, both thickness and abruptness are readily controlled [131], by means of material evaporation in ultra-high vacuum and refexion of high energy electron diffraction [131, 132].

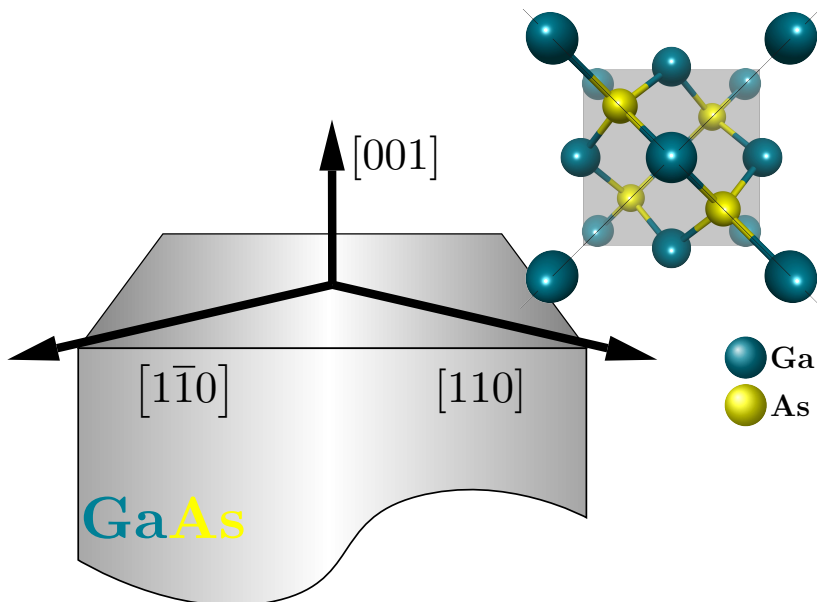


Figure 3.1: GaAs (001) substrate. The inset shows the atomic arrangement on the surface with no reconstruction as viewed at the [001] plane.

The samples studied in this work are made up of a GaAs (001) (Figure 3.1). The samples are based on GaAs and AlAs then these can have different thicknesses, $d_{\text{GaAs}} + d_{\text{AlAs}}$, and doping levels with Si atoms (n-type) and Be atoms (p-type). The result consists in an arrangement of $(\text{GaAs})_2 (\text{AlAs})_2$ superlattice, as a shown in Figure 3.2 or AB arrangement. In QWs structures, the width is the principal characteristic because quantum confinement is dependent on this, then MBE is the perfect choice to accomplish this.

The realistic structures present some details that can modify the experimental results, some of these are inevitability due to the complexity of growth. One of these is the interfaces between two different materials, *i.e.*, the typical structure of $\text{GaAs}/\text{Al}_x\text{Ga}_{1-x}\text{As}$ has an interface between these, then the problem is due to an imperfect mismatch of materials, therefore, they can cause anisotropy effects. Other details which usually are considered are surface, point defects along of structure, or strained caused by over layer in the epitaxial

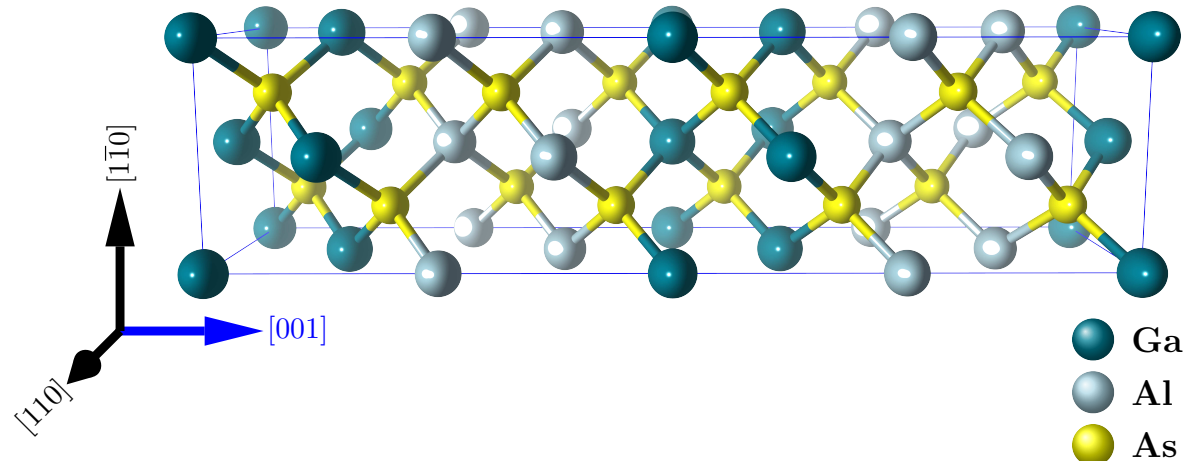


Figure 3.2: Atomic ordering in AlGaAs crystal structure grown along (001) direction.

process. Later, the interfacial detail gives the physical sense to RAS experiments in the symmetric CQWs structures.

Table 3.1 shows the sample's description. Each one has two QWs coupled by a thin barrier preferentially of $\text{Al}_x\text{Ga}_{1-x}\text{As}$ semiconductor, where Al content is important because of the potential barriers depend on this. This was taken into account in the numerical calculations to generate the potential profile. Commonly, for the case, $\text{Al}_x\text{Ga}_{1-x}\text{As}$ barriers x values are in the interval $0.1 < x < 0.4$. It is worth mentioning that the purpose of the first four samples (up to down in table) is that they were grown with the aim to measure indirect excitons (**IX**), and hence the structures are more complex, and that is why we omitted the value of n-doped since these samples are doped in both bottom and top to minimize the intrinsic electric field (screening field effect), so that external perturbation is applied through a voltage over the sample [133] and the n-doped enhance the external perturbation*.

After having carried out experiments over the four first samples and observed seemingly trions (\mathbf{X}^+ or \mathbf{X}^-) through PR spectroscopy, and an apparent increase of the RAS signal, it was decided to focus on experiments on these structures, which have a less complex composition as in the case of the first three samples in the table (see Table 3.1). Therefore, we took the sample M4_3141 as a reference, *i.e.*, same barriers widths both coupling barrier and adjacent barriers, obtained the samples M4_3521, M4_3522 and M4_3523 where sample M4_3522 is the same to sample M4_3521 in structure but with a different type of doping (p-type in M4_3522 and n-type in M4_3521), samples M4_3521 and M4_3522 have the same doping type (n-type in both) but one of the QW is more width to another, this means that the sample M4_3523 have the same thickness in both QWs (SCQWs) and sample M4_3521 have one QW thick more than the another (ACQWs).

*Non-published, the specific information about the doped in these growths, if you have a question about this, you can send email to Dr. Klaus Biermann biermann@pdi-berlin.de

3.1. Samples Description

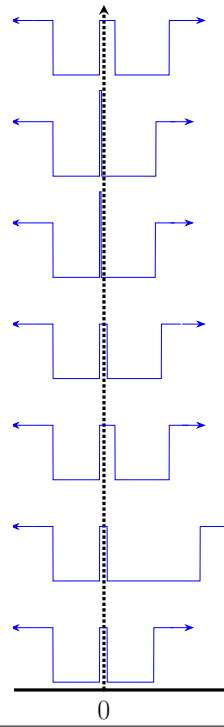
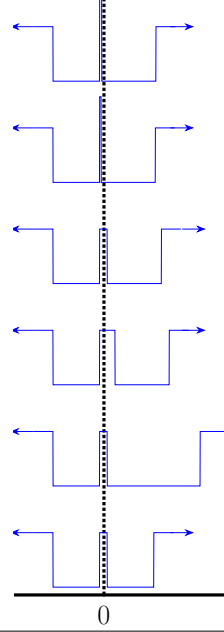
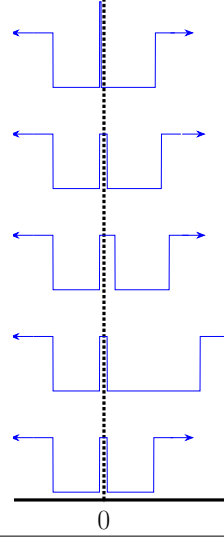
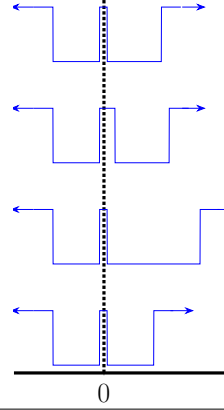
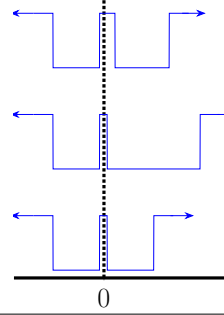
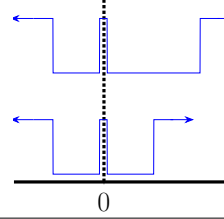
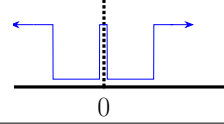
Sample	NW width (nm)	$V(z)$	WW width (nm)	Barrier width (nm)	Barrier	Adjacent barriers	Doped type	(cm $^{-3}$)	
M4_3171	11.87			13.85	3.960	AlGaAs	Al _{0.15} Ga _{0.85} As	n[Si]-i-n[Si]	6×10^{18}
M4_3172	11.87			13.85	0.565	AlAs	Al _{0.30} Ga _{0.70} As	n[Si]-i-n[Si]	6×10^{18}
M4_3226	11.87			13.85	0.424	AlAs	Al _{0.30} Ga _{0.70} As	n[Si]-i-n[Si]	6×10^{18}
M4_3140 (ACQWs-1)	11.87			13.85	1.980	AlGaAs	Al _{0.15} Ga _{0.85} As	i-n[Si]	6×10^{18}
M4_3141	11.87			13.85	3.960	AlGaAs	Al _{0.15} Ga _{0.85} As	i-n[Si]	6×10^{18}
M4_3521 (ACQWs-2)	11.87			23.74	1.980	AlGaAs	Al _{0.15} Ga _{0.85} As	i-n[Si]	6×10^{18}
M4_3522 (ACQWs-3)	11.87			23.74	1.980	AlGaAs	Al _{0.15} Ga _{0.85} As	i-p[Be]	5×10^{16}
M4_3523 (SCQWs)	11.87		11.87	1.980	AlGaAs	Al _{0.15} Ga _{0.85} As	i-n[Si]	6×10^{18}	

Table 3.1: CQWs structures studied in this work. CQWs potential profiles $V(z)$ are shown to observe the different shapes, composition parameters, and dimensions of structures studied. The dashed line determines the symmetric reference in the last samples in which we focused (M4_3141 , M4_3521 , M4_3522 , M4_3523), due to their characteristic results.

The Section 3.2 shows each experimental setup implemented for this investigation with their respective results. Starting with Section 3.2.1 that shows PL spectroscopy, their experimental setup implemented to obtain transitions energies values and compare with numerical results, after, in Section 3.2.2, it is shown the corresponding experimental setup and results of the PR spectroscopy, in order to assess information about the intrinsic electric field and the effects caused by this. Finally, Section 3.2.3 shows the RAS experimental setup and exposes the experiments that were realized to study the anisotropy caused by the asymmetry due to the relative thickness between the CQWs.

3.2

Spectroscopy: Experimental Setups and Results

OPTICAL SPECTROSCOPY is defined as a branch of physics that studies the light-matter interaction, in both linear and non-linear regimens. This is important because the simple definition of interaction covers a vast realm of physical phenomena from classical to quantum electrodynamics [134]. Therefore, optical spectroscopy is an essential tool in experimental solid state physics, as it paves the way to study optical and electronic properties of semiconductors, and their correlation.

The optical process in semiconductors consists of the study of response due to light-matter interaction, basically to the processes that can occur in the solids when photons fall onto it. These processes are basically classified into: absorption, reflectance, emission, and scatter, where all of this depends on electromagnetic spectra range; in our case this range includes from near-infrared to mid-infrared (700nm to 900nm). Although those processes are of the utmost importance, optical spectroscopies that uses in this work involve more interest in absorption and emission, being the latter probed in our experimental setups.

The experiments could not be carried out without the availability of optical detectors. To speak about optical detectors, it is impossible not to mention the photoelectric effect that in general terms is the transfer of energy from photons to electrons when the light spot on a surface [135]. So, this fundamental quantum phenomenon is the basis of detectors in spectroscopy; these detectors are called photodetectors, where these convert the light power (photons incidence over their sense area) into an electric signal, voltage, or current, then this signal we can measure and amplify it. The next sections will mention and discuss the PD implemented in the experimental setup, along with their drawbacks. It is important that the photo-cathode of the photo-detector corresponds to the spectral range of experiments; *i.e*, in our experiments the spectral range of interest is from 700nm to 900nm. The Table 3.2 shows some PD employed in our experiments and their main characteristics [30].

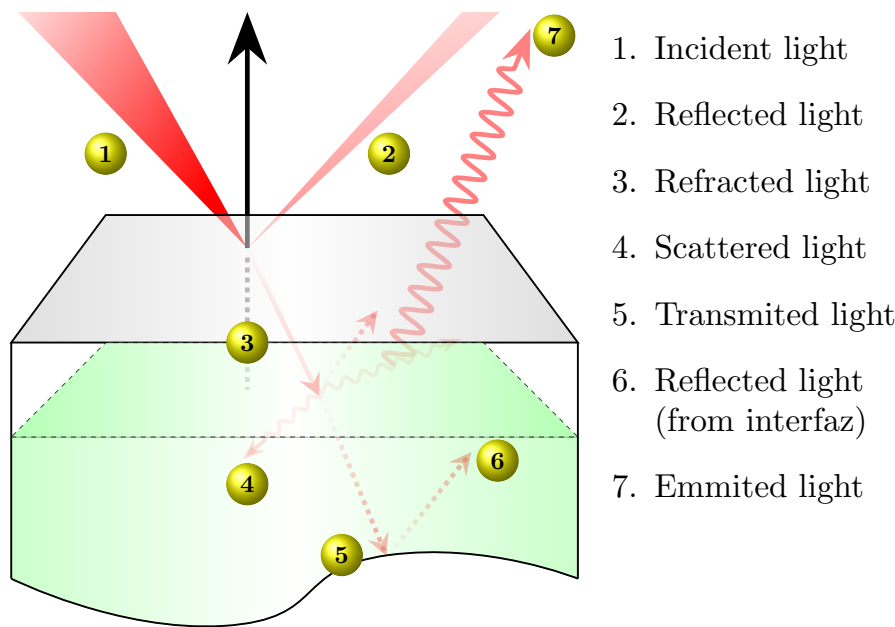


Figure 3.3: Processes that occur inside a solid in the light-matter interaction phenomena.

As a comment, it is important to denote that the CCD devices are being used in many setups in recent years and this is because these devices enlarged the range of experiments that can be realized with these, above all in other areas of physics as in the experimental astrophysics in which has obtained awfully important results. Nowadays, CCD devices in experimental solid-state physics have contributed to getting great experiments that previously were limited due to spatial resolution and time response. In the section 3.2.1, it discusses the advantages and cons of the detectors (PD and CCD) in PL spectroscopy context.

Cathode	Range (nm)	$\phi(\%)$	$\lambda(\text{nm})$	$i_d \text{ nA}$
bialkali (S-22)	300-630	26	400	0.1
multialkali (S-20)	180-800	20	480	0.2
extended red multialkali (S-25)	300-900	7	600	1
GaAs	300-920	15	700	2
Cs-Te	160-320	14	200	0.01

Table 3.2: Photo-cathodes, usually implemented in PD to the spectroscopy of semiconductors [30].

3.2.1 Photoluminescence Spectroscopy (PL)

PHOTOLUMINESCENCE spectroscopy is characterized by be a fast spectroscopy to investigate optical properties (*i.e.* band-gap) and transitions in semiconductor materials, for this reason the work began with PL spectroscopy with aim of searching optical transitions in each CQWs samples and compare with numerical solution of one-dimensional Schrödinger equation (see Table 2.1).

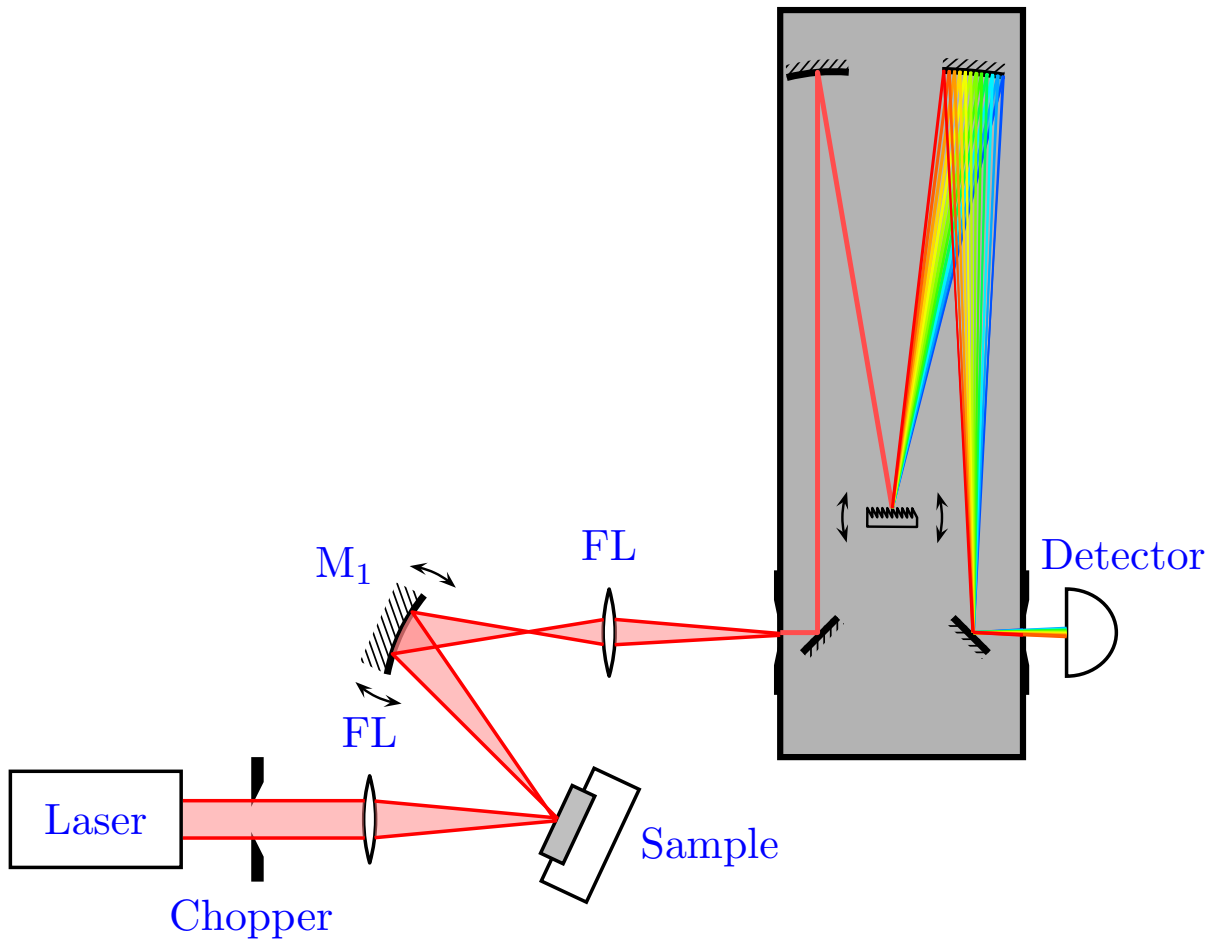


Figure 3.4: Scheme of photoluminescence setup allowing measurements at 14 K, a laser with wavelength of 685nm and a Si detector in tandem were used.

Although PL signal is characterized by be greater than other spectroscopies implemented in this work, the need to use a chopper is only to filter the signal to the external noise, this is achieved used a lock-in amplifier where the reference signal is the chopper and signal input is first measured by a multimeter and then input in the lock-in amplifier. In many other experimental setups the experimental measure are take fast, this is because implement a CCD device as a detector of experimental signals, where these devices are distinguished by fast time of acquisition (apart from other reasons). In our case the time

of measure it does not comparable with those, due the time in our experiments is about 2 hours (explained latter) and those are about several minutes. But why use lock-in amplifier if CCD devices shorter measured time?

Some experiments shown below correspond to Carlos's bachelor thesis [136], who implemented a simple and reliable PL system also he makes a computational code to fit PL spectra using numerical and experimental results (you can check Carlos's codes in our laboratory repository on GitHub*). These results were correlated with previously realized experiments taking into account the same parameters.

The experiments are organized by labels, how shows in Table 3.1, started with the samples M4_3171 , M4_3172 and M4_3226 where these samples were grown with objective the measure trions. The experimental parameters are shown in Table 3.3, in each experiment the optical setup was optimized to enhance the signal measured, the optimization process consisted in measure laser peak at a definite monochromator slits aperture then finely move the mirror until achieving a high response in multimeter, repeat this closing the slits and measuring the FWHM of the laser peak in each step, finally we obtained an optimal resolution about 1 nm in our PL experiments.

Sample	Laser	Range(nm)	λ step (nm)	No. of singnal acquisition	Slits aperature (μm)
M4_3171	680	800-820	0.1	20	75
M4_3172	680	780-840	0.1	15	75
M4_3226	680	800-820	0.1	20	100
M4_3140	680	800-820	0.1	20	100
M4_3141	680	800-820	0.1	20	100
M4_3521	680	800-820	0.1	20	100
M4_3522	680	800-820	0.1	20	100
M4_3523	680	800-820	0.1	20	100

Table 3.3: PL experimental parameters implemented in each sample, all experiments were carried about 14K and was used the same red (680 nm) laser diode. The measured parameters as a Wavelength step or number of acquisitions per step Wavelength were optimized as explains in the text.

An important detail about module laser ThorLabs and very remarkable in the Section 3.2.2 is related to power, the power of this was not stable in some time periods causing a variation in the results, this is the reason to use different experimental parameters and after some test were optimized the choice of the Wavelength step, number of acquisitions per λ step and slits aperture, this depending on each sample.

The PL spectra, corresponding to the samples showing in Figures 3.5(a) and 3.5(b), were more complicated to interpret and in experimental conditions as well. For this reason, we decided to calculate the absorption along of the structure that composes each sample because due to they have more layers. We speculated that this is the reason as to why it

*<https://github.com/NanophotonIICOs>

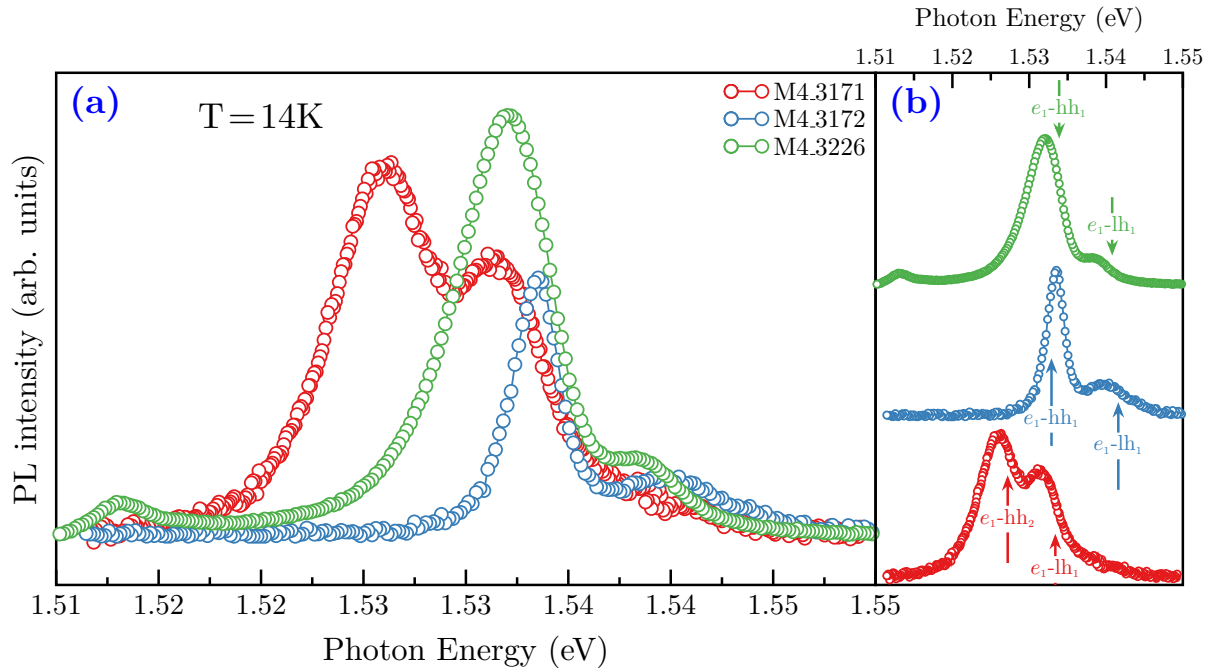


Figure 3.5: (a) shows PL experiments of the samples M4_3171 , M4_3172 and M4_3226 at 14K. Plots in how the comparison between these samples, where clearly can see the relative intensity among in each experiment. In (b) it can be seen each PL spectra with the respective direct transitions, numerically calculated, hh₁ and lh₁ indicates the first energy level that corresponds to heavy- and light-holes respectively.

is complex to realize the experiments and their analysis. As previously spoken, the study of light-matter interaction in solids can be a headache this is because in real experiments more than one interaction mechanism can be observed, especially in PL spectroscopy and, the objective is to measure only one of them, therefore, the experimental results can be affected and complicate their interpretation. The reason for starting with the samples of Figure 3.5 is that they have effects that modify the PL spectra and, although these effects are very interested in our case, they reduce the PL signal.

If started with the scoop, that the PL spectrum in semiconductors is given by an interband emission generated by recombination carriers, and this, in turn, is due to the absorption of photons provided by an excitation laser source. Therefore, the PL signal is due to absorption, it does not matter that they are opposite processes, the absorption, as well as many other mechanisms of light through the solid, can modify and generate the spectrum of PL. The absorption analysis was carried on in the macroscopic approach to light-matter interaction (in Chapter 4, talks about quantum processes and aspects of light-matter interaction in a microscopic environment), therefore, can use classical electrodynamics to study optical properties of semiconductors. One crucial property of semiconductors

is the dielectric function, this is proportional to the complex refractive index (later it is named only as refractive index) and with this, can be described the optical properties of semiconductors. It is important to mention that the refractive index describes how light propagates in a medium, and it expressed as [45, 137]:

$$\tilde{n} = n + i\kappa = \sqrt{\varepsilon(\omega)}, \quad (3.1)$$

where the real part (n) represents the refractive index and the imaginary part (κ) is the extinction coefficient. Even if the objective of this work does not rewrite and reinterpret the physics of these phenomena, we will try to focus on specific equations to reach the goal, which is the absorption model in semiconductors. Then the electric field inside a solid can be written as [137–139]:

$$\mathbf{E} = \mathbf{E}_0 \exp\left(\frac{-\kappa\omega z}{c}\right) \exp\left(-i\omega\left(\frac{nz}{c} - t\right)\right). \quad (3.2)$$

In Equation (3.2), can see the solution of Maxwell equation in a macroscopic picture of the photon-material interactions. This represents a wave propagating with dispersion and staying in terms of refractive index, but the principal idea is to establish a relationship that can help us to describe the absorption in terms of these principal parameters. The absorption is a process that occurs in any spectroscopy and is the absorption coefficient that defines such a feature in each medium. The extinction coefficient κ is the cause of the wave damping when the electromagnetic wave crosses in media, therefore it is related by absorption coefficient. Now in Figure 3.3 can see that there are three principal parts, that they are intensities that are reflected, transmitted, and absorbed. These three parts compose the original incident light through:

$$I_0 = I_R + I_T + I_A. \quad (3.3)$$

Finally, we call upon one of the most notable laws in spectroscopy, this basic expression relates the intensity of light absorbed with the absorption coefficient and is known as Beer-Lambert law [140, 141]:

$$I(z) = I_0 \cdot e^{-\alpha z}, \quad (3.4)$$

then this tell us how intensity decrease as a function of absorption coefficient. As a result of these basic principles in a real structure, we can define de absorption in each layer. After these general and quick basics of the macroscopic basis of light-matter interaction, let's move to a more realistic environment where the calculations are more complex and where it is decided that parameters have major physical priority. The numerical solutions

of absorption along structure were carried out using an exceptional Open-Source code called **SOLCORE** [6]* and our codes. As previously mentioned in a real calculation is frequently taken into account only parameters with major physical sense depending on the situation, arduous computational solutions, or for simplicity. From **SOLCORE**, we have the simplest model to calculate the absorption, despising all reflections at the interfaces having only the absorption as a function of wavelength and depth z expressed as:

$$A_n(\lambda, z) = \alpha_n(\lambda) \exp \left(- \sum_{i=1}^{n-1} \alpha_i(\lambda) d_i - \alpha_n(\lambda) (z - z_n) \right), \quad (3.5)$$

where α_n is the absorption of layer n , d_i is the thickness and z_n the position of beginning of the layer[†].

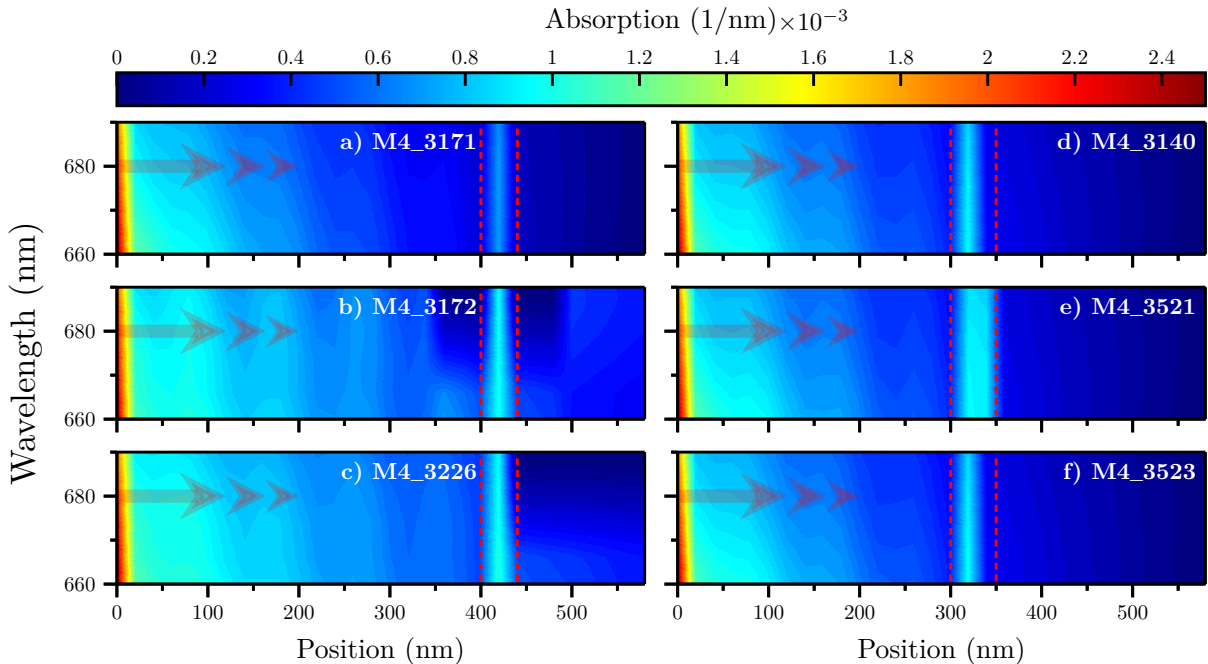


Figure 3.6: Absorption calculated as a function of sample depth. Dashed lines closed the CQWs region, left: Figures 3.6(a) to 3.6(c). Here the samples have $\text{Al}_x\text{Ga}_{1-x}\text{As}$ layers with different compositions $x = 0.15$, $x = 0.2$ and $x = 0.3$; this results in a change of refractive index then also in the absorption. Right: Figures 3.6(d) to 3.6(f) these samples are equal in structure but different on their width of one of the QWs, therefore the absorption manifests strongly homogenous than the first three samples.

The samples with extra layers have characteristics that do not present in samples with fewer layers, one of this is which the fundamental transition around the GaAs gap does not

*You can test and contribute this code, visiting their GitHub repository at <https://github.com/qpv-research-group/solcore5.git>.

[†]In eq. (3.5) originally the thickness is represented how w_i , by confusion issues it was decided to change the notation.

possible to observe in these samples, the amplitude in these samples in comparison with sample M4_3141 for example, is around of twenty times smaller than this, opposite case in samples M4_3140, M4_3421, M4_3523. We take these samples because these are the basis of this work, the complete set of PL experiments corresponds to the work previously mentioned. So, why is the important to get the PL results and calculate absorption? The answers are simple, the importance to get PL spectra to help us to get experimentally energy transitions, which have a very important role in the next experiments and in the basis of our model to explain the increase in anisotropy in the ACQWs. Also, the experimental PL results are the basis to compare that our numerical calculations are consistent with the experiments. Numerical calculations get more complicated in bigger structures, this means, while the structure is conformed with more layers and these layers are thicker, the probability to get a divergence in calculations is great, this is the reason which not all models work. In fact, in our numerical calculations the energy transitions in samples with more layers (M4_3171, M4_3172, M4_3226) we had to be careful at the moment to choice energy binding, the reasons are many and in the PL is complicated to get unique information and even less in structures with high doped, the charge recombination they play us dirty to understand the results.

The case of absorption calculations is a guide to explain the difficulty to carried out PL experiments and put to discussion if doping is a reason to generate or not intrinsic electric field, after all the absorption is part of field solutions.

Figures 3.6(a) to 3.6(c) shows the calculations of absorptions as a function of depth. In these figures indicate that, in a range of 650 nm to 700 nm, the wavelengths are absorbed with major proportion in the first layer; this is due to the structures starts with a GaAs doped(n- or p-type) or undoped layer. Deeper inside these structures, we can also observe a decrease in absorption to short wavelengths, and a notably increased around of the coupled quantum wells.

These calculations make sense in the next section where PR spectroscopy is a powerful tool that can used to measure the optical properties due to the modulation without external perturbation, this means that the modulation depends on the intrinsic properties of the structure. The generalizability of the results is limited by the classical regime, as previously mentioned, it has taken into account the refractive index where the absorption can obtain from the complex part of this, that is the extinction coefficient. The common use of the PL is to determine the band gap and optical transitions in semiconductors, especially in QS as quantum wells, but what happens if consider PL regardless of the penetration depth? In our case it is important does not, due to the structures studied have wide layers before of coupled quantum wells region, this can observe in figure 4 where shows the results of samples: M4_3171, M4_3172, M4_3226, M4_3140, M4_3521, and M4_3523. In the PL experiments carried out here, it was used as a show in Figure 3.4 a red laser diode of $\lambda = 685$ nm, although the laser energy is chosen in respect to energy gap therefore short wavelengths are preferable but how we can see these wavelengths are absorbed in the first

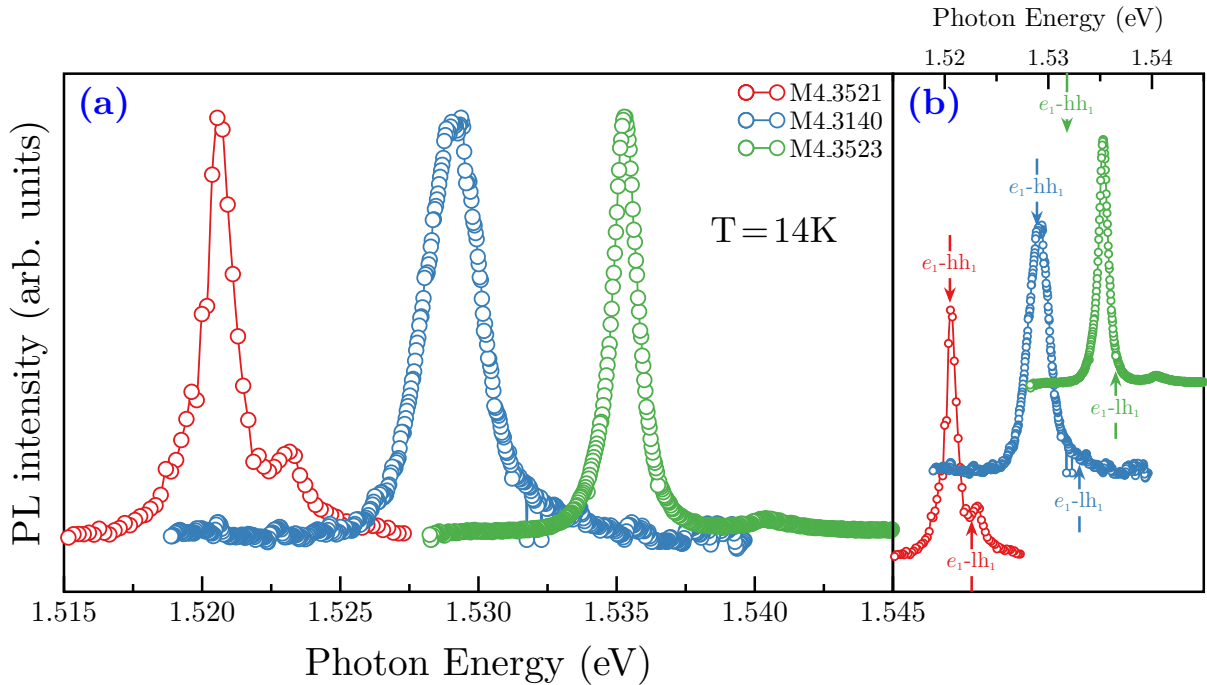


Figure 3.7: (a) Shows the PL spectra of samples M4_3140, M4_3521 and M4_3523, in this comparison is clear the shift between these in respect to first transitions. The relative change in width of one of the QW modifies the energy transitions being the sample 3521 the lowest energy. (b) It is plotted each PL spectra result with the correspondent $e_1\text{-}hh_1$ and $e_1\text{-}lh_1$ transitions energies.

layer due to the samples ends in a GaAs layer, even the laser used is absorbed in large proportion.

Contrary to the samples measured first, the samples M4_3140, M4_3521, and M4_3526 exhibits the most spectral resolution this means that exhibit a more homogenous behavior due to the QWs have quantized energy, therefore, the electron-hole recombination is more probably to measure than the other samples which present width spectrums so that these results may be due to the several internal mechanisms of which can be: impurities, large carrier density due doped, defects, among others [142, 143]. In each of these PL spectra, Figures 3.5 and 3.7 present the most intense peaks associates with heavy- and light-holes exciton transitions denoted by $e_1\text{-}hh_1$ and $e_1\text{-}lh_1$ respectively.

In discussion with the before mentioned, several mechanisms can contribute to getting an inhomogeneous spectrum, even it can say that the two peaks which correspond to exciton transitions are thick and merge this can be related with the high doped level this is because very high dopant concentration causes an overlap of the impurity band with the free-carrier continuum [143]. Table 5 shows the comparison between experimental transitions energies get with PL and the numerical results. It is important to mentioned that the approximation of numerical calculations are closed to experimental, the difference

Transition		M4_3171	M4_3172	M4_3226	M4_3140	M4_3521	M4_3523
e1-hh1	(E)	1.5270	1.5341	1.5329	1.5170	1.5207	1.5354
	(N)	1.5313	1.5342	1.5339	1.5292	1.5196	1.5354
e1-lh1	(E)	1.5318	1.5402	1.5286		1.5234	1.5406
	(N)	1.5370	1.5414	1.5408	1.5335	1.5220	1.5366

Table 3.4: Comparison table between experimental transitions obtained through PL measures and numerical transitions calculated as explained in Section 2.3

is about of 5 meV for the PL case. It is well-known that the PL signal is increased as a function of decrease well widths, as shown.

Table 3.4 shows the comparison between experimental transitions energies get with PL and the numerical results. It is important to mention that the approximation of numerical calculations is closed to experimental, the difference is about 5 meV for the PL case. It is well-known that the PL signal is increased as a function of decrease well widths, this due to the energy of the confined particle state depends on strongly in it and this is demonstrated in Figure 3.7 this due to structures does not have top n-type epitaxial layer these structures are i-n type, staying only barriers structures and PL line shape presents strong confinement [144–146].

3.2.2 Photoreflectance spectroscopy (PR)

POTOREFLECTANCE belongs to the group of modulation spectroscopy, being one of the most important to determine field effects without external perturbations, this means that there is no need for an external source that generates the electric field on the sample. There exists another kind of modulation spectroscopies, where the type of modulation depends on the physical property of interest. These can be phenomena linked with temperature (thermoreflectance), strain (piezoreflectance), electric (electroreflectance), etc. There is a great amount of information that can be retrieved from these techniques. Unlike the PL, the PR is the reflectance measured, as a function of modulation of an external secondary pump beam on the sample studied. eq. (3.1) expresses the refractive index with their real and imaginary part respectively and these are proportional to dielectric function. If the PR is the change in R which is due to modulation of an intrinsic electric field generated by doped layer o layers in the sample (later discuss this mechanism) this mean that:

$$\frac{\Delta R}{R} = \frac{R_{\text{off}} - R_{\text{on}}}{R_{\text{off}}}, \quad (3.6)$$

where R_{off} and R_{on} are the reflectivity when the perturbation (laser) are activated or not are the reflectivity when the perturbation (laser) are activated or not, this mean that the

results falls on perturbation that is the laser.

The PR as modulation spectroscopy is a powerful tool to perform the study of semiconductors, their modulation mechanism occurs when the built-in field is screening by photoexcited carriers created through incident photons, which involves contactless and non-destructive. In many cases, this spectroscopy technique is preferred due to it can measure transitions in heterostructures at room temperature in comparison with the PL or PLE [147] that are measured at low temperature. Therefore, the highlighter characterize of the PR is the modulation of the built-in electric field, in part, this is due to the structure characteristics but in fact, the PR spectra is the change that generated electric field in the dielectric function, this is expected because is the result of measured the changes in reflectivity generated by the laser, in other words, the laser induces an excess of carriers which neutralize intrinsic field. This is well-known to study in the bulk materials, the models show as the reflectivity change is very well approximated by a first-derivative [148–151] but in QWs structures that are dominates by excitonic transitions then the PR line shapes can be understood in terms of modulation of dielectric function appropriate for excitons [147, 152–154].

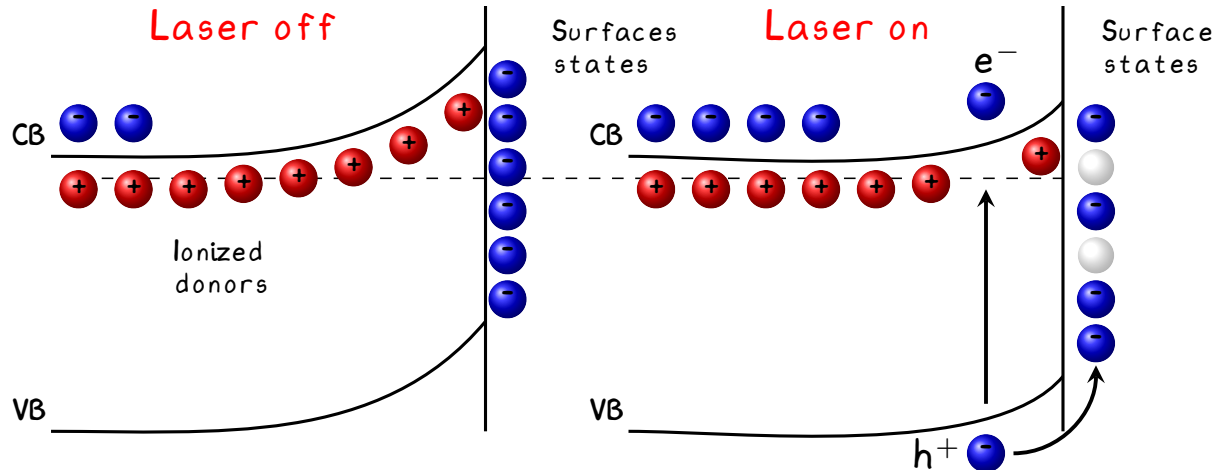


Figure 3.8: Scheme of the PR effect showing the carrier dynamics involved in the mechanism. Right and Left: the corresponding photoinduced changes when the laser is off and on, respectively.

Under the objective of this thesis, we have not focused on doing a traditional study of the line shape with their respective model, the study over PR lineshape is complex, the interpretation starting from changes in dielectric function like a derivative shape and depending on magnitude perturbation, *i.e.*, does not is same the PR analysis on structures with free carriers in solid that the confine particles in QWs structures, the bounded particles are not accelerated by built-in field modulation, so the energy spectrum is discrete and not continuous like free particles. The capability to implement a lineshape fit, renders PR be a great tool. It has been mentioned which the photoreflectance process is due to the built-in electric field modulation, therefore we are considering that the sample was grown considering desired characteristics to generate an intrinsic field, this means that sample

contains n-type doped layers, impurities, unintentional strain mechanisms which generate a space charge region. In the case of an n-type doped layer in a structure, create a space charge region, this region creates the field therefore the conduction and valence bands are bending as a show in the Figure 3.8 and the Fermi energy are pinning at the surface. Photoexcited electron-hole pairs are separated by the built-in field, with the minority carrier (holes in this case) being swept towards the surface.

At the surface, the holes neutralize the trapped charge, reducing the built-in field [150]. That is the general explanation to the PR modulation, before we mentioned that a characteristic of the PR, is to fit as a derivative-like and the order depends on structure, also, we mentioned which in quantum wells the confinement and bound states modify the line shape and the respective fit. So, in this situation, the modulation of field causes the binding energy change of excitons, in other words, this is a Stark effect but in an inverse case because of the field it already exists. The electron-hole pairs depend on binding energy, if that is modified, then the intensity of the transition varies.

The experimental setup to PR experiments implemented in this work, shown in Figure 3.9.

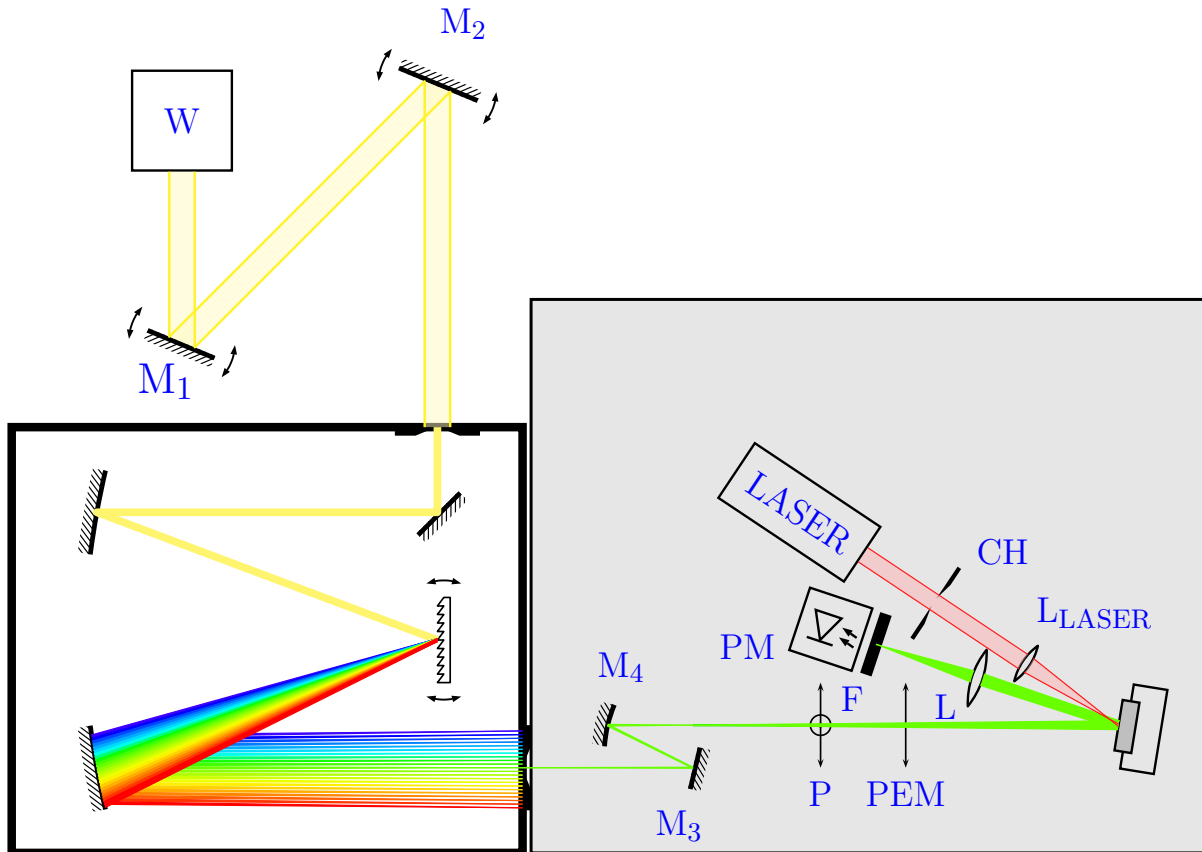


Figure 3.9: Photoreflectance setup used in these experiments, the setup implemented is commonly called dark configuration this due that photo-detector are exposed, then keeping closed to ambient light. W: tungsten lamp, M₁ to M₄ variable mirrors, P: polarizer, PEM: photoelastic modulator, L: focus lens, F: filter, PM: photomultiplier, L_{LASER}: focus lens for laser, CH: mechanical chopper.

The setup start with the probe light from a tungsten lamp, the beam is led by two silver mirrors to monochromator entrance slit, then the monochromatic beam passes through a polarizer and a photoelastic modulator finally affects on sample. The reflected light is focused to the PM with a focus lens. Modulation of the electric field in the sample is caused by photo-excited electron-hole pairs created by the pump source in our case is a red laser that illuminates the same spot of the monochromatic beam and is chopped to a certain frequency, in this setup we use a mechanical chopper at 1KHz. It is important to mention that the reflected light in addition to being focused by a lens, is filtered before inside at PEM, this is important because the reflected laser light by the sample can modify the modulated R signal, do not forget that the PL signal is involved too.

Although the R signal is modulated by the chopper at 1KHz, after is measure by a lock-in amplifier due to the change in the R is very small about of 1×10^{-4} , in comparison with the PL signal, R change is less than PL as one million times. This is the reason by which any modulated spectroscopy commonly uses a lock-in amplifier. In our case, the setup is called Dark [150] setup because the PM is exposed to room light, therefore the system is keep closed. The Dark configuration has some advantages, one of these is, that the R changes are subtracted intrinsically therefore the use of the filter is enough to the dispersion of laser is not a problem. We refer intrinsically to the R signal modulation. If the PL signal achieves to be detected, the system will perform subtraction as shown in Equation (3.6), if the PL signal mixes with the R in both cases this will cancel because it is constant, staying only the change in R.

The result of PR signals associated with band to band and quantum level transitions, in case of samples M4_43171, M4_43172 and M4_43226 the built-in electric field is low due to the structure n-i-n, this in principle is canceled or screen, this mean that the field create by carriers is opposite. The Figure 3.10 shows the result of PR experiments on samples mentioned above and are a bit informative. In fact, GaAs gap is not visible in these samples, many mechanisms can affect the PR results in these. The first one and more representative undoubtedly is the low built-in field, if the structures are n-i-n the field expected is so low although the field can affect the interfaces and contribute but in general this is canceled by opposite photo-carrier directions. Frequently the PR is used tool to calculate or estimate intrinsic fields, this is possible in intermediate-field regimen, this known as Franz-Keldysh oscillations (FKOs) by electric field along z-direction [155]. So, the in PR spectra is observed oscillations and the period is determined by the field in the structure, where typically only about 3-4 FKO can be detected in the space charge region of a doped sample. In this case for these samples and as will be explained later, the PR experiments are complex in context to determine all transitions that occur in them and the field is smaller, therefore does not are candidates to have FKO.

The samples n-i-n type as shown in the Figure 3.10 the FKO does not exist and this is clearly observable because these experiments does not have any oscillations, as before mentioned this behavior may be occurred because the directions of photocarriers generated

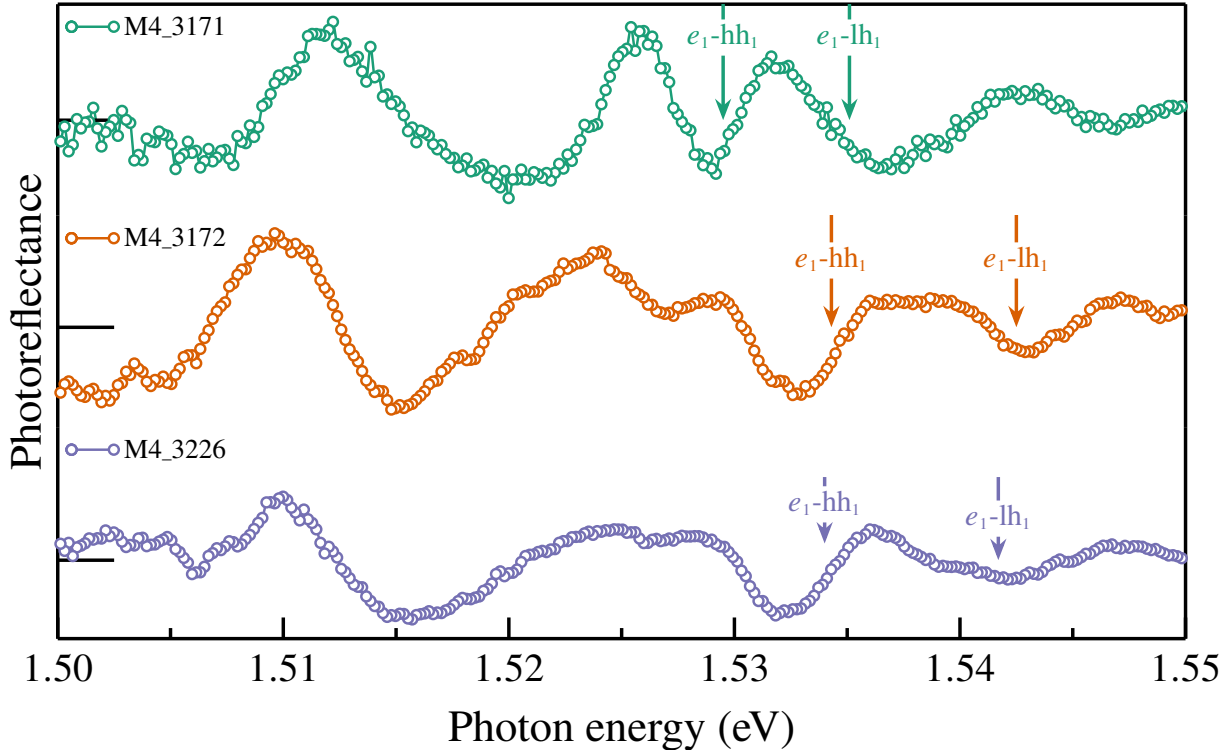


Figure 3.10: PR experiments of samples M4_3171, M4_3172, and M4_3226 at 30K. Arrows point the calculated transitions for each sample. As pump probe a laser with a wavelength similar to the PL experiments was used, with an average power of 5mW. Dashed line indicated the GaAs substrate fundamental transition.

are opposite, then the intrinsic field is canceled. Thus, the PR measured spectra are the result of modulation of intrinsic residual electric field or nonuniform fields effects [156]. In contrast, with the n-i-n type samples, the i-n type samples exposes clearly the direct transitions even associated to transitions with more energy (next levels energies), although the intrinsic field is not enough to generate FKOs.

In the Figure 3.11 can see the direct transitions numerically calculated for samples M4_3140, M4_3141, M4_3521, M4_3522 and M4_3523. The sample M4_3521 was taken as reference in terms of amplitude, in the sample M4_3140 was performed experiments as a function of power laser, being the power 2.5 mW the closest at 5mW, this is one of the reasons for that the result spectra was approx four times smaller than the sample M4_3521. The sample M4_3522 p-type, maybe can be five times smaller than their n-type analogous sample (M4_3521), but the line shape resultant does not have any response, *i.e.*, in terms of amplitude is smaller, but the transitions are not clarified or not resolved. This is one of our keys to final results because it has to do with carrier distribution and the nonexistence of the built-in electric field. For the sample M4_3141 the PR spectra is similar to the sample M4_3140, the difference between these structures is the barrier width, but in spectra the transitions are more resolved in the sample M4_3141.

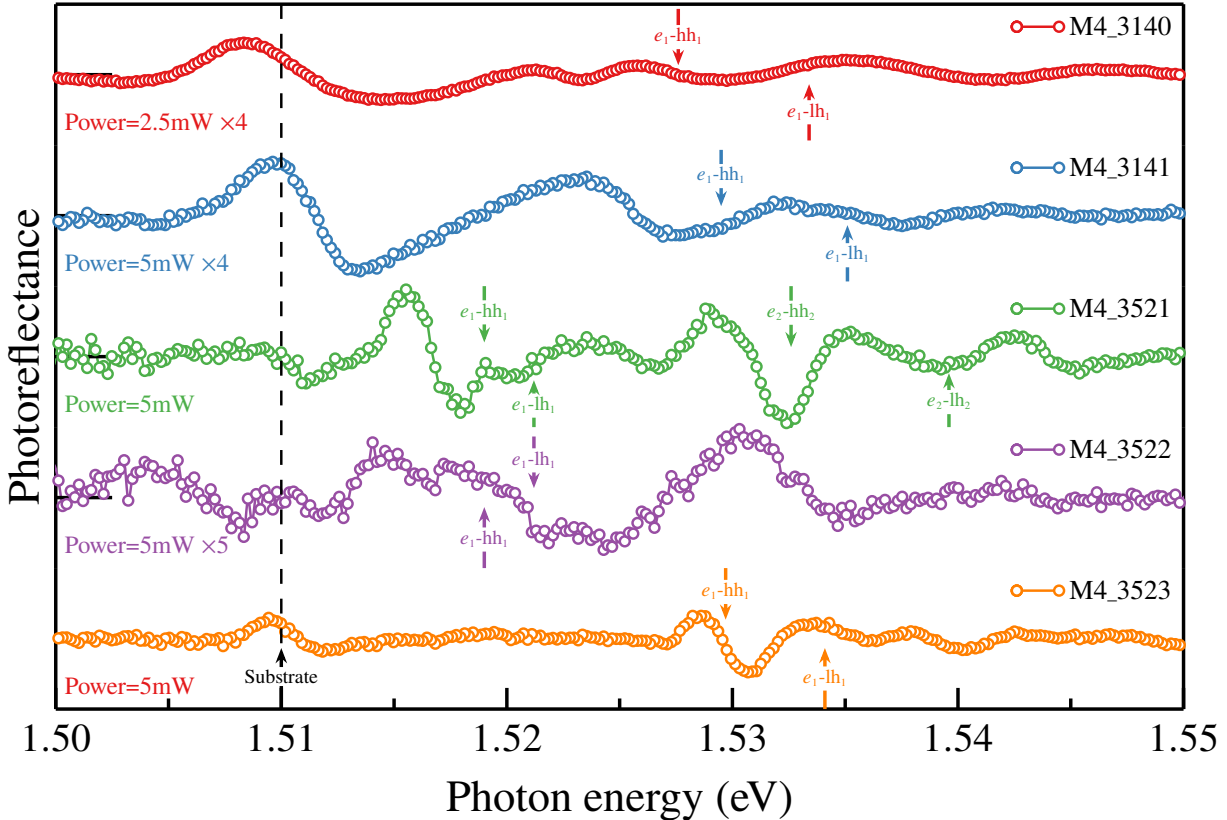


Figure 3.11: PR experiments of samples: M4_3140, M4_3141, M4_3521, M4_3522 and M4_3523 at 30K. Arrows point to calculated transitions for each sample, the used laser wavelength was the same, which in PL experiments and the previous PR experiments. Dashed line indicate the GaAs substrate, in these samples this transition is well located. The PR spectra of sample M4_3522 p-type doped (orange) is five times smaller than their corresponding n-type, the sample M4_3521. The experiments in sample M4_3140 was performed at 2.5mW, then was multiply it by four in according to samples M4_3521 and M4_3523, in case of the sample M4_3141 even if, was performed at a power = 5mW the result was 5 times smaller than sample M4_3521. The discussion concerning this is explained in the text.

From now on, we focus on the samples : M4_3140, M4_3521, M4_3522 and M4_3523, these samples are similar in structure, if shows experiments of the n-i-n type samples and the rest of i-n type samples is only to remark the importance of our results.

Even though in many works about the PR is normal to submit a line shape fit model to clarify the effects of modulated intrinsic fields around of critical points or transitions and as before mentioned this does not the interest of this work. Although, the study and models of line shape for modulated spectroscopy as the PR are essential in the experimental study of semiconductor physics [157, 158]. Nevertheless, in our experiments although the PR mechanism is observable in general around of the Gap (E_0) and direct transitions, the mechanism of modulation over the low intrinsic field, exhibit effects which is not frequently in the PR experiments, as it is shown in the following section.

3.2.2.1 Excitonic Effects

THE CQWs structures are useful to study excitonic effects under external perturbations of an applied electric field. These structures are coupled by the thin barrier, then the electrons overlap over both wells, this behavior is very studied by the confinement effects and possibility to create combines based on electron properties. In this work, we focus on the samples which exhibit exciton effects that commonly are observed under external field apply in our case, without external fields or external perturbations and nor any structure modifies*. Starting with a comparison between ACQWs n- and p-type these are the M4_3521 and M4_3522 samples respectively, Figure 3.12(a) shows the PR of both samples(left), where the p-type sample is approx five times smaller than the n-type sample, therefore we can conclude that the mechanism of photo-carriers generated in these are different even if it has the same CQWs structure.

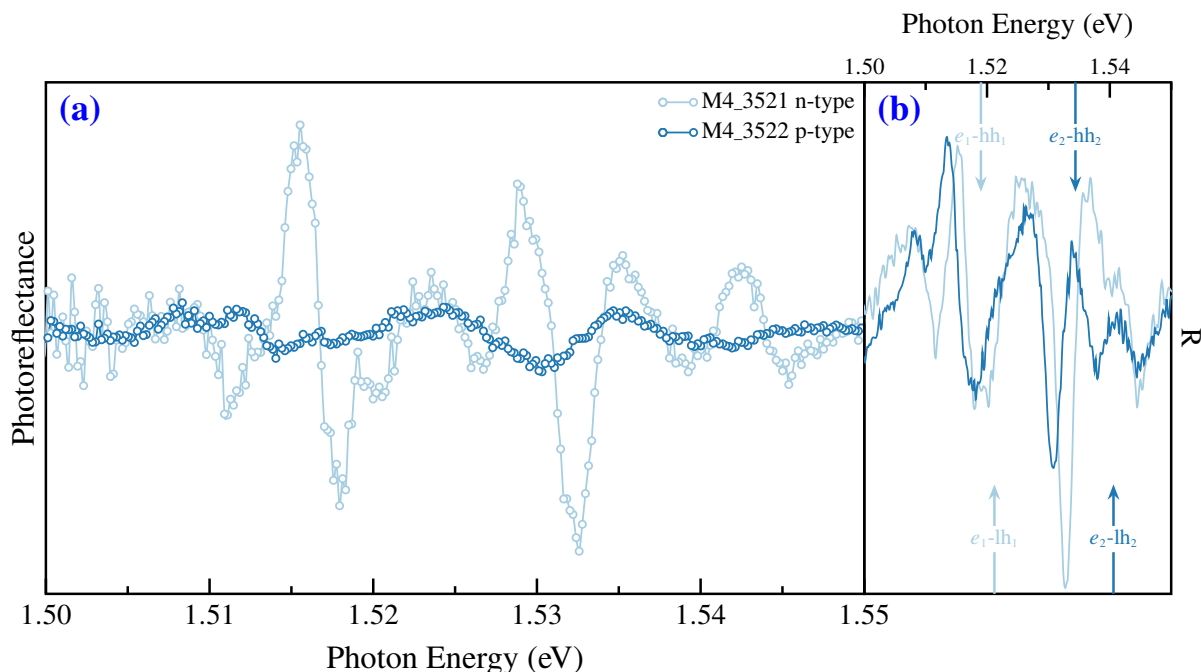


Figure 3.12: Comparison of : (a) PR spectra of the 3521 (n-type) and 3522 (p-type) samples, the p-type sample is 5 times smaller than n-type sample. (b) R spectra obtained at same time in each experiment, the arrows point to each direct transitions for two first confined energies. The line shape is practically the same in both spectra.

Also, the R spectra as shows the Figure 3.12(b) obtained synchronously at each experimental measured, this is the DC signal detected by photomultiplier and reading by the multimeter. These signals are practically the same, according to equation eq. (3.6) the change originated

*This refers to create strain by polish over the samples or mechanisms which generates strain, external perturbations also refers to temperature changes, applied currents, and others.

by the laser source does not enough, *i.e.*, $\Delta R = R_{\text{off}} - R_{\text{on}}$ is smaller. In another way, the comparison of samples M4_3521 (ACQWs-2) and M4_3523 (SCQWs), shown in the figure Figure 3.13 exhibits the difference in amplitude at same power laser but around de E_0 is well resolved in both. In case of the SCQWs sample the direct transitions are well resolved, but in ACQWs-2 sample, could be present forbidden transitions, pointed at Figure 3.13 with same color of its correspond PR spectra. This behavior it has been observed previously [159] in MQWs structures even at 300K [160]. The nomenclature to allowed transitions (direct transitions) is: $e_n\text{-}hh_m$ for electron-heavy hole and $e_n\text{-}lh_m$ for electron-light hole, n index represent the n-th conduction subband and m-th valence subband. So, when $n=m$ its refer to direct transitions or allowed transitions, in ACQWs appear peaks related to transitions between first electron energy where electron wave function is predominantly in the wide well, but this wave function is overlapping to narrow well even if in minor percent, this mean that $n \neq m$ then the heavy- and light-holes confined at narrow well can create $e_1\text{-}hh_2$, $e_1\text{-}lh_2$ transitions, or the electrons in second confined energy that predominantly are at narrow well but, they can penetrate (tunneling) to the another well (wide well) as seen in Figure 3.13 can generate another forbidden transitions. It is important to mentioned that this behavior is presented at low-field regime, therefore can not associate this to modulation of the built-in electric field, this being discussed since some years ago [160, 161], even though can this associated, with the behavior which have the electron, heavy- and light-holes in CQWs structures, with a specific barrier width and the height of the potential barriers (or depth of wells) [26, 162]. The electron and holes tunneling depends on those parameters and, in our case, the barriers potential depends on Al percent in the alloy $\text{Al}_x\text{Ga}_{1-x}\text{As}$, therefore $x = 0.15$ then the barriers they are not so tall, and the coupling barrier width is very thin ($< 2 \text{ nm}$).

These structures, become an interesting platform to study the phenomenology and behavior of confined electrons, heavy- and light-holes, and their respective interactions. Another interesting phenomenon, which we could observe, was the triions (\mathbf{X}^+ or \mathbf{X}^-) formation through the PR experiments. When were carried out the set of PR experiments over the samples i-n type, occurred a peculiar event while we performed and established the correct measure parameters, to be specific while we determined the laser power. This does not mean that our experiments are wrong, as a matter of fact, this peculiar event made us test the experimental setup several times and carried out experiments as a function of laser power. This event started with the M4_3140 (ACQWs-1) sample, this sample has a well with a slightly wide width and because of that the wave function overlapping in major percent than the others samples, by this reason is reasonable or expected, that the triions formation it is more likely as explain later. While they were being carried out, the PR experiments in ACQWs-1 sample, at higher power laser allowed by our device, in fact, this was trouble, because the laser power does not stable, so it was decided to turn on the laser previously before performing each experiment, this was around of eight hours before to start experiments. After detecting the problem with the laser power, it was tarterd

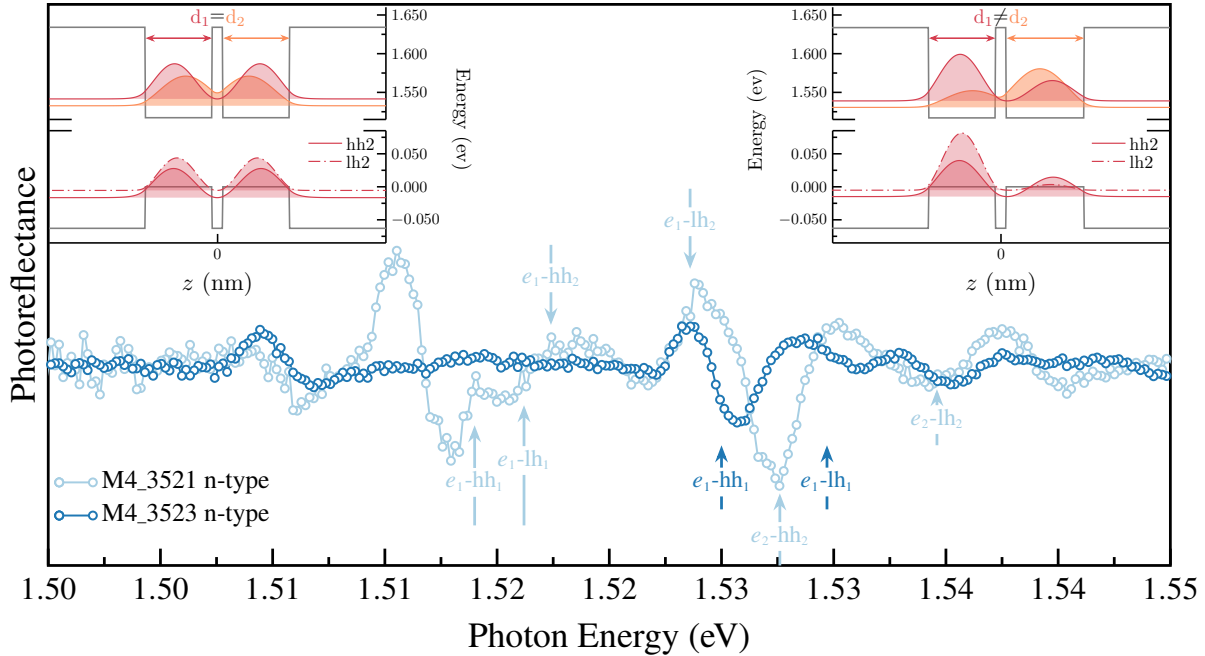


Figure 3.13: The PR comparison between samples M4_3521 (ACQWs-2) and M4_3523 (SCQWs), the electron wave function are plotted for each sample where, the SCQWs sample at top left and at top right to ACQWs sample. The top arrows pointed to forbidden transitions in ASQWs-1 sample, while the bottom arrows pointed to the direct transitions in both samples.

the PR experiments at higher laser power, the results were peculiar due to appearing a higher peak with respect to direct transitions, in fact, the direct transitions did not was observable. These experiments were realized several times and the behavior was kept, then we decided to increase the spectral resolution to try to understand the nature of this peak, previously all experiments were carried out with the monochromator slits at 1500μ this to enhance the light collected by PM. The Figure 3.14 shows the evolution of these experiments at $P=50\text{mW}$ as a function of the slits aperture, it is clearly that does not about of experimental contraption or another external thing which can contribute or being the cause of this behavior.

From these results it decided all experiments with these apertures of slits, although we try to enhance the spectra resolutions at $750\mu\text{m}$ was they got the best results. In the Figure 3.15 shows the evolution of the PR spectra as a function of laser power, starting with 1mW of power and finished with 50mW . Remember previously mentioned that the laser power is unstable and this trouble it did not allow performing the experiments increases power in one way more uniform, this is the reason that the experiments were carried out with powers at 1mW , 3mW , 8mW , 30mW , and 50mW . The spectra with power less than 8mW are relatively similar, therefore, after that power it can see a change in peak width and that peak tends to shift at less energy.

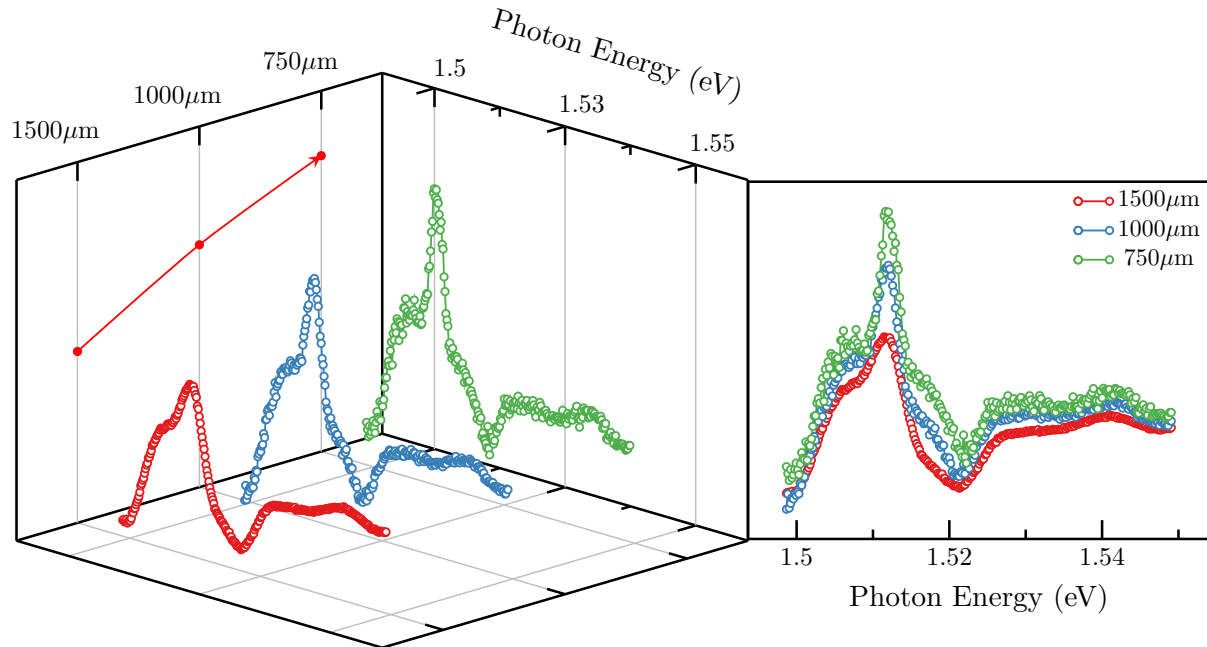


Figure 3.14: PR spectra of the ACQWs-1 sample designed as a function of slits aperture, where it can see the increase of peak resolution as decrease the aperture of slits.

Now, we establish the physical background of that rare behavior in the PR experiments. In semiconductors, the electron-hole pairs are the reason for many special phenomena and are commonly called the hydrogen atoms in semiconductors. But to understand the nature of excitons and their consequent behaviors, it needs to start with a specific platform to keep or extend their life and interactions. As above-mentioned, the life of the excitons in QWs is extended for several reasons, of which; well width and low temperatures enhance the binding energy [163, 164]. When the light interacts with these structures, the electron-hole pair associated with the absorption of a photon with enough energy results in an exciton (general explanation), but if inside the structure the electron density is great [165], the excitons and all possible interactions which can occur as exciton-exciton, exciton-hole (X^-), exciton-electron (X^+), electron-electron, even, LO-phonon-exciton interaction. All of this presents in a modification of the line shape resultant, in terms of the PL experiments it is possible to observe unexpected transitions as a slight modification in the line shape. In spite of the physics involved in this mechanism is very complex, the hard work in this theme has generated valuable results.

Since the 50s Lampert [166] suggested the existence of charged excitons also called *trions* in semiconductors and after almost 40 years it is proved experimentally [165, 167], and as expected the trions X^+ or X^- they were observed in QWs. The electron concentration has a role important in trion formation, for this reason, they usually modulated n- or p-type doping in the QWs structures. Also, the external perturbations as the electric* or

*In this case the trions formation is due a relative position of the Fermi level when the low electric

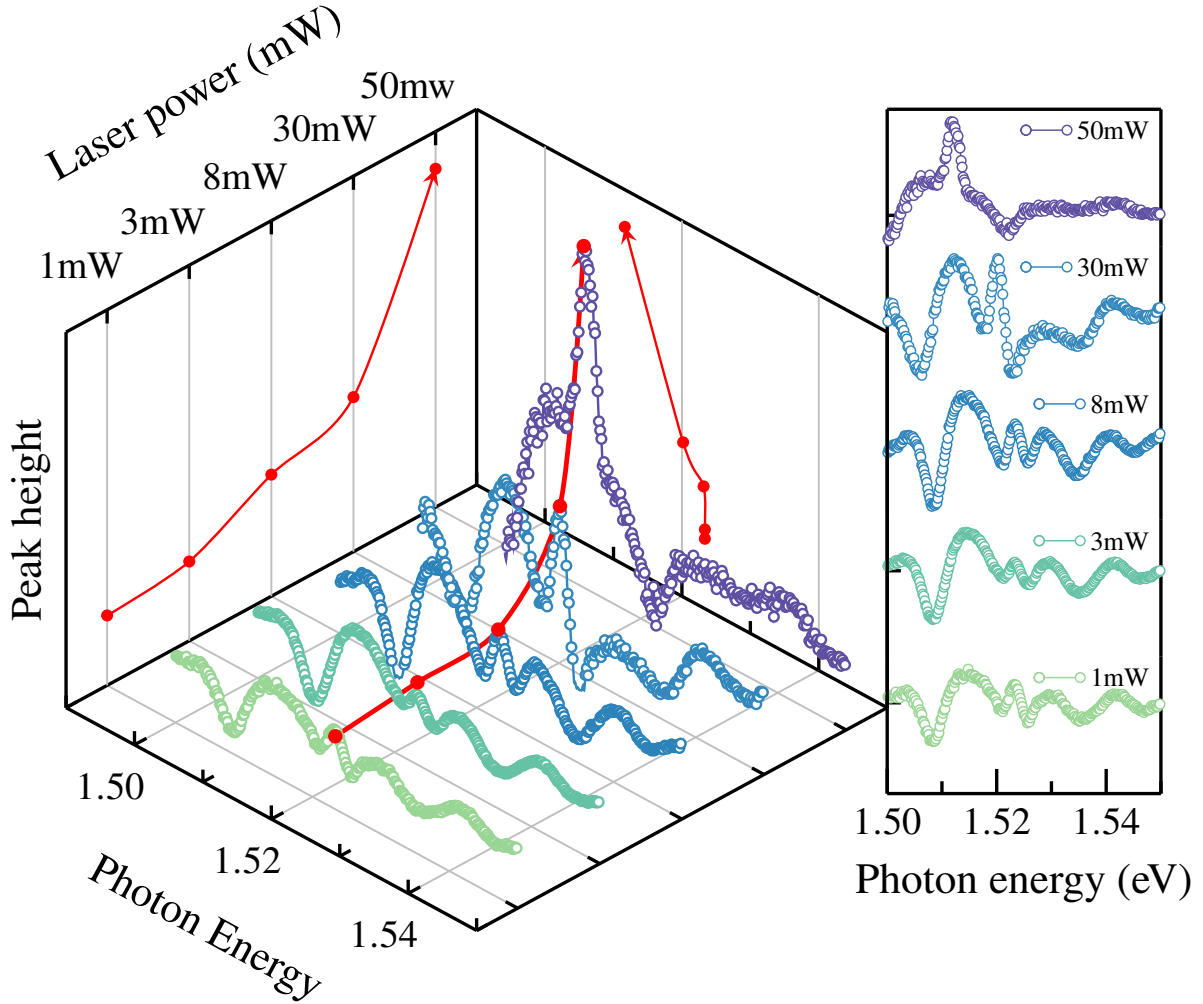


Figure 3.15: The peak tends to height as increase the laser power, which also is very observable as a redshift.

magnetic fields commonly used to enhance the trions transitions, in the magnetic field case, the trions involved acquiring a triplet state nature, so the Zemman splitting is expected, therefore the transitions are well resolved. At zero field, the ground state of trion is a singlet [168], this is, two electrons with opposite spin, these electrons are bound with a hole as shows the scheme in Figure 3.16(a).

In our case, the trions formation is due to photo-excited carriers induced by the laser source, if we suppose that the doped layer is the absolute answer of this, the other samples as SCQWS-1 and ACQWS-2 would have similar results in their PR spectra when it increases laser power, but this is not observed, in fact, in these cases the line shape kept but noisily,

field is applied, in fact, the mechanism involves indirect transitions and is easy that the indirect exciton interact with electrons or holes [133].

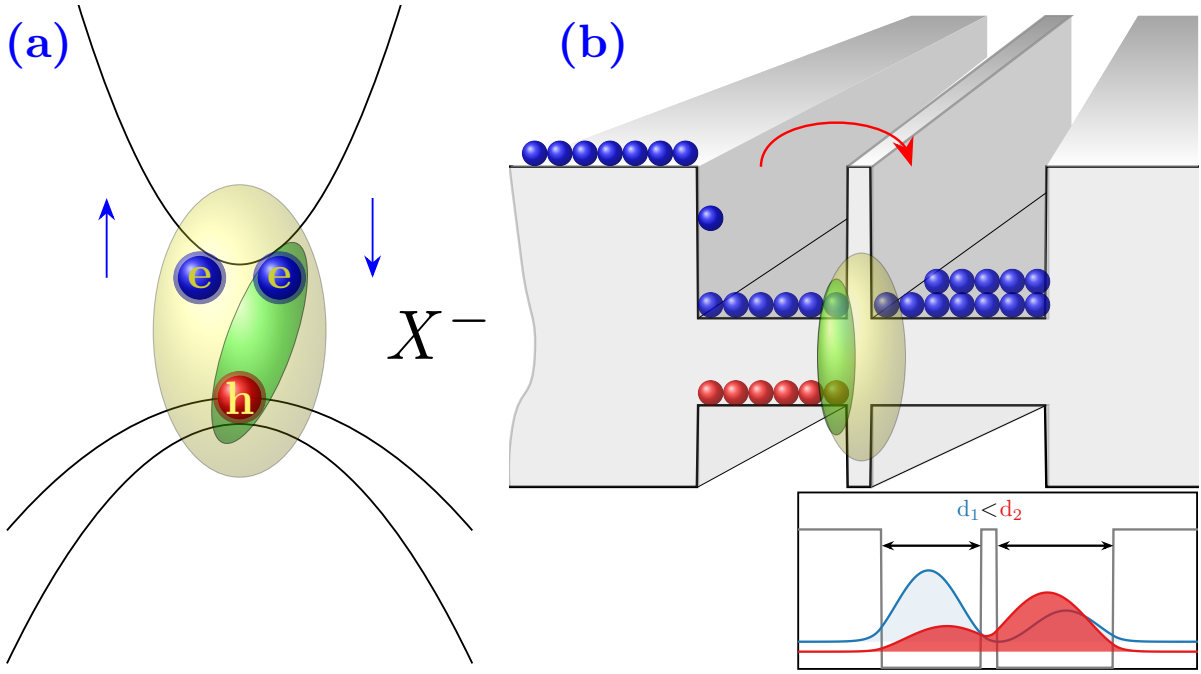


Figure 3.16: Trions formation scheme in terms of band structure (a) in this case, the exciton is bound to an electron in the conduction band leading to a three-body system knew as negative trion \mathbf{X}^- . On the other hand, in (b) it presents the possible formation of \mathbf{X}^- due to a slight width of one in the CQWS, consequently, the narrow well transfers electrons through tunneling to a wide well, if it is calculated the wave functions of this structure, the wave functions have the characteristic of to be distributed asymmetrically as in the case of the applied electric field along z [26, 27].

then if we adjudicate the trion formation to photo-excited carriers, which is the cause that enables trions in the ACQWs-2 sample?. The answer is a hypothesis that needs extra experiments but is part of the future objectives of this work. The electron and holes (hh, lh) wave functions in samples slightly asymmetric in wells widths, *i.e.*, one of the wells is slightly width than the other, these wave functions have similar behavior as the case when de electric filed is applied. This behavior enhances the electron tunneling from the narrow well to the other well (wide well) as shows in Figure 3.16(b), if all-important samples contain the doped layer with the same n-type concentration if we suppose that this layer modifies the Fermi level thus generating a small electron gas (2DEG), its possible think that this electron gas has a function of electron reservoir [169, 170]. Then the photo-carriers generates by the laser source step up carriers dynamics, doing that the narrow well is yielding continuously electrons to wide well through tunneling and, these electrons are recombining with the excitons confined in the plane of the narrow well, therefore results in a three-body system $\mathbf{X}^- = (e, e, h)$ or $\mathbf{X}^+ = (e, h, h)$. As it is known, the trion is a charged exciton where the sign depends on its formation, in the case of $\mathbf{X}^- = (e, e, h)$ their transition is under the first transition of X_{hh} , and their energy evolution tends to redshift as can see in Figure 3.15. Therefore in our case, which was

also has been reported [165, 169–172], the shift evolution correspond to an \mathbf{X}^- trion, however still missing more experiments to strengthen this hypothesis. On the other hand, what happens if the 2DEG does not consider? It is very important to emphasize this argument because the objective of this work is to demonstrate that CQWS structures especially ACQWs shows effects of symmetry breaking does not see in structures without external perturbation(application of: electric or magnetic field, strain, etc.) or intentional modification (growing of interfaces that unbalance the QWs region, differences in the potential of the barriers), by this reason is importantly empathized that regardless of exist a 2DEG whichever is their electron density and the built-in electric field which can this generate, as a matter of fact, that field does not represent the cause of the phenomena presented in this work, more later this is discussed with more detail. On the other hand, is relatively easy to corroborate that the presence of the electric field on those samples can be regarded as despise, what is the reason to asseverate this if the PR has a principal characteristic the built-in field modulation? As before mentioned the non-existence of the FKOs is a point to assert the field regime is low, moreover, in comparison with the n-i-n-type samples, also remain in this regime notwithstanding of be designed to reduce the built-in field. However, it is can be estimated by means of Schrödinger-Poisson, so as to, the equation Equation (2.5) it is coupled Poisson equation [24, 173]

$$\left(\frac{d}{dz} \varepsilon(z) \frac{d}{dz} \right) V_p(z) = \rho(z) \quad (3.7)$$

$$\left(\frac{d}{dz} \varepsilon(z) \frac{d}{dz} \right) V_p(z) = e \left[n_D(z) - \sum_i n_i^s |\psi_i(z)|^2 \right] \quad (3.8)$$

With the objective of present the behavior and the causes of the high doping in the $\text{Al}_x\text{Ga}_{1-x}\text{As}$ layer, we implement a simple code, starting off our numerical codes and helping us with already implemented codes as Aestimo [7], we calculated numerically Schrödinger-Poisson equation. It is important to mention which solution is self-consistent, therefore the code is implemented with all parameters to divergence avoid, in our case is due to high doping and this is too large.

For this reason, it is inevitable that the codes do not converge, although it can be considered a factor damping to speed convergence [174]. We consider the damping factor, and we decided to calculate a structure as GaAs/n-type doped $\text{Al}_x\text{Ga}_{1-x}\text{As}/\text{Al}_x\text{Ga}_{1-x}\text{As}$, where the width of lateral layers is fixed and the width of the doped layer varies from 15nm to 300 nm with the same n-type doped $6 \times 10^{18} \text{ cm}^{-3}$. In general, the self-consistent Schrödinger-Poisson equation, is a process that starts with the calculation of the confined energies in the potential profile defined as $V(z)$, in this profile are included each parameter of the material that makes up the heterojunction as the doping quantity in each layer if this is doped. After, as shown in Equation (3.8), is evaluating the space charge with their respective charged donors and their concentration n_D , n_i^s is the electron sheet density of the confined levels and corresponding wavefunctions $\psi_i(z)$. To calculates the electron density in each level i frequently is applied Fermi-Dirac statistics [47, 175, 176].

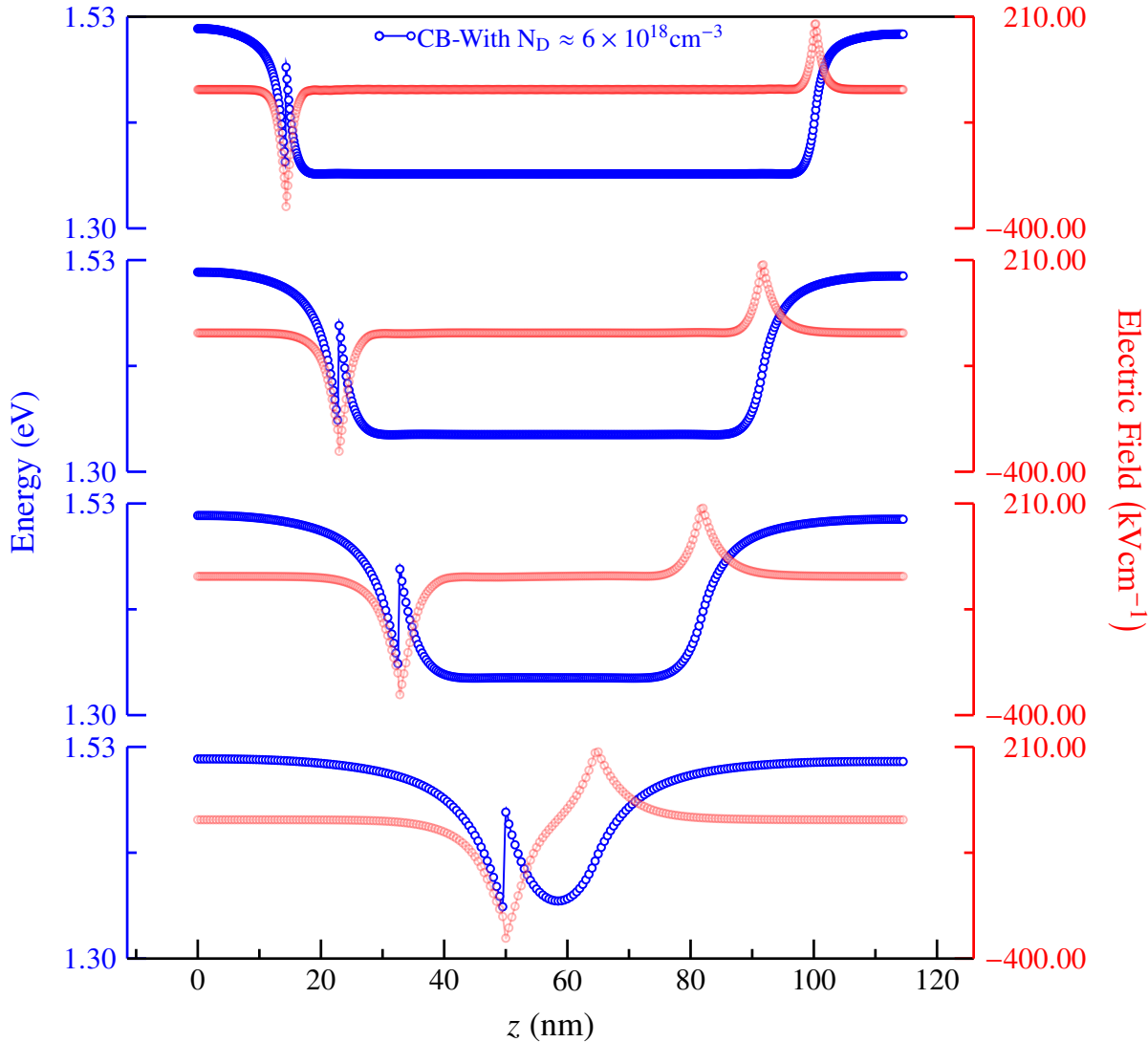


Figure 3.17: Results to self-consistently Schrödinger-Poisson equation, in order with down to top the n-type layer $\text{Al}_{0.15}\text{Ga}_{0.85}\text{As}$ doped ($6 \times 10^{18} \text{ cm}^{-3}$) is increasing in width from 15nm, 75nm, 150nm to 300nm. The goal of this is to calculate in a general way the effects of the doped layer, specifically due to the electric field induced by this. The strength of the field is expressed in kV/cm units, although this magnitude is great, we assume that does not significantly, latter we explained this.

This charge distribution in the structure gives rise to space charge effects, resulting in an additional electrostatic potential V_p which causes conduction band bending [173, 177]. The total potential V is the result of $V = V_0 + V_p$, where the V_0 is the original potential profile, so, this is the iterative part of calculations, in our case, we established the difference between $e_{1\text{new}} - e_{1\text{old}} < 1 \times 10^{-5}$ as convergence factor. Previously mentioned the damping factor is defined for fast convergence, in our case α_{damp} is about 1×10^{-3} . The results are shown in Figure 3.17 to a structure : $\text{GaAs}/\text{Al}_{0.15}\text{Ga}_{0.85}\text{As}(\text{n-type } 6 \times 10^{18} \text{ cm}^{-3})/\text{Al}_{0.15}\text{Ga}_{0.85}\text{As}$ with four different widths (15nm, 75nm, 150nm, and 300nm) for the layer doped.

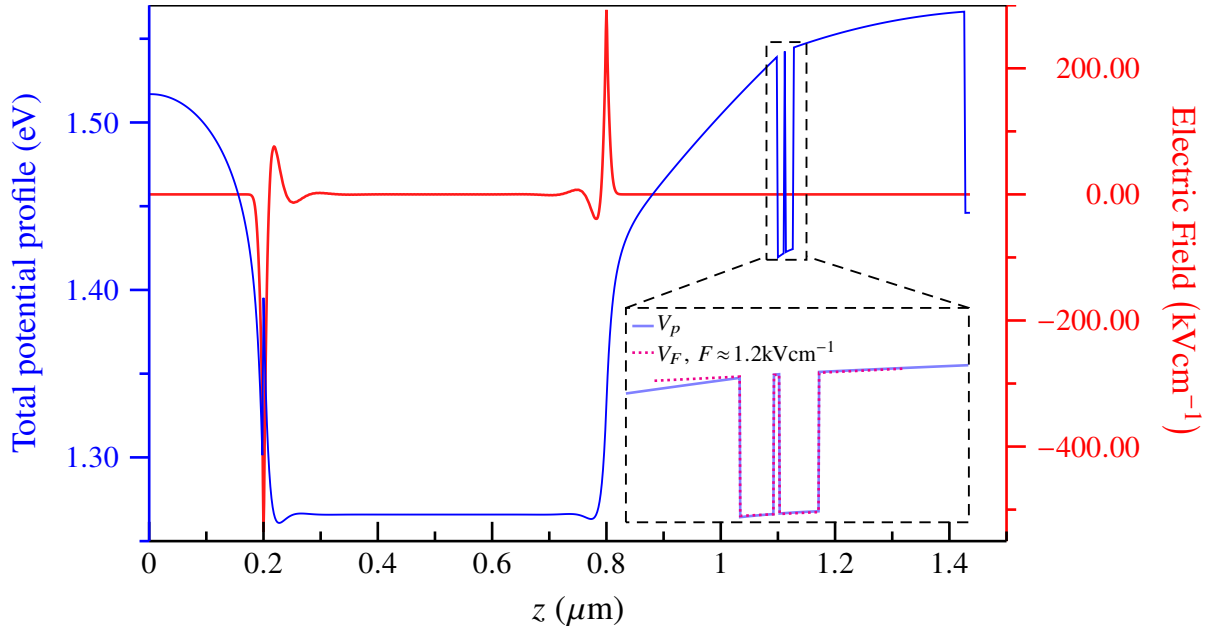


Figure 3.18: Band conduction profile $V(z)$ calculated by numerical solution of self-consistent Schrödinger-Poisson equation. The calculations were performed considering the width of the doped n-type 6×10^{18} layer with 600nm. The zoom inset shows the comparison between total potential calculated (blue) and when applied field $F \approx 1.2\text{kVcm}^{-1}$ (dotted magenta), where at around of CQWs zone are similar.

In the next chapter, we expose the RAS experiments and their significance in the wonderful results of this work, following, is important to define and explain the role of the doping layer that as can see may be generated a significant intrinsic field which in contrast with the RAS results and our model the built-in electric field does not significantly important in the symmetry breaking ($D_2 \rightarrow C_{2v}$). Therefore, we calculate the possible conduction band bending due to the built-in electric field as can see in Figure 3.18. We have taken into account a total structure width with an n-type doped layer, we remember that the high doping and large width can cause the calculations does not converge by this we implemented a damping factor to accelerate the convergence, also we calculated a potential profile considering an external electric field applied around of $F \approx 1.2\text{kVcm}^{-1}$.

The results show that practically the total V_p and electric field (line-shape and magnitude) are kept as shown in Figure 3.17, if we compare the potential profiles V_p and V_F as see in Figure 3.18, it can observe that practically the band bending which is generated by electric field so much as by doped layer, as an external field applied are very similar if the external potential is around of $F \approx 1.2\text{kVcm}^{-1}$. This means that, if exists an electric field but is comparable with surface field [178], hence is a small field. Therefore, we can say that the effects of the trions are associated with the asymmetry of the QWs as before mentioned.

3.2.2.2 The PR Summary

In conclusion, the PR remains a powerful tool for experimental solid-state physics, especially in semiconductors study the facility to implement it, and the great information which gives as about fundamental transitions that in comparison with other spectroscopy is still better. Along with the experimental work, we could notice that the PR has the capability of detect behaviors which does not common in this spectroscopy as trions measured, and although this work is still in progress, the satisfaction to propound a novel source to study of an excitonic behavior as the trions, through easy spectroscopy without external perturbations. On the other side, the ACQWs has a large potential to study quantum phenomena, especially the interactions and process due to the exciton confined, in this case, something so simple as the relative widths in the CQWs generates a surprising behavior.

3.2.3 Reflectance Anisotropy Spectroscopy (RAS)

THE RAS is the experimental tool that completes the set in this work, without the intention of replicates the physical background and interpretations about RAS, we focus on specific terms to detail our great results. This spectroscopy, is a powerful tool in the studying of semiconductors physics, being characterized as default anisotropy study tool. This experimental technique, was developed by Aspnes [149, 179, 180] to measure *surface-induced* optical anisotropy in cubic semiconductors, although this can be applied around of near-band-edge [181]. So, to our purposes, RAS is an excellent experimental tool to study optical anisotropies in CQWs structures. In our case both RAS and PR setup is the same with their exceptions, in the PR case is necessary to add the laser to modulated spectroscopy while in the RAS the modulation it is realized by the PEM, which changes the polarization state. As schemes in Figure 3.19, the monochromatic light first times trough over polarizer prism and the PEM to finally being focused onto the sample with spot size of 5.00mm diameter. The light reflected by the sample is collected and detected by the multialkali photomultiplier tube (before discussed in Section 3.1 and shows in Table 3.2). A detailed description of the RAS technique can be found elsewhere [182]. As shows in Figure 3.19, the RAS signal is proportional to:

$$\frac{\Delta R}{R} = 2 \frac{R_{[110]} - R_{[1\bar{1}0]}}{R_{[110]} + R_{[1\bar{1}0]}} \quad (3.9)$$

where denotes the orientations $[110]$ and $[1\bar{1}0]$ over crystalline directions(see Figure 3.1). In our experiments the RAS signal is around of 10^{-4} . As well's known if the RAS signal it is detected, the structure exhibits an optical anisotropy for in-plane light propagation [12]. The experiments, as the PR case, were it performed at 30K.

In accordance with Chapter 2, the anisotropy into these structures entails into interesting physical phenomena, overall about of optical properties. This IOA it is due to the hole mixing, as a long as the structures being under symmetry reduction, in this case from $D_{2d} \rightarrow C_{2v}$. If we measured RAS over SCQWs, it is expected that this does not exhibit an IOA or failing that this being smaller due to abrupt interfaces are non-ideal. The first part of experiments were carried out over the samples: M4_3171, M4_3172 and M4_3226, we remember that these samples are the type n-i-n, this means that they consist in more growth layers, therefore it is expected that the RAS signal being smaller. The Figure 3.20 shows the results to these samples, in top to bottom order, in left side plots the RAS while in right side it is plotted the R spectra. The R spectra plotted to each sample is the average of all experiments performed, this means which in each RAS experiment, the R was simultaneously measured, then to each sample it is taking the average. In order to discuss the result of that samples, we can observe that in general therms these samples gets a smaller signal of RAS, although in R it does not happen, the direct transitions can being locate in accordance with the numerical results as shows with arrows. Although

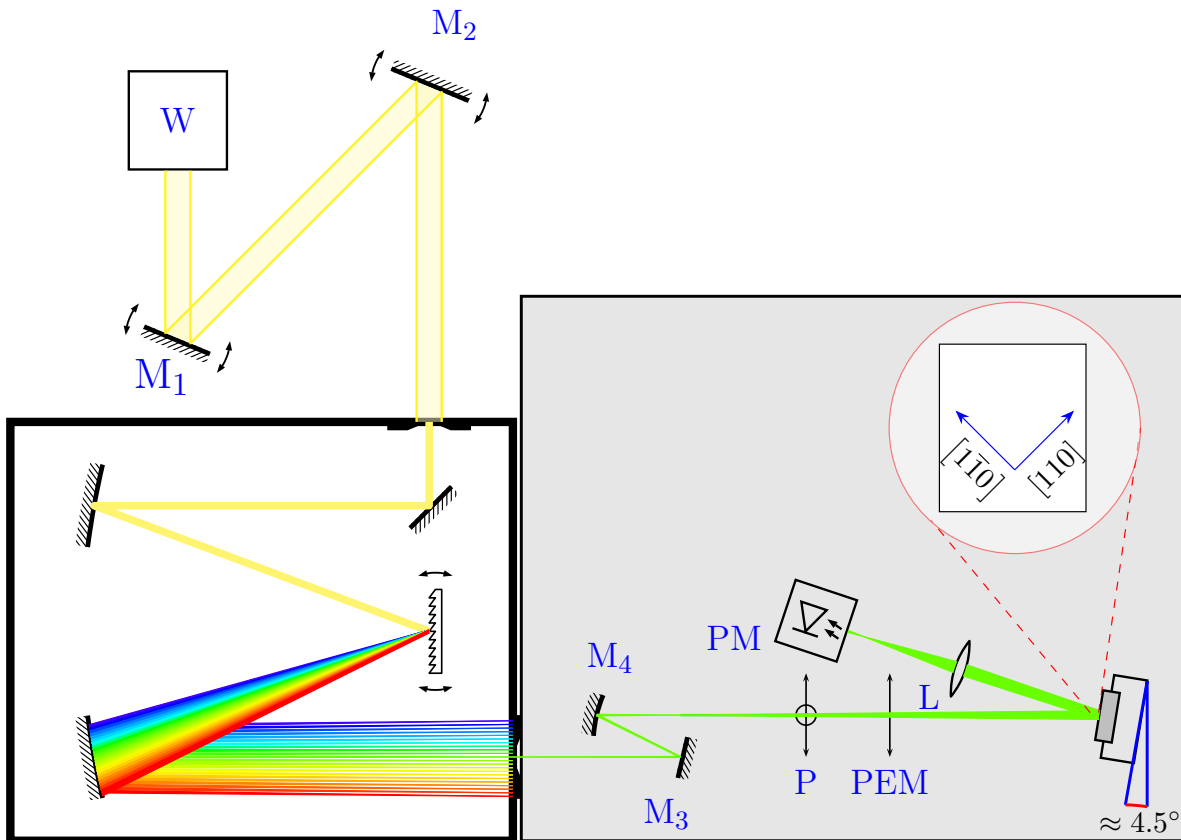


Figure 3.19: RAS setup implemented in this work, as before explained in the PR setup, this is a dark configuration this due that photo-detector are exposed, then keeping closed to ambient light. The optical array is the same as the PR, with the difference which the role of polarization and PEM. This figure also schemes the incidence angle which is about of 4.5° and the directions of linear polarization.

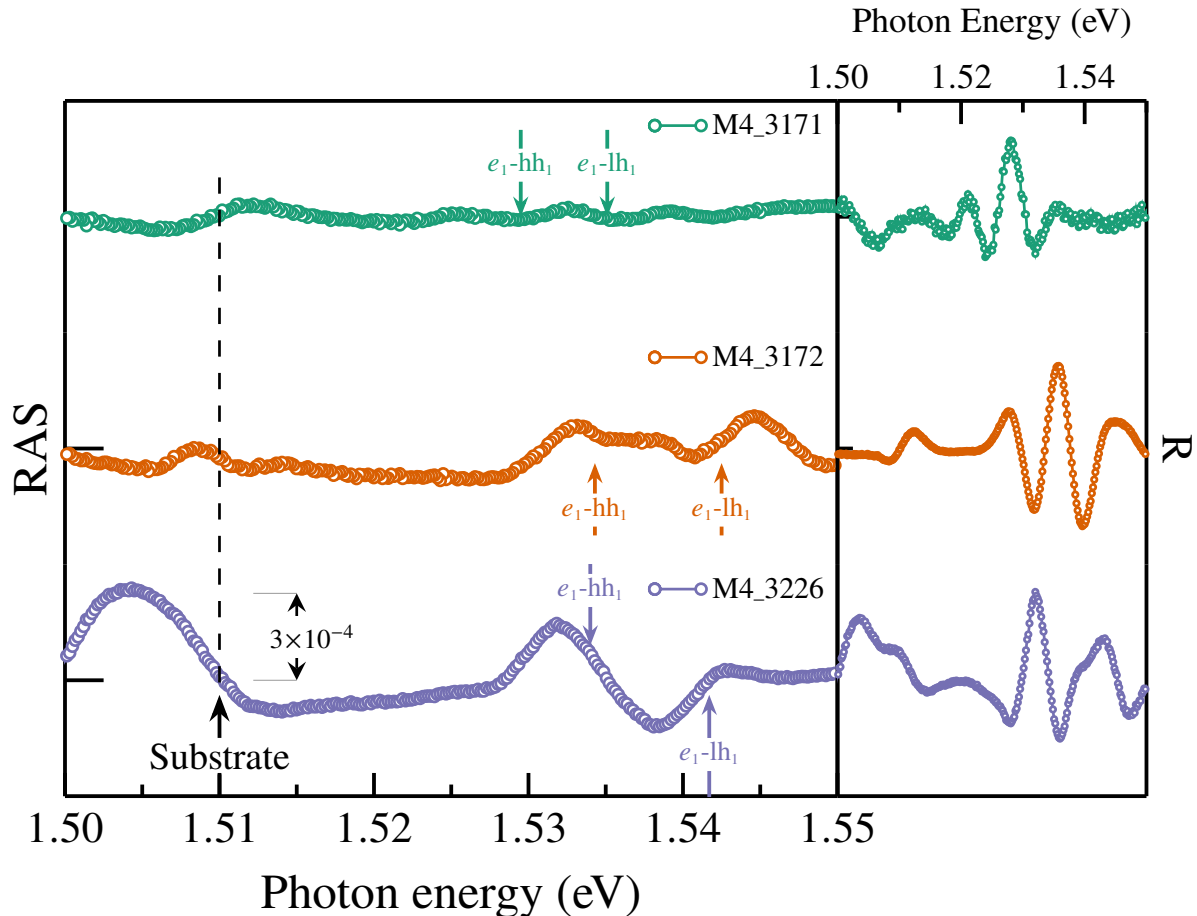


Figure 3.20: Experimental results from samples: M4_3171, M4_3172 and M4_3226, from top to bottom respectively. In left, shows the RAS result where with a dashed line it is denote the substrate transition, in each sample denotes the direct transitions with arrows. The right side, show the plots of R spectra, which is the average result of all experiments carried in each correspond sample.

these three samples consists in more several growth layers, it is possible to measure an in-plane anisotropy were in samples: M4_3171 and M4_3226 the signal amplitude it is relatively same in contrast with the sample M4_3171. The first RAS results even they are an asymmetric CQWs structures, the RAS spectra it is higher in the samples with AlAs barrier (M4_3172 and M4_3226), then the potential barrier is higher than in the sample M4_3171, but the width of these barriers is small, therefore we have a case with samples they consist; in high coupled barrier and thinner. In the other sample, where the RAS spectra is smaller (M4_3171), the coupled barrier is small in potential in comparison with the other samples, but is more wide. Although, it was expected that the spectra relatively same in these three samples, the coupled barrier plays an important role this due to the tunneling process, wells it returns a RAS spectra more definite (better line-shape) than the sample with less tunneling, this means, the coupled barrier is wide. Then, the sample M4_3171 is approx three times smaller. These samples are relatively common with barrier

exception, in sample M4_3226 that better has RAS response posses a coupled barrier with a width of 0.424 nm, while the second with a better RAS response is the sample M4_3172 which has a barrier width of 0.565 nm.

In the next set of samples: M4_3140, M4_3141, M4_3521, M4_3522 and M4_3523, as is explained in Section 3.1, consists in samples with coupled barrier of $\text{Al}_{0.15}\text{Ga}_{0.9}\text{As}$, where the difference in this set samples, is one of these samples (M4_43141) has a coupled barrier twice wider than the other samples, and the relative width of the wells.

Figure 3.21 shows the results of RAS experiments carried out on these samples. These results are interesting in comparison with the before set, the most notorious is the evolution of RAS signal in the more asymmetric structures, in these structures the peaks associated with direct transitions are seen more clearly, being those with an opposite concavity. In these peaks the larger one it is the heavy-hole (down concavity) while the smaller one it is the light-hole transition (up concavity). It is totally evident that the samples M4_3521 and M4_3522 (also called as ACQWs-1 and ACQWs-2) exhibits great RAS response, then, in accordance with the model anisotropy has a major hole mixing. Also, the R spectra is well resolved in both samples, with a peculiarity in the transitions concavities, which in both, is up concavity.

3.2.3.1 RAS Strength Discussion and the Physical Model Justification

To enter into discussion, its purpose is to focus on the three samples before mentioned, aiming to expose the principal objective of this work, which is denoted the RAS strength in ACQWs as importance in the optical properties and excitonic effects in these structures. The Figure 3.22 exposes the evolution of RAS strength, in this plot it is indisputable that the signal increases, because the comparison between the three samples where it is starting with a symmetric structure, then with a lightly asymmetric structure and finally with a very asymmetric structure, the RAS signal associated with each transition have opposite concavities and redshift as the structure is more asymmetric.

Due to the fact that the wave-function probability density of sample SCQWs is distributed symmetrically along the QW structure, the IOA strength is expected to be similar to that obtained for a single QW. In fact, a RAS signal of the order of magnitude of 0.1×10^{-3} has been reported for an 8 nm single QW [79], which has the same order of magnitude as the spectra of Figure 3.23(c). This IOA is attributed to the inequivalent $\text{Al}_x\text{Ga}_{1-x}\text{As} / \text{GaAs}$ interfaces along the SCQWs structure. It is important every clear the role of tunneling in the coupled wells, the difficulty to get a model to explain this structures does not it the same as the single QW structure.

As pointed out before (Section 2.5), the strength of the IOA signal is produced by an intermixing of the heavy- and light-hole states in the valence band that is proportional to $\langle \psi_{hhn} | \mathcal{H} | \psi_{lhn} \rangle$ according to Equation (2.13). For the lowest heavy- and light-hole levels ($n = 1$), there is an estimated separation in energy of around $\Delta E_1 = 2.0, 4.1$, and 4.4 meV

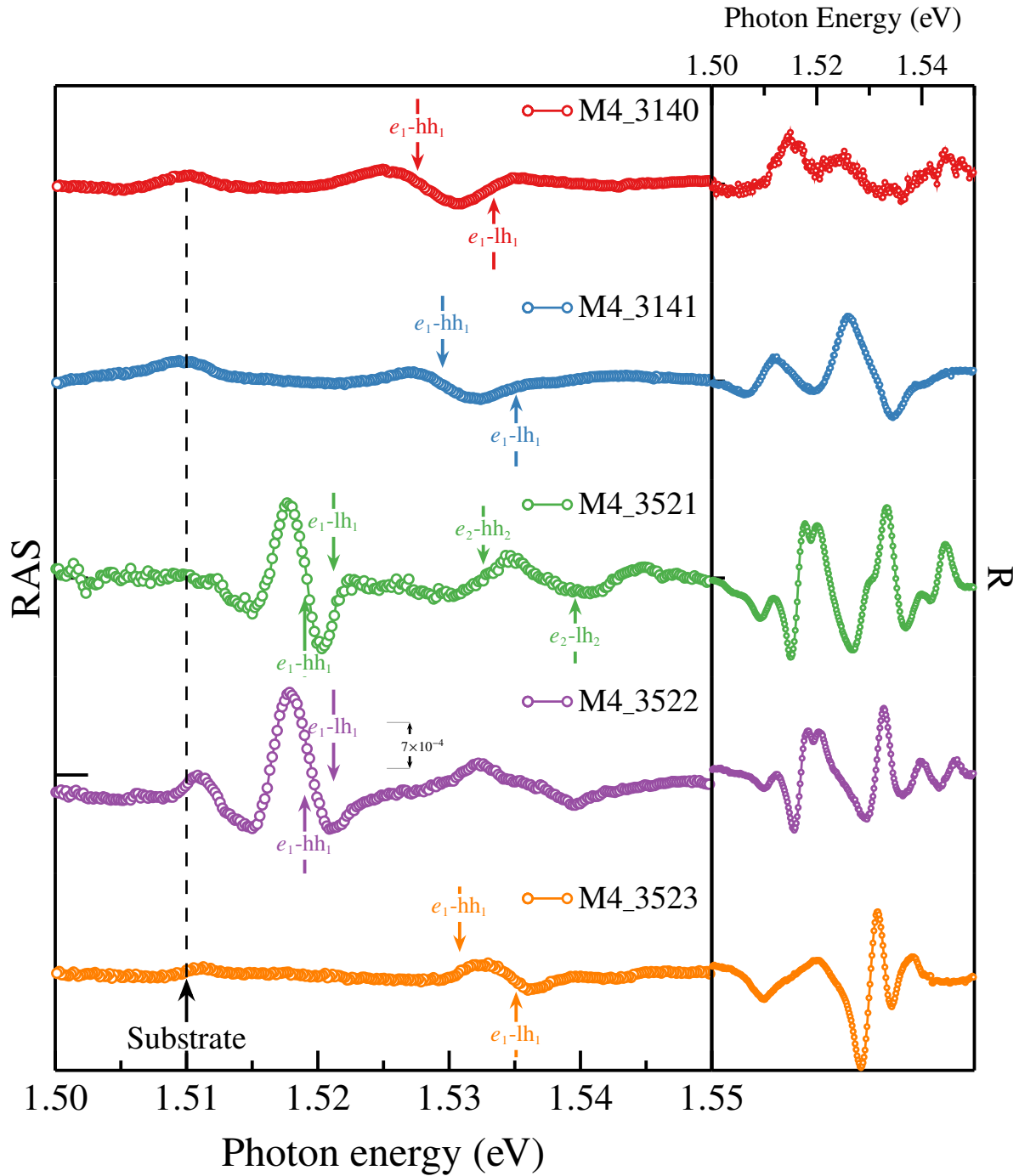


Figure 3.21: Experimental results of samples: M4_3140, M4_3141, M4_3521, M4_3522 and M4_3523, from top to bottom, respectively. In left, shows the RAS result where a dashed line denotes the substrate transition. In each spectrum the direct transitions with arrows are remarked. The right side show the plots of the R spectra, which is the average result of all experiments carried out. The direct transitions are located by two peaks with opposite concavity where we can attest that the larger one transition is $e_1\text{-}hh_1$ and a smaller, one associated with the $e_1\text{-}lh_1$

for samples ACQWs-2 (ACQWs-3), ACQWs-1, and SCQWs, respectively. The mixing $\langle \psi_{hhn} | \mathcal{H} | \psi_{lhn} \rangle$ can be estimated by considering that the transitions are direct (n is the same for the valence and conduction band) and then the overlapping terms in Equation (2.13) must be approximately the same for each sample. For transitions $n = 1$ it can be seen in Figure 3.22 that amplifier ratios of the spectra between ACQWs-2 and ACQWs-1 with respect to SCQWs are 1.5 and 3.7, respectively. Thus from Equation (2.13) we estimate ratios of $\langle \psi_{hh1} | \mathcal{H}_{ACQWs-1} | \psi_{lh1} \rangle / \langle \psi_{hh1} | \mathcal{H}_{SCQWs} | \psi_{lh1} \rangle \sim 1.4$ for sample ACQWs-1 and $\langle \psi_{hh1} | \mathcal{H}_{ACQWs-2} | \psi_{lh1} \rangle / \langle \psi_{hh1} | \mathcal{H}_{SCQWs} | \psi_{lh1} \rangle \sim 1.7$ for sample ACQWs-2.

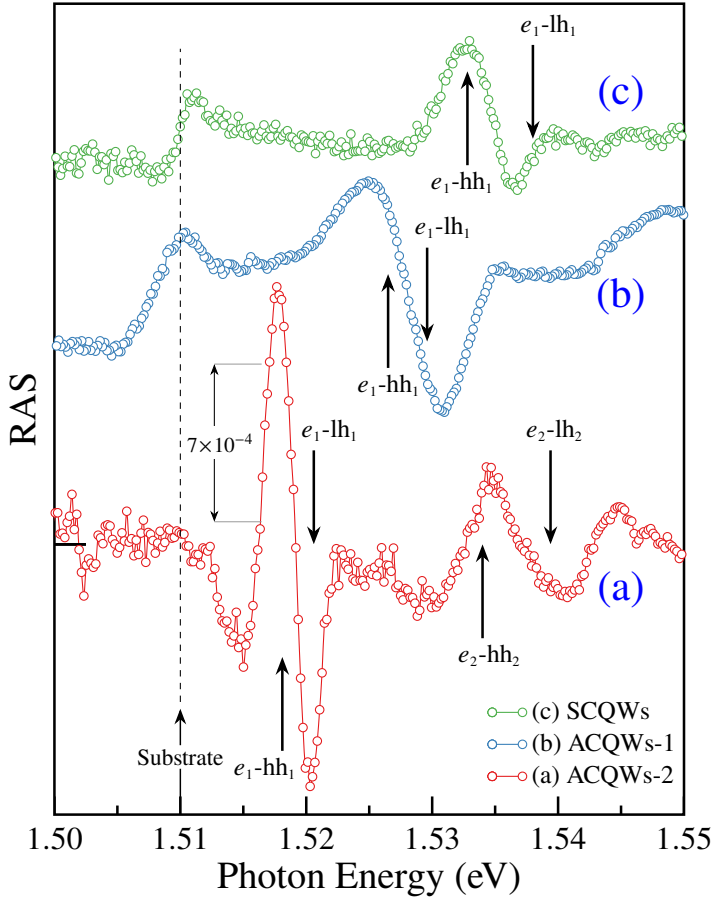


Figure 3.22: RAS spectra for the (a), (b), asymmetric and (c) symmetric CQWs. The dashed vertical line indicates the expected energy of the excitonic transition of the GaAs substrate. Above this energy, the optical transitions come from the CQWs. The inset shows the PL spectra measured for each sample. Two peaks can be identified in each spectrum, a larger one associated with the transition $e_1\text{-}hh_1$ and a much smaller one associated with the $e_1\text{-}lh_1$ (for spectrum (b) this peak is observed as a shoulder). The energies obtained from the PL spectra are indicated by the arrows in the RAS spectra. Note that the structures associated with $e_1\text{-}hh_1$ and $e_1\text{-}lh_1$ increase their strength when the CQWs become more asymmetric. The RAS spectra were measured at 30 K.

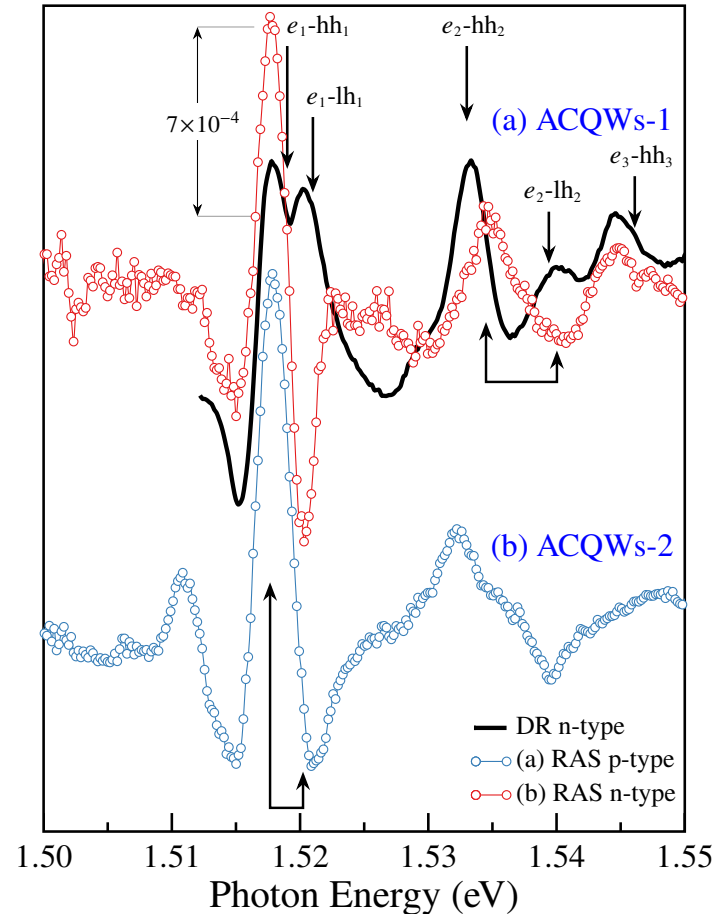
In accordance with our estimation based on the anisotropy model, the Table 3.5 contains the energies considered. If well, the large IOA in general, it is attributed to interfaces in our case the reason is due to non-equivalence due to the width asymmetric into coupled QWs, this originates a mixing of hh-lh states and therefore these it coupled strongest as the states close in energy [85]. The Table 3.5 and Figure 2.10 confirms this, in the ACQWs-2 this energy between hh₁ and lh₁ states are close, in counterpart with the SCQWs this energy is large.

Sample	$e_1\text{-hh}_1$	$e_1\text{-lh}_1$	ΔE_e (meV)	ΔE_{hh} (meV)	ΔE_{lh} (meV)	ΔE_n (meV)
SCQWs	(N)1.5328 (E)1.5297	(N)1.5380 (E)1.5341	8.9	0.9	6.9	$\Delta E_1 = 4.4$ $\Delta E_2 = 10.5$
ACQWs-1	(N)1.5265 (E)1.5273	(N)1.5296 (E)1.5314	8.4	1.3	6.4	$\Delta E_1 = 4.1$ $\Delta E_2 = 9.2$
ACQWs-2	(N)1.5181 (E)1.5190	(N)1.5206 (E)1.5210	11.8	3.4	7.5	$\Delta E_1 = 2.0$ $\Delta E_2 = 6.4$

Table 3.5: Comparative of experimental (E) and numerical calculations (N) of first level transition energies (in eV). δE_e , δE_{hh} and δE_{lh} corresponds to the difference between electrons, heavy- light holes states, respectively. ΔE_n is the numerical calculation of energy splitting for transitions 1 and 2 ($n = 1, 2$).

In order to elucidate the physical origin of the RAS in the ACQWs, we compare in Figure 3.24 the RAS and the DR spectra of the ACQWs-2. DR spectra is obtained by the numerical subtraction of the reflection (R) spectra recorded at 30K and 300K followed by the normalization to the 300K spectrum. The subtraction highlights the excitonic

Figure 3.24: Reflection anisotropy (RAS, (a), (b)) and differential reflection (DR, solid line) spectra for ACCQWs-2 and ACQWs-3, grown on an AlGaAs n-type and p-type layer respectively. Note that while for the heavy hole transitions ($e_1\text{-hh}_1$ and $e_2\text{-hh}_2$) in the RAS and DR spectra have the same concavity, for light holes transitions ($e_1\text{-lh}_1$ and $e_2\text{-lh}_2$) the concavities are opposite and DR spectra shows the highest level transitions. The bottom arrows point to the experimental transitions for the two first levels, whereas the top arrows show the calculated energies to three energy levels. The RAS and DR spectra were measured at 30K.



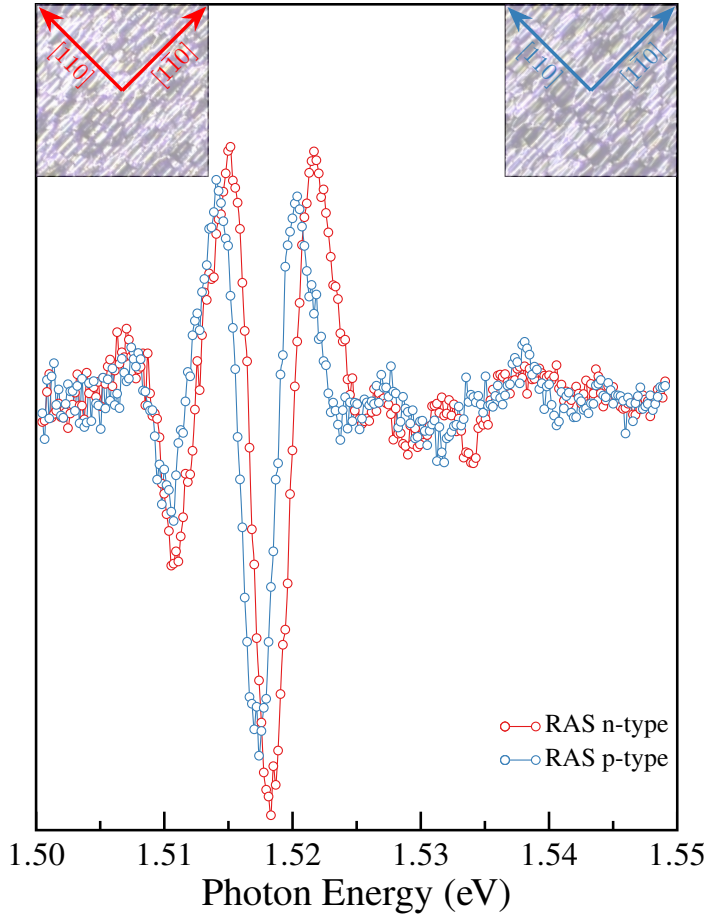


Figure 3.26: RAS experiment designed to demonstrate the non-existence of built-in electric field trough sequential measured along the preferential direction, in this case, it was chosen along the pits $[1\bar{1}0]$ [28]. The signal result in both samples practically is the same, the sign is conserving. At top left and right located the images recorded with a microscope of back substrate which shows typical and well known etch pits elongated [29] along of $[1\bar{1}0]$ direction.

features, which are very weak (and energy shifted) at 300K. The comparison between RAS and DR spectra allows us to contrast the contribution of the heavy and light holes transitions. Around 1.5175 eV, the DR spectrum shows two peaks corresponding to $e_1\text{-hh}_1$ and $e_1\text{-lh}_1$ transitions. Note that in the RAS spectrum, the structure associated to $e_1\text{-hh}_1$ transition has the same concavity as the corresponding for the DR spectrum, while the $e_1\text{-lh}_1$ transition has the opposite concavity. This is an indication of the transfer of oscillator strength between the levels due to the intermixing of heavy- and light- holes, thus supporting our anisotropy model. The same behavior applies for the $e_2\text{-hh}_2$ and $e_2\text{-lh}_2$ transitions at around 1.5375 eV. Transition $e_2\text{-hh}_3$ is also indicated and it has the same concavity for RAS and DR spectra, as in the case of the $e_1\text{-hh}_1$ and $e_2\text{-hh}_2$ transitions. The arrows at the bottom of Figure 3.24 indicate the energy of the states $e_n\text{-hh}_n$ and $e_n\text{-lh}_n$ (for $n = 1$ and 2) obtained from the maximum and minimum of the RAS spectrum. From the numerical calculation results summarized in Table 3.5, the energy splitting between transitions $e_n\text{-hh}_n$ and $e_n\text{-lh}_n$ are $\Delta E_1 = 2.0$ meV and $\Delta E_2 = 6.4$ meV. In accordance with Equation (2.13), the IOA amplitude is proportional to $1/\Delta E_n$. Considering the same valued for the overlapping and the mixing $\langle \psi_{hhn} | \mathcal{H} | \psi_{lhn} \rangle$ we estimate an amplitude ratio of 3.25 between these transitions. This value is close to the value of 3.9 obtained by the RAS spectrum of Figure 3.24 supporting our interpretation.

Finally, we discuss the possible contribution to the RAS amplitude by a built-in electric field across the CQWs both symmetric and asymmetric. To study this contribution, we have compared the RAS spectra of asymmetric samples ACQWs-2 and ACQWs-3. The difference between them is the doping of the AlGaAs layer (see Table 3.1). While for ACQWs-2 it is n-type, for ACQWs-3 it is p-type. Assuming that the built-in electric field originates from charge transfer between surface states and the AlGaAs doped layer (n or p), this field is expected to have opposite signs for samples ACQWs-2 and ACQWs-3. Thus, the linear contribution of the electric field to the RAS should be reversed in sign for such samples. Figure 3.26 shows the comparison between the RAS spectra of samples ACQWs-2 and ACQWs-3, this with aim to demonstrate that in the case of existed a field the sign is opposite. The experiment, it was designed to measure both samples in a sequence way along the same preferential direction, in this case we choose the direction of pits [1 $\bar{1}$ 0] [28], if existed a field we expected a opposite RAS signal, but this does not occur, the sign in signal it was conserved in both samples. The Figure 3.26 shows the results of this experiment, in top left and right it is placed the images of both samples of the pits orientation, this to corroborate that the direction of measured. As can be seen (Figure 3.24), RAS spectra are equivalent in shape and have the same sign, thus indicating that the contribution of the electric field to the RAS signal is very small.

It is natural to suppose that the built-in electric field contributes to increase of the RAS signal, and although we estimate that this field is small, it is still important to discussed it and show different ways to affirms that the built-in field is not the reason of the IOA. We conclude, thus, that the dominant contribution to RAS spectra is the asymmetry of the CQWs system.

3.2.3.2 The RAS summary

To conclude, we found a simple yet accurate description of optical anisotropies occurring at interfaces made up of GaAs/AlAs, that has been a long-standing challenge because of the lack of a systematic investigations of well prepared coupled quantum wells. Indeed, even for simple quantum wells, for which interface C_{2V} symmetry had been proposed, previous experimental results were unable to give a definite conclusion. This thesis tacked such issue and even paves the way to tailor anisotropic spin-related phenomena.

4

CONCLUSIONS AND FUTURE WORK

This chapter summarizes the principal conclusions of this work and presents the future experiments on these structures in the wake of obtained results.

THE AIM of this work finally resulted in important publications and stress the fact that the CQWs offer an excellent platform to study optical and quantum mechanical properties. The main results can be summarized as follows:

- I) The principal idea to expose our results was planned to simplify specific the physical basis, starting by explaining a single QW and structural properties and then raising the relevance of symmetry context to understand the physical behavior of electrons. We also exposed the symmetry importance and its fundamental role in the emergence of the IOA. Then we focused on symmetry reduction (symmetry breaking) which is the cause of the appearance of interesting physical properties, in our case optical properties. The perturbative model purposed to understand the IOA is simple yet very useful, as this mainly depends on the grade of asymmetry in the CQWs system, the more asymmetry, the bigger the RAS signal. Also, this model is supported by numerical calculations with a good approximation. When we had obtained the results of the first, we purposed to develop codes to generate numerical results and although this represented a new area to explore, we decided to dedicate enough time to get a new tool to support our experimental work.
- II) Already inside in numerical solutions area, we realized the complexity of generating reliable results, and the overall existence of numerous proposals to get it, then we decided to implement the simple context. Our numerical results are simple but reliable in accordance with the experimental energies and, by this reason we create a [GitHub](#) repository [183] with the aim to develop new codes and numerical models that in future work can be implemented.
- III) In the experimental part, the results are proof of the arduously work that it was inverted, along with the project it was realized experiments to study and understand the physics which involves the CQWs systems, although this has been studied for several years ago, our contribution is novel.

The quantum confinement is the key to these structures, if we consider the symmetry breaking by coupled wells width asymmetry exhibits wonderful physics, from spin dynamics to excitonic effects. With respect to spin dynamics into CQWs structures, it was realized experiments of circularly polarized PL over the samples shown in this work, reveal that the spin relaxation time τ_s . It has been demonstrated that the degree of circular polarization is directly related to the asymmetry of the CQWs [94].

The excitonic properties shown in the Section 3.2.2.1 are really interesting, the PR experiments performed as a laser power function reveal a non-common transition in these experiments, this transition associated with a trion, commonly occurs in structures under external disturbance as an electric field is applied, in our case, we not only detect the trion transition, but also it modulated with a light source. This means this can be applied as a laser transistor. These PR results are very relevant, in fact as future work we planned to publish them.

Finally, in the RAS experiments it is clearly the wonderful physics that exhibits ACQWs structures, the results obtained are the principle of an experiments series which we are thinking to carry out. Without the intention of being repetitive since the results prove our work, we purpose to take further the RAS technique to explore with more detail the ACQWs structures. The first upgrade of RAS experiments, it is do it spin sensitive, which means, spin-resolved RAS experiments. The principal idea is to enhance the RAS setup to measure spin response. Our proposal is to carry out the experiments just by changing the modulated PEM polarization. In the RAS setup (as can see in Figure 3.19) the monochromatic beam is first polarized to then modulated linear polarization by the PEM between mutual perpendicular polarization states, to finally spot on sample along [110] and $[1\bar{1}0]$ directions. Then, in the spin resolve RAS experiments, it is purposed to modify PEM polarization modulation, to this it is possible to the choice that the modulation being right circular and left circular polarization, in the PEM device this is $\lambda/4$ and $3\lambda/2$ which in contrast with the $\lambda/2$ of the traditional RAS experiments.

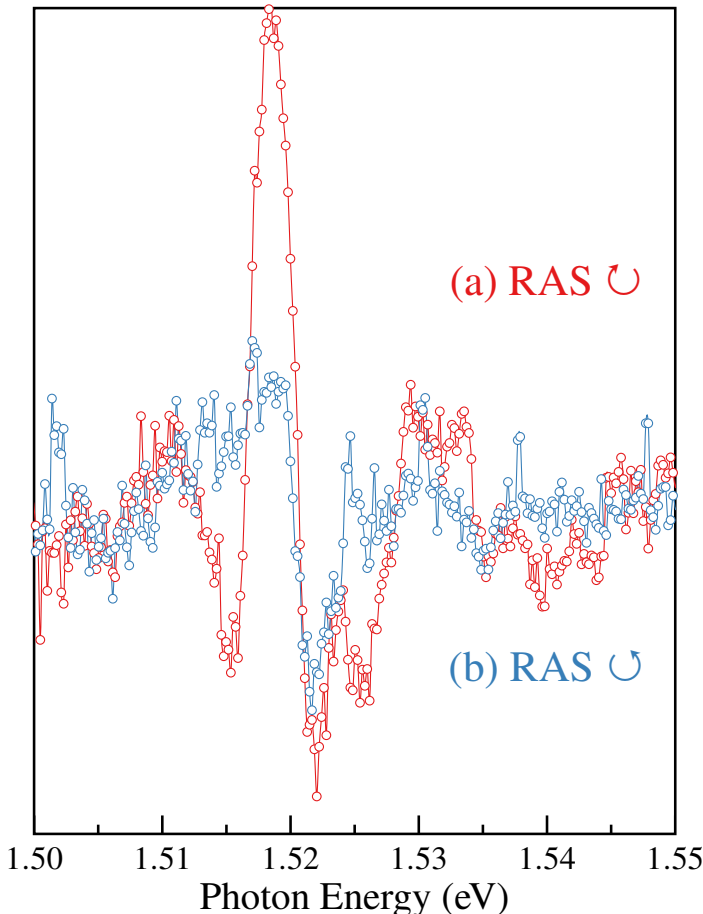


Figure 4.1: Spin resolve RAS experiments worked on ACQWs-2 sample, this experiments carried out in sequential way, firstly measured with one polarization state and then the second state. The sample it was placed along preferential direction ($[1\bar{1}0]$), maybe this be a reason can observer a structural signal of RAS, this means, the line shape of anisotropy due to the asymmetry structure. Although, it's notable the difference between mutual polarization states.

The first results obtained from worked on ACQWs-2 sample shows in Figure 4.1, these experiments were it performed with the sample position in a preferential direction [110] and as a sequential way, this means, firstly with a polarization state then the other state.

The results shown in Figure 4.1 are the average of sequential experiments, each of one with their respective polarization. The signals results exhibit an interest difference, although, maybe the line-shape has a remainder of structural anisotropy due to the asymmetry in the structure (C_{2v}). Even if, these results are really first approximations, the technique has powerful to explore spin properties. The second RAS upgrade to spin resolving, as a proposal, instead of polarization states with the PEM will be used a laser beam circular (left and right) focused on the sample, while theRAS signal it is measured traditionally. We expected that these upgrades the RAS experiments, turning a tool for spin study.

BIBLIOGRAPHY

- [1] O. Ruiz-Cigarrillo and G. Martinez-Cepeda, “Coupled quantum wells codes,” 2018. [Online]. Available: <https://github.com/NanophotonIICOs/cqws-codes.git> (Cited on pages IV and 33.)
- [2] J. Bezanson, A. Edelman, S. Karpinski, and V. B. Shah, “Julia: A fresh approach to numerical computing,” *SIAM Review*, vol. 59, no. 1, pp. 65–98, 2017. [Online]. Available: <https://pubs.siam.org/doi/10.1137/141000671> (Cited on page IV.)
- [3] G. Martinez-Cepeda and O. Ruiz-Cigarrillo, “ $\mathbf{k} \cdot \mathbf{p}$ julia package,” 2022. [Online]. Available: <https://github.com/NanophotonIICOs/kp-nanoiiico-group.git> (Cited on page IV.)
- [4] A. H. Larsen, J. J. Mortensen, J. Blomqvist, I. E. Castelli, R. Christensen, M. Dułak, J. Friis, M. N. Groves, B. Hammer, C. Hargus, E. D. Hermes, P. C. Jennings, P. B. Jensen, J. Kermode, J. R. Kitchin, E. L. Kolsbjerger, J. Kubal, K. Kaasbjerger, S. Lysgaard, J. B. Maronsson, T. Maxson, T. Olsen, L. Pastewka, A. Peterson, C. Rostgaard, J. Schiøtz, O. Schütt, M. Strange, K. S. Thygesen, T. Vegge, L. Vilhelmsen, M. Walter, Z. Zeng, and K. W. Jacobsen, “The atomic simulation environment—a python library for working with atoms,” *Journal of Physics: Condensed Matter*, vol. 29, no. 27, p. 273002, 2017. [Online]. Available: <http://stacks.iop.org/0953-8984/29/i=27/a=273002> (Cited on page IV.)
- [5] A. Togo and I. Tanaka, “Spglib: a software library for crystal symmetry search,” 2018. (Cited on page IV.)
- [6] D. Alonso-Álvarez, T. Wilson, P. Pearce, M. Führer, D. Farrell, and N. Ekins-Daukes, “Solcore: a multi-scale, python-based library for modelling solar cells and semiconductor materials,” *Journal of Computational Electronics*, vol. 17, no. 3, pp. 1099–1123, 2018. (Cited on pages IV and 52.)
- [7] H. Hebal, Z. Koziol, S. Lisesivdin, and R. Steed, “General-purpose open-source 1d self-consistent schrödinger-poisson solver: Aestimo 1d,” *Computational Materials Science*, vol. 186, p. 110015, 2021. [Online]. Available: <https://www.sciencedirect.com/science/article/pii/S0927025620305061> (Cited on pages IV and 67.)
- [8] K. Momma and F. Izumi, “it VESTA3 for three-dimensional visualization of crystal, volumetric and morphology data,” *Journal of Applied Crystallography*, vol. 44, no. 6, pp. 1272–1276, Dec 2011. [Online]. Available: <https://doi.org/10.1107/S0021889811038970> (Cited on page IV.)

- [9] T. Tantau, “Pgf/tikz,” 2007. [Online]. Available: <https://github.com/pgf-tikz/pgf.git> (Cited on page IV.)
- [10] C. Bersch, “pst-optexp, drawing optical experimental setups,” 2022. [Online]. Available: <https://github.com/cbersch/pst-optexp> (Cited on page IV.)
- [11] M. Fox, “Optical properties of solids,” 2002. (Cited on pages VI, 6, and 12.)
- [12] B. Koopmans, B. Koopmans, P. Santos, P. Santos, and M. Cardona, “Microscopic reflection difference spectroscopy on semiconductor nanostructures,” *physica status solidi (a)*, vol. 170, no. 2, pp. 307–315, 1998. (Cited on pages VII, 24, 25, 39, and 70.)
- [13] E. A. de Andrade e Silva, G. C. La Rocca, and F. Bassani, “Spin-orbit splitting of electronic states in semiconductor asymmetric quantum wells,” *Phys. Rev. B*, vol. 55, pp. 16 293–16 299, Jun 1997. [Online]. Available: <https://link.aps.org/doi/10.1103/PhysRevB.55.16293> (Cited on pages VII, 23, and 25.)
- [14] D. J. English, J. Hübner, P. S. Eldridge, D. Taylor, M. Henini, R. T. Harley, and M. Oestreich, “Effect of symmetry reduction on the spin dynamics of (001)-oriented gaas quantum wells,” *Phys. Rev. B*, vol. 87, p. 075304, Feb 2013. [Online]. Available: <https://link.aps.org/doi/10.1103/PhysRevB.87.075304> (Cited on pages VII, 24, and 25.)
- [15] P. S. Eldridge, J. Hübner, S. Oertel, R. T. Harley, M. Henini, and M. Oestreich, “Spin-orbit fields in asymmetric (001)-oriented gaas/al_xga_{1-x}as quantum wells,” *Phys. Rev. B*, vol. 83, p. 041301, Jan 2011. [Online]. Available: <https://link.aps.org/doi/10.1103/PhysRevB.83.041301> (Cited on pages VII, 24, and 25.)
- [16] J. L. Yu, S. Y. Cheng, Y. F. Lai, Q. Zheng, Y. H. Chen, and C. G. Tang, “Tuning of in-plane optical anisotropy by inserting ultra-thin inas layer at interfaces in (001)-grown gaas/algaas quantum wells,” *Journal of Applied Physics*, vol. 117, no. 1, p. 015302, 2015. (Cited on pages VII, 24, 25, and 39.)
- [17] D. J. English, P. G. Lagoudakis, R. T. Harley, P. S. Eldridge, J. Hübner, and M. Oestreich, “Strain-induced spin relaxation anisotropy in symmetric (001)-oriented gaas quantum wells,” *Phys. Rev. B*, vol. 84, p. 155323, Oct 2011. [Online]. Available: <https://link.aps.org/doi/10.1103/PhysRevB.84.155323> (Cited on pages VII and 25.)
- [18] C. G. Tang, Y. H. Chen, B. Xu, X. L. Ye, and Z. G. Wang, “Well-width dependence of in-plane optical anisotropy in (001) gaas/algaas quantum wells induced by in-plane uniaxial strain and interface asymmetry,” *Journal of Applied Physics*, vol. 105, no. 10, p. 103108, 2009. (Cited on pages VII, 25, and 39.)

- [19] Y. Li, F. Liu, X. Ye, Y. Liu, J. Wang, and Y. Chen, “Quantitative investigation of intrinsic shear strain and asymmetric interface conditions in semiconductor superlattices,” *Journal of Applied Physics*, vol. 126, no. 6, p. 065704, 2019. (Cited on pages VII, 25, and 39.)
- [20] S. H. Kwok, H. T. Grahn, K. Ploog, and R. Merlin, “Giant electropoleochroism in gaas-(al,ga)as heterostructures: The quantum-well pockels effect,” *Phys. Rev. Lett.*, vol. 69, pp. 973–976, Aug 1992. [Online]. Available: <https://link.aps.org/doi/10.1103/PhysRevLett.69.973> (Cited on pages VII and 25.)
- [21] O. Ruiz-Cigarrillo, L. F. Lastras-Martínez, E. A. Cerdá-Méndez, G. Flores-Rangel, C. A. Bravo-Velazquez, R. E. Balderas-Navarro, A. Lastras-Martínez, N. A. Ulloa-Castillo, K. Biermann, and P. V. Santos, “Optical anisotropies of asymmetric double gaas (001) quantum wells,” *Phys. Rev. B*, vol. 103, p. 035309, Jan 2021. [Online]. Available: <https://link.aps.org/doi/10.1103/PhysRevB.103.035309> (Cited on pages VII, 25, and 34.)
- [22] E. O. Kane, “Band structure of indium antimonide,” *Journal of Physics and Chemistry of Solids*, vol. 1, no. 4, pp. 249–261, 1957. [Online]. Available: <https://www.sciencedirect.com/science/article/pii/0022369757900136> (Cited on pages VII, 26, and 28.)
- [23] E. G. Novik, A. Pfeuffer-Jeschke, T. Jungwirth, V. Latussek, C. R. Becker, G. Landwehr, H. Buhmann, and L. W. Molenkamp, “Band structure of semimagnetic $hg_{1-y}mn_yte$ quantum wells,” *Phys. Rev. B*, vol. 72, p. 035321, Jul 2005. [Online]. Available: <https://link.aps.org/doi/10.1103/PhysRevB.72.035321> (Cited on pages VII, 27, and 28.)
- [24] P. Harrison and A. Valavanis, *Numerical solutions*. John Wiley & Sons, Ltd, 2016, ch. 3, pp. 81–130. (Cited on pages VII, 33, 34, and 67.)
- [25] Nextnano, “Nextnano software.” [Online]. Available: https://www.nextnano.com/manual/nextnanoplus_tutorials/1D/double_qw.html (Cited on pages VII, 33, and 34.)
- [26] K. Sivalertporn, “Effect of barrier width on the exciton states in coupled quantum wells in an applied electric field,” *Physics Letters A*, vol. 380, no. 22, pp. 1990–1994, 2016. [Online]. Available: <https://www.sciencedirect.com/science/article/pii/S0375960116300664> (Cited on pages IX, 35, 62, and 66.)
- [27] N. Debbar, S. Hong, J. Singh, P. Bhattacharya, and R. Sahai, “Coupled gaas/algaas quantum-well electroabsorption modulators for low-electric-field optical modulation,” *Journal of Applied Physics*, vol. 65, no. 1, pp. 383–385, 1989. [Online]. Available: <https://doi.org/10.1063/1.342554> (Cited on pages IX and 66.)

- [28] J. L. Weyher and J. J. Kelly, *Defect-Selective Etching of Semiconductors*. Berlin, Heidelberg: Springer Berlin Heidelberg, 2010, pp. 1453–1476. [Online]. Available: https://doi.org/10.1007/978-3-540-74761-1_43 (Cited on pages XI, 77, and 78.)
- [29] I. Yonenaga and K. Sumino, “Behaviour of dislocations in gaas revealed by etch pit technique and x-ray topography,” *Journal of Crystal Growth*, vol. 126, no. 1, pp. 19–29, 1993. [Online]. Available: <https://www.sciencedirect.com/science/article/pii/002202489390223J> (Cited on pages XI and 77.)
- [30] N. V. Tkachenko, *Optical spectroscopy: methods and instrumentations*. Elsevier, 2006. (Cited on pages XII, 46, and 47.)
- [31] M. SUNDARAM, S. A. CHALMERS, P. F. HOPKINS, and A. C. GOSSARD, “New quantum structures,” *Science*, vol. 254, no. 5036, pp. 1326–1335, 1991. [Online]. Available: <https://science.sciencemag.org/content/254/5036/1326> (Cited on page 2.)
- [32] M. P. McDonald, R. Chatterjee, J. Si, B. Jankó, and M. Kuno, “Dimensional crossover in semiconductor nanostructures,” *Nature communications*, vol. 7, no. 1, pp. 1–5, 2016. (Cited on page 2.)
- [33] C. Argyropoulos, “Asymmetric control of light at the nanoscale,” *Nature Photonics*, vol. 16, no. 8, pp. 556–557, Aug 2022. [Online]. Available: <https://doi.org/10.1038/s41566-022-01045-4> (Cited on page 2.)
- [34] J. Piprek, *Handbook of Optoelectronic Device Modeling and Simulation: Fundamentals, Materials, Nanostructures, LEDs, and Amplifiers, Vol. 1*. CRC Press, 2017. (Cited on pages 2, 3, and 4.)
- [35] H. Alloul, *Introduction to the Physics of Electrons in Solids*. Springer Science & Business Media, 2010. [Online]. Available: <https://doi.org/10.1007/978-3-642-13565-1> (Cited on page 2.)
- [36] M. Cardona and Y. Y. Peter, *Fundamentals of semiconductors*. Springer, 2005, vol. 619. (Cited on pages 2, 6, 10, and 18.)
- [37] K. W. Böer and U. W. Pohl, *Semiconductor physics*. Springer, 2018. [Online]. Available: <https://doi.org/10.1007/978-3-319-06540-3> (Cited on page 3.)
- [38] I. Vurgaftman, M. P. Lumb, and J. R. Meyer, *Bands and Photons in III-V Semiconductor Quantum Structures*. Oxford University Press, 2020, vol. 25. (Cited on pages 4, 26, and 27.)
- [39] P. Vogl, H. P. Hjalmarson, and J. D. Dow, “A semi-empirical tight-binding theory of the electronic structure of semiconductors†,” *Journal of Physics and Chemistry of Solids*, vol. 44, no. 5, pp. 365–378, 1983. [Online]. Available:

- <https://www.sciencedirect.com/science/article/pii/0022369783900641> (Cited on pages 5 and 18.)
- [40] R. Muller, “Tight binding program to compute the band structure of simple semiconductors.” 2017. [Online]. Available: <https://github.com/qftphys/Simple-SPS-tight-binding-code-based-on-parameters-from-Vogl-Hjalmarson-Dow> (Cited on page 5.)
- [41] J. Leonard, *Exciton Transport Phenomena in GaAs Coupled Quantum Wells*. Springer, 2017. (Cited on page 7.)
- [42] C. Tanguy, “Optical dispersion by wannier excitons,” *Phys. Rev. Lett.*, vol. 75, pp. 4090–4093, Nov 1995. [Online]. Available: <https://link.aps.org/doi/10.1103/PhysRevLett.75.4090> (Cited on page 7.)
- [43] P. Harrison and A. Valavanis, *Quantum wells, wires and dots: theoretical and computational physics of semiconductor nanostructures*. John Wiley & Sons, 2016. (Cited on pages 9, 10, 12, 13, 26, 29, 30, 32, and 33.)
- [44] W. Pauli, “Über den Zusammenhang des Abschlusses der Elektronengruppen im Atom mit der Komplexstruktur der Spektren,” *Zeitschrift für Physik*, vol. 31, no. 1, pp. 765–783, 1925. (Cited on page 10.)
- [45] S. Chuang, *Physics of Optoelectronic Devices*, ser. Wiley Series in Pure and Applied Optics. Wiley, 1995. [Online]. Available: <https://books.google.com.mx/books?id=ect6QgAACAAJ> (Cited on pages 12 and 51.)
- [46] J. Singh, *Electronic and Optoelectronic Properties of Semiconductor Structures*. Cambridge University Press, 2003. (Cited on page 12.)
- [47] G. Bastard, *Wave mechanics applied to semiconductor heterostructures*. Wiley, 1990. (Cited on pages 12, 30, and 67.)
- [48] J. H. Davies, *The physics of low-dimensional semiconductors: an introduction*. Cambridge university press, 1998. (Cited on page 12.)
- [49] L. De La Peña, *Introducción a la mecánica cuántica*. Fondo de Cultura económica, 2014. (Cited on page 12.)
- [50] D. J. Griffiths and D. F. Schroeter, *Introduction to quantum mechanics*. Cambridge University Press, 2018. (Cited on page 12.)
- [51] J. J. Sakurai and E. D. Commins, “Modern quantum mechanics, revised edition,” 1995. (Cited on page 12.)
- [52] C. Cohen-Tannoudji, B. Diu, and F. Laloë, *Quantum Mechanics, Volume 1: Basic Concepts, Tools, and Applications*. John Wiley & Sons, 2019. (Cited on page 12.)

- [53] N. Rivera and I. Kaminer, “Light–matter interactions with photonic quasiparticles,” *Nature Reviews Physics*, vol. 2, no. 10, pp. 538–561, 2020. (Cited on page 13.)
- [54] B. C. Van Fraassen, *Laws and symmetry*. Clarendon Press, 1989. (Cited on page 15.)
- [55] R. C. Powell, *Symmetry, group theory, and the physical properties of crystals*. Springer, 2010, vol. 824. (Cited on pages 15 and 17.)
- [56] K. Tapp, *Symmetry: A mathematical exploration*. Springer Nature, 2021. (Cited on page 15.)
- [57] J. F. Cornwell, *Group theory in physics: An introduction*. Academic press, 1997. (Cited on page 15.)
- [58] U. Müller, *Symmetry relationships between crystal structures: applications of crystallographic group theory in crystal chemistry*. OUP Oxford, 2013, vol. 18. (Cited on page 15.)
- [59] C. Kittel and P. McEuen, *Kittel’s Introduction to Solid State Physics*. John Wiley & Sons, 2018. (Cited on pages 15 and 16.)
- [60] J. Sólyom, *Fundamentals of the Physics of Solids: Volume 1: Structure and Dynamics*. Springer Science & Business Media, 2007, vol. 1. (Cited on page 15.)
- [61] S. K. Chatterjee, *Crystallography and the World of Symmetry*. Springer Science & Business Media, 2008, vol. 113. (Cited on pages 16 and 17.)
- [62] J. McKelvey, *Solid State and Semiconductor Physics*, ser. A Harper international edition. Harper & Row, 1966. [Online]. Available: <https://books.google.com.mx/books?id=MQNRAAAAMAAJ> (Cited on page 16.)
- [63] C. Malgrange, C. Ricolleau, and M. Schlenker, *Symmetry and Physical Properties of Crystals*. Springer, 2014. (Cited on page 17.)
- [64] N. Ashcroft, A. W. N. Mermin, W. Ashcroft, D. Mermin, N. Mermin, and B. P. Company, *Solid State Physics*, ser. HRW international editions. Holt, Rinehart and Winston, 1976. [Online]. Available: <https://books.google.com.mx/books?id=1C9HAQAAIAAJ> (Cited on page 17.)
- [65] R. C. Powell, *Symmetry in Solids*. New York, NY: Springer New York, 2010, pp. 1–24. [Online]. Available: https://doi.org/10.1007/978-1-4419-7598-0_1 (Cited on page 17.)
- [66] M. S. Dresselhaus, G. Dresselhaus, and A. Jorio, *Group theory: application to the physics of condensed matter*. Springer Science & Business Media, 2007. (Cited on pages 18 and 19.)

- [67] R. H. Parmenter, “Symmetry properties of the energy bands of the zinc blende structure,” *Phys. Rev.*, vol. 100, pp. 573–579, Oct 1955. [Online]. Available: <https://link.aps.org/doi/10.1103/PhysRev.100.573> (Cited on page 18.)
- [68] P. N. Butcher, N. H. March, and M. P. Tosi, *Crystalline semiconducting materials and devices*. Springer Science & Business Media, 2013. (Cited on page 18.)
- [69] G. Bir and G. Pikus, *Symmetry and Strain-induced Effects in Semiconductors*, ser. A Halsted Press book. Wiley, 1974. [Online]. Available: <https://books.google.com.mx/books?id=38m2QgAACAAJ> (Cited on pages 18 and 19.)
- [70] W. A. Harrison, “Bond-orbital model and the properties of tetrahedrally coordinated solids,” *Phys. Rev. B*, vol. 8, pp. 4487–4498, Nov 1973. [Online]. Available: <https://link.aps.org/doi/10.1103/PhysRevB.8.4487> (Cited on page 18.)
- [71] J. C. Slater and G. F. Koster, “Simplified lcao method for the periodic potential problem,” *Phys. Rev.*, vol. 94, pp. 1498–1524, Jun 1954. [Online]. Available: <https://link.aps.org/doi/10.1103/PhysRev.94.1498> (Cited on pages 18 and 26.)
- [72] P. Curie, “Sur la symétrie dans les phénomènes physiques, symétrie d'un champ électrique et d'un champ magnétique,” *Journal de physique théorique et appliquée*, vol. 3, no. 1, pp. 393–415, 1894. (Cited on pages 19 and 22.)
- [73] K. Brading, E. Castellani, and N. Teh, “Symmetry and Symmetry Breaking,” in *The Stanford Encyclopedia of Philosophy*, Fall 2021 ed., E. N. Zalta, Ed. Metaphysics Research Lab, Stanford University, 2021. (Cited on pages 19 and 22.)
- [74] R. Magri and A. Zunger, “Anticrossing and coupling of light-hole and heavy-hole states in (001) GaAs/ al_xga_{1-x} As heterostructures,” *Phys. Rev. B*, vol. 62, pp. 10 364–10 372, Oct 2000. [Online]. Available: <https://link.aps.org/doi/10.1103/PhysRevB.62.10364> (Cited on pages 19, 20, and 22.)
- [75] E. L. Ivchenko, A. Y. Kaminski, and U. Rössler, “Heavy-light hole mixing at zinc-blende (001) interfaces under normal incidence,” *Phys. Rev. B*, vol. 54, pp. 5852–5859, Aug 1996. (Cited on pages 19, 20, 38, and 39.)
- [76] P. Tronc, Y. E. Kitaev, A. G. Panfilov, M. F. Limonov, G. Wang, and V. P. Smirnov, “Bound-state symmetries and optical transitions in gaas/ala_xs quantum wells and superlattices with impurities and defects,” *Phys. Rev. B*, vol. 61, pp. 1999–2007, Jan 2000. [Online]. Available: <https://link.aps.org/doi/10.1103/PhysRevB.61.1999> (Cited on pages 19 and 20.)
- [77] M. Glazov, *Electron & Nuclear Spin Dynamics in Semiconductor Nanostructures*, ser. Series on Semiconductor Scienc. OXFORD University Press, 2018. (Cited on pages 20, 23, and 41.)

- [78] O. Krebs and P. Voisin, “Giant optical anisotropy of semiconductor heterostructures with no common atom and the quantum-confined pockels effect,” *Phys. Rev. Lett.*, vol. 77, pp. 1829–1832, Aug 1996. (Cited on page 20.)
- [79] Y. H. Chen, X. L. Ye, J. Z. Wang, Z. G. Wang, and Z. Yang, “Interface-related in-plane optical anisotropy in gaas/al_xga_{1-x}As single-quantum-well structures studied by reflectance difference spectroscopy,” *Phys. Rev. B*, vol. 66, p. 195321, Nov 2002. (Cited on pages 20, 38, 39, and 73.)
- [80] E. L. Ivchenko and S. D. Ganichev, *Spin-Photogalvanics*. Berlin, Heidelberg: Springer Berlin Heidelberg, 2008, pp. 245–277. (Cited on pages 20, 23, and 41.)
- [81] N. Chand and S. N. G. Chu, “Origin and improvement of interface roughness in algaas/gaas heterostructures grown by molecular beam epitaxy,” *Applied Physics Letters*, vol. 57, no. 17, pp. 1796–1798, 1990. [Online]. Available: <https://doi.org/10.1063/1.104025> (Cited on page 21.)
- [82] K. Tillmann, M. Luysberg, P. Specht, and E. Weber, “Direct compositional analysis of algaas/gaas heterostructures by the reciprocal space segmentation of high-resolution micrographs,” *Ultramicroscopy*, vol. 93, no. 2, pp. 123–137, 2002. [Online]. Available: [https://doi.org/10.1016/S0304-3991\(02\)00153-5](https://doi.org/10.1016/S0304-3991(02)00153-5) (Cited on page 21.)
- [83] A. SHUBNIKOV, “On the works of pierre curie on symmetry††originally appeared in russian in uspekhi fizicheskikh nauk 59, 591-602 (1956). translated by l. i. man.” in *Crystal Symmetries*, ser. International Series in Modern Applied Mathematics and Computer Science, I. HARGITTAI and B. VAINSHTEIN, Eds. Amsterdam: Pergamon, 1988, pp. 357–364. [Online]. Available: <https://www.sciencedirect.com/science/article/pii/B9780080370149500078> (Cited on page 22.)
- [84] J.-W. Luo, G. Bester, and A. Zunger, “Supercoupling between heavy-hole and light-hole states in nanostructures,” *Phys. Rev. B*, vol. 92, p. 165301, Oct 2015. [Online]. Available: <https://link.aps.org/doi/10.1103/PhysRevB.92.165301> (Cited on page 23.)
- [85] R. Winkler, *Spin-orbit coupling effects in two-dimensional electron and hole systems*. Springer, 2003, vol. 191. (Cited on pages 23 and 75.)
- [86] S. Döhrmann, D. Hägele, J. Rudolph, M. Bichler, D. Schuh, and M. Oestreich, “Anomalous spin dephasing in (110) gaas quantum wells: Anisotropy and intersubband effects,” *Phys. Rev. Lett.*, vol. 93, p. 147405, Sep 2004. [Online]. Available: <https://link.aps.org/doi/10.1103/PhysRevLett.93.147405> (Cited on page 23.)

- [87] L. V. Butov, A. Zrenner, G. Abstreiter, G. Böhm, and G. Weimann, “Condensation of indirect excitons in coupled alas/gaas quantum wells,” *Phys. Rev. Lett.*, vol. 73, pp. 304–307, Jul 1994. [Online]. Available: <https://link.aps.org/doi/10.1103/PhysRevLett.73.304> (Cited on page 24.)
- [88] L. Butov, C. Lai, A. Ivanov, A. Gossard, and D. Chemla, “Towards bose-einstein condensation of excitons in potential traps,” *Nature*, vol. 417, no. 6884, pp. 47–52, 2002. (Cited on page 24.)
- [89] G. Grosso, J. Graves, A. Hammack, A. High, L. Butov, M. Hanson, and A. Gossard, “Excitonic switches operating at around 100 k,” *Nature Photonics*, vol. 3, no. 10, pp. 577–580, 2009. (Cited on page 24.)
- [90] A. T. Hammack, L. V. Butov, J. Wilkes, L. Mouchliadis, E. A. Muljarov, A. L. Ivanov, and A. C. Gossard, “Kinetics of the inner ring in the exciton emission pattern in coupled gaas quantum wells,” *Phys. Rev. B*, vol. 80, p. 155331, Oct 2009. [Online]. Available: <https://link.aps.org/doi/10.1103/PhysRevB.80.155331> (Cited on page 24.)
- [91] J. E. Golub, K. Kash, J. P. Harbison, and L. T. Florez, “Long-lived spatially indirect excitons in coupled gaas/al_xga_{1-x}as quantum wells,” *Phys. Rev. B*, vol. 41, pp. 8564–8567, Apr 1990. [Online]. Available: <https://link.aps.org/doi/10.1103/PhysRevB.41.8564> (Cited on page 24.)
- [92] K. Sivalertporn, L. Mouchliadis, A. L. Ivanov, R. Philp, and E. A. Muljarov, “Direct and indirect excitons in semiconductor coupled quantum wells in an applied electric field,” *Phys. Rev. B*, vol. 85, p. 045207, Jan 2012. [Online]. Available: <https://link.aps.org/doi/10.1103/PhysRevB.85.045207> (Cited on pages 24, 35, and 36.)
- [93] A. G. Winbow, J. R. Leonard, M. Remeika, Y. Y. Kuznetsova, A. A. High, A. T. Hammack, L. V. Butov, J. Wilkes, A. A. Guenther, A. L. Ivanov, M. Hanson, and A. C. Gossard, “Electrostatic conveyer for excitons,” *Phys. Rev. Lett.*, vol. 106, p. 196806, May 2011. [Online]. Available: <https://link.aps.org/doi/10.1103/PhysRevLett.106.196806> (Cited on page 24.)
- [94] C. A. Bravo-Velázquez, L. F. Lastras-Martínez, O. Ruiz-Cigarrillo, G. Flores-Rangel, L. E. Tapia-Rodríguez, K. Biermann, and P. V. Santos, “Photoluminescence of double quantum wells: Asymmetry and excitation laser wavelength effects,” *physica status solidi (b)*, vol. n/a, no. n/a, p. 2100612. [Online]. Available: <https://onlinelibrary.wiley.com/doi/abs/10.1002/pssb.202100612> (Cited on pages 24 and 80.)

- [95] J. M. Luttinger and W. Kohn, “Motion of electrons and holes in perturbed periodic fields,” *Phys. Rev.*, vol. 97, pp. 869–883, Feb 1955. [Online]. Available: <https://link.aps.org/doi/10.1103/PhysRev.97.869> (Cited on page 26.)
- [96] A. Yariv, C. Lindsey, and U. Sivan, “Approximate analytic solution for electronic wave functions and energies in coupled quantum wells,” *Journal of Applied Physics*, vol. 58, no. 9, pp. 3669–3672, 1985. [Online]. Available: <https://doi.org/10.1063/1.335726> (Cited on page 26.)
- [97] T. Fromherz, “Floquet states and intersubband absorption in strongly driven double quantum wells,” *Phys. Rev. B*, vol. 56, pp. 4772–4777, Aug 1997. [Online]. Available: <https://link.aps.org/doi/10.1103/PhysRevB.56.4772> (Cited on page 26.)
- [98] E. Rosencher and B. Vinter, *Optoelectronics*. Cambridge University Press, 2002. (Cited on page 26.)
- [99] C. Galeriu, “ $k \cdot p$ theory of semiconductor nanostructures,” *PhD Dissertations. Worcester Polytechnic Institute, Worcester*, 2005. (Cited on page 26.)
- [100] H. Yeo, J. S. Lee, M. E. Khan, H. S. Kim, D. Y. Jeon, and Y.-H. Kim, “First-principles-derived effective mass approximation for the improved description of quantum nanostructures,” *Journal of Physics: Materials*, vol. 3, no. 3, p. 034012, jul 2020. [Online]. Available: <https://doi.org/10.1088/2515-7639/ab9b61> (Cited on page 26.)
- [101] M. G. Burt, “A new effective-mass equation for microstructures,” *Semiconductor Science and Technology*, vol. 3, no. 12, pp. 1224–1226, dec 1988. [Online]. Available: <https://doi.org/10.1088/0268-1242/3/12/013> (Cited on page 26.)
- [102] B. A. Foreman, “Effective-mass hamiltonian and boundary conditions for the valence bands of semiconductor microstructures,” *Phys. Rev. B*, vol. 48, pp. 4964–4967, Aug 1993. [Online]. Available: <https://link.aps.org/doi/10.1103/PhysRevB.48.4964> (Cited on page 26.)
- [103] M. G. Burt, “The justification for applying the effective-mass approximation to microstructures,” *Journal of Physics: Condensed Matter*, vol. 4, no. 32, pp. 6651–6690, aug 1992. [Online]. Available: <https://doi.org/10.1088/0953-8984/4/32/003> (Cited on page 26.)
- [104] M. Marchewka, “Finite-difference method applied for eight-band kp model for $Hg_{1-x}Cd_xTe/HgTe$ quantum well,” *International Journal of Modern Physics B*, vol. 31, no. 20, p. 1750137, 2017. [Online]. Available: <https://doi.org/10.1142/S0217979217501375> (Cited on page 27.)

- [105] B. A. Foreman, “Envelope-function formalism for electrons in abrupt heterostructures with material-dependent basis functions,” *Phys. Rev. B*, vol. 54, pp. 1909–1921, Jul 1996. [Online]. Available: <https://link.aps.org/doi/10.1103/PhysRevB.54.1909> (Cited on page 30.)
- [106] D. J. BenDaniel and C. B. Duke, “Space-charge effects on electron tunneling,” *Phys. Rev.*, vol. 152, pp. 683–692, Dec 1966. (Cited on page 30.)
- [107] T. Kamizato and M. Matsuura, “Excitons in double quantum wells,” *Phys. Rev. B*, vol. 40, pp. 8378–8384, Oct 1989. [Online]. Available: <https://link.aps.org/doi/10.1103/PhysRevB.40.8378> (Cited on page 30.)
- [108] J. P. Killingbeck, *Microcomputer algorithms: action from algebra*. CRC Press, 2020. (Cited on page 32.)
- [109] E. R. Davidson and W. J. Thompson, “Monster matrices: their eigenvalues and eigenvectors,” *Computers in Physics*, vol. 7, no. 5, pp. 519–522, 1993. (Cited on page 32.)
- [110] E. Anderson, Z. Bai, C. Bischof, S. Blackford, J. Demmel, J. Dongarra, J. Du Croz, A. Greenbaum, S. Hammarling, A. McKenney, and D. Sorensen, *LAPACK Users’ Guide*, 3rd ed. Philadelphia, PA: Society for Industrial and Applied Mathematics, 1999. (Cited on page 33.)
- [111] C. R. Harris, K. J. Millman, S. J. van der Walt, R. Gommers, P. Virtanen, D. Cournapeau, E. Wieser, J. Taylor, S. Berg, N. J. Smith, R. Kern, M. Picus, S. Hoyer, M. H. van Kerkwijk, M. Brett, A. Haldane, J. F. del Río, M. Wiebe, P. Peterson, P. Gérard-Marchant, K. Sheppard, T. Reddy, W. Weckesser, H. Abbasi, C. Gohlke, and T. E. Oliphant, “Array programming with NumPy,” *Nature*, vol. 585, no. 7825, pp. 357–362, Sep. 2020. [Online]. Available: <https://doi.org/10.1038/s41586-020-2649-2> (Cited on page 33.)
- [112] D. F. Nelson, R. C. Miller, and D. A. Kleinman, “Band nonparabolicity effects in semiconductor quantum wells,” *Phys. Rev. B*, vol. 35, pp. 7770–7773, May 1987. [Online]. Available: <https://link.aps.org/doi/10.1103/PhysRevB.35.7770> (Cited on page 33.)
- [113] J. D. Cooper, A. Valavanis, Z. Ikonić, P. Harrison, and J. E. Cunningham, “Finite difference method for solving the schrödinger equation with band nonparabolicity in mid-infrared quantum cascade lasers,” *Journal of Applied Physics*, vol. 108, no. 11, p. 113109, 2010. [Online]. Available: <https://doi.org/10.1063/1.3512981> (Cited on page 33.)
- [114] Y. Varshni, “Temperature dependence of the energy gap in semiconductors,” *Physica*, vol. 34, no. 1, pp. 149–154, 1967. [Online]. Available: <https://www.sciencedirect.com/science/article/pii/0031891467900626> (Cited on page 33.)

- [115] I. Vurgaftman, J. R. Meyer, and L. R. Ram-Mohan, “Band parameters for iii–v compound semiconductors and their alloys,” *Journal of Applied Physics*, vol. 89, no. 11, pp. 5815–5875, 2001. (Cited on pages 33 and 34.)
- [116] L. W. Molenkamp, R. Eppenga, G. W. ’t Hooft, P. Dawson, C. T. Foxon, and K. J. Moore, “Determination of valence-band effective-mass anisotropy in gaas quantum wells by optical spectroscopy,” *Phys. Rev. B*, vol. 38, pp. 4314–4317, Aug 1988. [Online]. Available: <https://link.aps.org/doi/10.1103/PhysRevB.38.4314> (Cited on pages 33 and 34.)
- [117] S. Adachi, *Properties of semiconductor alloys: group-IV, III-V and II-VI semiconductors*. John Wiley & Sons, 2009, vol. 28. (Cited on pages 33 and 34.)
- [118] L. C. Lew Yan Voon and M. Willatzen, *Heterostructures: Basic Formalism*. Berlin, Heidelberg: Springer Berlin Heidelberg, 2009, pp. 273–362. (Cited on page 33.)
- [119] O. Donmez, F. Nutku, A. Erol, C. M. Arikan, and Y. Ergun, “A study of photomodulated reflectance on staircase-like, n-doped gaas/al_xga_{1-x}as quantum well structures,” *Nanoscale Research Letters*, vol. 7, no. 1, p. 622, 2012. (Cited on pages 33 and 35.)
- [120] D. Zhou and B. F. Usher, “Deviation of the AlGaAs lattice constant from Vegard’s law,” *Journal of Physics D: Applied Physics*, vol. 34, no. 10, pp. 1461–1465, May 2001, publisher: IOP Publishing. [Online]. Available: <https://doi.org/10.1088/0022-3727/34/10/304> (Cited on page 33.)
- [121] S. Birner, T. Zibold, T. Andlauer, T. Kubis, M. Sabathil, A. Trellakis, and P. Vogl, “nextnano: General purpose 3-d simulations,” *IEEE Transactions on Electron Devices*, vol. 54, no. 9, pp. 2137–2142, 2007. (Cited on page 33.)
- [122] Y. Takahashi, Y. Kato, S. S. Kano, S. Fukatsu, Y. Shiraki, and R. Ito, “The effect of electric field on the excitonic states in coupled quantum well structures,” *Journal of Applied Physics*, vol. 76, no. 4, pp. 2299–2305, 1994. (Cited on page 35.)
- [123] R. L. Greene, K. K. Bajaj, and D. E. Phelps, “Energy levels of wannier excitons in GaAs – ga_{1-x}al_xAs quantum-well structures,” *Phys. Rev. B*, vol. 29, pp. 1807–1812, Feb 1984. (Cited on page 35.)
- [124] N. S. Averkiev, L. E. Golub, A. S. Gurevich, V. P. Evtikhiev, V. P. Kochereshko, A. V. Platonov, A. S. Shkolnik, and Y. P. Efimov, “Spin-relaxation anisotropy in asymmetrical (001) al_xga_{1-x}As quantum wells from hanle-effect measurements: Relative strengths of rashba and dresselhaus spin-orbit coupling,” *Phys. Rev. B*, vol. 74, p. 033305, Jul 2006. [Online]. Available: <https://link.aps.org/doi/10.1103/PhysRevB.74.033305> (Cited on page 36.)

- [125] L. V. Kotova, A. V. Platonov, V. N. Kats, V. P. Kochereshko, S. V. Sorokin, S. V. Ivanov, and L. E. Golub, “Optical activity of quantum wells,” *Phys. Rev. B*, vol. 94, p. 165309, Oct 2016. [Online]. Available: <https://link.aps.org/doi/10.1103/PhysRevB.94.165309> (Cited on page 36.)
- [126] C. Schönhuber, M. P. Walser, G. Salis, C. Reichl, W. Wegscheider, T. Korn, and C. Schüller, “Inelastic light-scattering from spin-density excitations in the regime of the persistent spin helix in a gaas-algaas quantum well,” *Phys. Rev. B*, vol. 89, p. 085406, Feb 2014. [Online]. Available: <https://link.aps.org/doi/10.1103/PhysRevB.89.085406> (Cited on page 36.)
- [127] P. Tronc, “Spin phenomena in asymmetrical [001] GaAs/Al_xGa_{1-x}As quantum wells,” *Semiconductor Science and Technology*, vol. 27, no. 5, p. 055016, apr 2012. [Online]. Available: <https://doi.org/10.1088/0268-1242/27/5/055016> (Cited on page 36.)
- [128] X.-L. Ye, Y. H. Chen, J. Z. Wang, Z. G. Wang, and Z. Yang, “Determination of the values of hole-mixing coefficients due to interface and electric field in gaas/al_xga_{1-x}As superlattices,” *Phys. Rev. B*, vol. 63, p. 115317, Mar 2001. [Online]. Available: <https://link.aps.org/doi/10.1103/PhysRevB.63.115317> (Cited on page 38.)
- [129] O. Krebs, D. Rondi, J. L. Gentner, L. Goldstein, and P. Voisin, “Inversion asymmetry in heterostructures of zinc-blende semiconductors: Interface and external potential versus bulk effects,” *Phys. Rev. Lett.*, vol. 80, pp. 5770–5773, Jun 1998. [Online]. Available: <https://link.aps.org/doi/10.1103/PhysRevLett.80.5770> (Cited on pages 38 and 39.)
- [130] X. Ye, Y. H. Chen, J. Z. Wang, B. Xu, Z. G. Wang, and Z. Yang, “In-plane optical anisotropy of symmetric and asymmetric (001) gaas/al(ga)as superlattices and quantum wells,” *Journal of Applied Physics*, vol. 90, no. 3, pp. 1266–1270, 2001. [Online]. Available: <https://doi.org/10.1063/1.1383018> (Cited on pages 38 and 39.)
- [131] J. W. Orton and T. Foxon, *Molecular beam epitaxy: a short history*. Oxford University Press, USA, 2015. (Cited on page 43.)
- [132] M. Grundmann, *Physics of semiconductors*. Springer, 2010, vol. 11. (Cited on page 43.)
- [133] M. Yuan, A. Hernández-Mínguez, K. Biermann, and P. V. Santos, “Tunneling blockade and single-photon emission in gaas double quantum wells,” *Phys. Rev. B*, vol. 98, p. 155311, Oct 2018. (Cited on pages 44 and 65.)
- [134] J. Weiner and F. Nunes, *Light-matter interaction: physics and engineering at the nanoscale*. Oxford University Press, 2017. (Cited on page 46.)

- [135] A. Einstein, “Über die von der molekularkinetischen theorie der wärme geforderte bewegung von in ruhenden flüssigkeiten suspendierten teilchen,” *Annalen der Physik*, vol. 322, no. 8, pp. 549–560, 1905. [Online]. Available: <https://onlinelibrary.wiley.com/doi/abs/10.1002/andp.19053220806> (Cited on page 46.)
- [136] C. A. Bravo-Velazques, “Sistema de fotoluminiscencia para caracterización de pozos cuánticos acoplados,” 2 2020, bachelor Thesis to obtain Engineering Physicist degree. (Cited on page 49.)
- [137] J. Jimenez and J. W. Tomm, *Spectroscopic Analysis of optoelectronic semiconductors*. Springer, 2016, vol. 202. (Cited on page 51.)
- [138] W. Lu and Y. Fu, *Spectroscopy of Semiconductors*. Springer International Publishing, 2018. [Online]. Available: <https://doi.org/10.1007/978-3-319-94953-6> (Cited on page 51.)
- [139] D. W. Ball, *The basics of spectroscopy*. Spie Press, 2001, vol. 49. (Cited on page 51.)
- [140] W. Demtr̄der, *Electrodynamics and Optics*. Springer Nature, 2019. (Cited on page 51.)
- [141] J. Solé, L. Bausa, and D. Jaque, *An introduction to the optical spectroscopy of inorganic solids*. John Wiley & Sons, 2005. (Cited on page 51.)
- [142] H. Khmissi, L. Sfaxi, L. Bouzaïene, F. Saidi, H. Maaref, and C. Bru-Chevallier, “Effect of carriers transfer behavior on the optical properties of inas quantum dots embedded in algaas/gaas heterojunction,” *Journal of Applied Physics*, vol. 107, no. 7, p. 074307, 2010. [Online]. Available: <https://doi.org/10.1063/1.3371356> (Cited on page 54.)
- [143] J. Kundrotas, A. Čerškus, S. Ašmontas, G. Valušis, B. Sherlike, M. P. Halsall, M. J. Steer, E. Johannessen, and P. Harrison, “Excitonic and impurity-related optical transitions in be δ -doped GaAs/AlAs multiple quantum wells: Fractional-dimensional space approach,” *Phys. Rev. B*, vol. 72, p. 235322, Dec 2005. [Online]. Available: <https://link.aps.org/doi/10.1103/PhysRevB.72.235322> (Cited on page 54.)
- [144] J. Singh, K. Bajaj, and S. Chaudhuri, “Theory of photoluminescence line shape due to interfacial quality in quantum well structures,” *Applied physics letters*, vol. 44, no. 8, pp. 805–807, 1984. (Cited on page 55.)
- [145] F.-Y. Juang, J. Singh, P. K. Bhattacharya, K. Bajema, and R. Merlin, “Field-dependent linewidths and photoluminescence energies in gaas/algaas multiquantum well modulators,” *Applied physics letters*, vol. 48, no. 19, pp. 1246–1248, 1986. (Cited on page 55.)

- [146] J. Maluenda and P. M. Frijlink, “Abrupt transitions in composition and doping profile in GaAs/Ga_{1-x}Al_xAs heterostructures by atmospheric pressure movpe,” *Journal of Vacuum Science & Technology B: Microelectronics Processing and Phenomena*, vol. 1, no. 2, pp. 334–337, 1983. [Online]. Available: <https://avs.scitation.org/doi/abs/10.1116/1.582552> (Cited on page 55.)
- [147] B. V. Shanabrook, O. J. Glembocki, and W. T. Beard, “Photoreflectance modulation mechanisms in gaas-al_xga_{1-x}as multiple quantum wells,” *Phys. Rev. B*, vol. 35, pp. 2540–2543, Feb 1987. [Online]. Available: <https://link.aps.org/doi/10.1103/PhysRevB.35.2540> (Cited on page 56.)
- [148] B. O. Seraphin and D. E. Aspnes, “Electric field effects in optical and first-derivative modulation spectroscopy,” *Phys. Rev. B*, vol. 6, pp. 3158–3160, Oct 1972. [Online]. Available: <https://link.aps.org/doi/10.1103/PhysRevB.6.3158> (Cited on page 56.)
- [149] D. Aspnes and D. Sell, “Surface field effects in reflectance and first-derivative modulation spectra,” *Solid State Communications*, vol. 13, no. 5, pp. 519–522, 1973. (Cited on pages 56 and 70.)
- [150] J. Misiewicz, G. Sęk, and P. Sitarek, “Photoreflectance spectroscopy applied to semiconductors and semiconductor heterostructures.” *Optica Applicata*, vol. 29, no. 3, pp. 327–363, 1999. (Cited on pages 56, 57, and 58.)
- [151] M. Sydor, J. Angelo, J. J. Wilson, W. C. Mitchel, and M. Y. Yen, “Photoreflectance from gaas and gaas/gaas interfaces,” *Phys. Rev. B*, vol. 40, pp. 8473–8484, Oct 1989. [Online]. Available: <https://link.aps.org/doi/10.1103/PhysRevB.40.8473> (Cited on page 56.)
- [152] W. M. Theis, G. D. Sanders, C. E. Leak, K. K. Bajaj, and H. Morkoc, “Excitonic transitions in gaas/ga_xal_{1-x}as quantum wells observed by photoreflectance spectroscopy: Comparison with a first-principles theory,” *Phys. Rev. B*, vol. 37, pp. 3042–3051, Feb 1988. [Online]. Available: <https://link.aps.org/doi/10.1103/PhysRevB.37.3042> (Cited on page 56.)
- [153] W. M. Theis, G. D. Sanders, K. R. Evans, L. L. Liou, C. E. Leak, K. K. Bajaj, C. E. Stutz, R. L. Jones, and Y.-C. Chang, “Extrinsic contributions to photoreflectance of al_xga_{1-x}as/gaas quantum wells: An investigation of the “donor-related” feature,” *Phys. Rev. B*, vol. 39, pp. 11 038–11 043, May 1989. [Online]. Available: <https://link.aps.org/doi/10.1103/PhysRevB.39.11038> (Cited on page 56.)
- [154] I. Gontijo, Y. Tang, R. De La Rue, C. Sotomayor Torres, J. Roberts, and J. Marsh, “Photoreflectance and photoluminescence of partially intermixed gaas/algaas double quantum wells,” *Journal of applied physics*, vol. 76, no. 9, pp. 5434–5438, 1994. (Cited on page 56.)

- [155] H. Shen and M. Dutta, “Franz–keldysh oscillations in modulation spectroscopy,” *Journal of Applied Physics*, vol. 78, no. 4, pp. 2151–2176, 1995. [Online]. Available: <https://doi.org/10.1063/1.360131> (Cited on page 58.)
- [156] R. Del Sole and D. E. Aspnes, “Effect of surface and nonuniform fields in electroreflectance: Application to ge,” *Phys. Rev. B*, vol. 17, pp. 3310–3317, Apr 1978. [Online]. Available: <https://link.aps.org/doi/10.1103/PhysRevB.17.3310> (Cited on page 59.)
- [157] M. Cardona, “Modulation spectroscopy,” *Solid State Phys.*, vol. 11, 1969. (Cited on page 60.)
- [158] B. O. Seraphin and N. Bottka, “Band-structure analysis from electro-reflectance studies,” *Phys. Rev.*, vol. 145, pp. 628–636, May 1966. [Online]. Available: <https://link.aps.org/doi/10.1103/PhysRev.145.628> (Cited on page 60.)
- [159] A. M. Fox, D. A. B. Miller, G. Livescu, J. E. Cunningham, and W. Y. Jan, “Excitonic effects in coupled quantum wells,” *Phys. Rev. B*, vol. 44, pp. 6231–6242, Sep 1991. [Online]. Available: <https://link.aps.org/doi/10.1103/PhysRevB.44.6231> (Cited on page 62.)
- [160] H. Shen, P. Parayanthal, F. Pollak, A. Smirl, J. Schulman, R. McFarlane, and I. D’Haenens, “Observation of symmetry forbidden transitions in the room temperature photoreflectance spectrum of a gaas/gaalas multiple quantum well,” *Solid State Communications*, vol. 59, no. 8, pp. 557–560, 1986. [Online]. Available: <https://www.sciencedirect.com/science/article/pii/003810988690058X> (Cited on page 62.)
- [161] H. Shen, X. C. Shen, F. H. Pollak, and R. N. Sacks, “Photoreflectance and photoreflectance-excitation spectroscopy of a gaas/ga_{0.67}al_{0.33}as multiple-quantum-well structure,” *Phys. Rev. B*, vol. 36, pp. 3487–3490, Aug 1987. [Online]. Available: <https://link.aps.org/doi/10.1103/PhysRevB.36.3487> (Cited on page 62.)
- [162] Z. M. Fang, A. Persson, and R. M. Cohen, “Allowed 3h-1e transition in semiconductor quantum wells,” *Phys. Rev. B*, vol. 37, pp. 4071–4075, Mar 1988. [Online]. Available: <https://link.aps.org/doi/10.1103/PhysRevB.37.4071> (Cited on page 62.)
- [163] G. Bastard, E. E. Mendez, L. L. Chang, and L. Esaki, “Exciton binding energy in quantum wells,” *Phys. Rev. B*, vol. 26, pp. 1974–1979, Aug 1982. [Online]. Available: <https://link.aps.org/doi/10.1103/PhysRevB.26.1974> (Cited on page 64.)
- [164] Y. Shinozuka and M. Matsuura, “Wannier exciton in quantum wells,” *Phys. Rev. B*, vol. 28, pp. 4878–4881, Oct 1983. [Online]. Available: <https://link.aps.org/doi/10.1103/PhysRevB.28.4878> (Cited on page 64.)

- [165] K. Kheng, R. T. Cox, M. Y. d' Aubigné, F. Bassani, K. Saminadayar, and S. Tatarenko, "Observation of negatively charged excitons x^- in semiconductor quantum wells," *Phys. Rev. Lett.*, vol. 71, pp. 1752–1755, Sep 1993. [Online]. Available: <https://link.aps.org/doi/10.1103/PhysRevLett.71.1752> (Cited on pages 64 and 67.)
- [166] M. A. Lampert, "Mobile and immobile effective-mass-particle complexes in nonmetallic solids," *Phys. Rev. Lett.*, vol. 1, pp. 450–453, Dec 1958. [Online]. Available: <https://link.aps.org/doi/10.1103/PhysRevLett.1.450> (Cited on page 64.)
- [167] B. Stébé and A. Ainane, "Ground state energy and optical absorption of excitonic trions in two dimensional semiconductors," *Superlattices and Microstructures*, vol. 5, no. 4, pp. 545–548, 1989. [Online]. Available: <https://www.sciencedirect.com/science/article/pii/0749603689903820> (Cited on page 64.)
- [168] P. Aceituno and A. Hernández-Cabrera, "The role of excitons and trions on electron spin polarization in quantum wells," *Journal of Applied Physics*, vol. 110, no. 1, p. 013724, 2011. [Online]. Available: <https://doi.org/10.1063/1.3603031> (Cited on page 65.)
- [169] A. Manassen, E. Cohen, A. Ron, E. Linder, and L. N. Pfeiffer, "Exciton and trion spectral line shape in the presence of an electron gas in gaas/alaas quantum wells," *Phys. Rev. B*, vol. 54, pp. 10 609–10 613, Oct 1996. [Online]. Available: <https://link.aps.org/doi/10.1103/PhysRevB.54.10609> (Cited on pages 66 and 67.)
- [170] G. Finkelstein, H. Shtrikman, and I. Bar-Joseph, "Negatively and positively charged excitons in GaAs/ $\text{Al}_x\text{Ga}_{1-x}\text{As}$ quantum wells," *Phys. Rev. B*, vol. 53, pp. R1709–R1712, Jan 1996. [Online]. Available: <https://link.aps.org/doi/10.1103/PhysRevB.53.R1709> (Cited on pages 66 and 67.)
- [171] N. N. Sibeldin, M. L. Skorikov, and V. A. Tsvetkov, "Formation of charged excitonic complexes in shallow quantum wells of undoped GaAs/AlGaAs structures under below-barrier and above-barrier photoexcitation," *Nanotechnology*, vol. 12, no. 4, pp. 591–596, nov 2001. [Online]. Available: <https://doi.org/10.1088/0957-4484/12/4/344> (Cited on page 67.)
- [172] I. Bar-Joseph, "Trions in GaAs quantum wells," *Semiconductor Science and Technology*, vol. 20, no. 6, pp. R29–R39, may 2005. [Online]. Available: <https://doi.org/10.1088/0268-1242/20/6/r01> (Cited on page 67.)
- [173] C. Jirauschek and T. Kubis, "Modeling techniques for quantum cascade lasers," *Applied Physics Reviews*, vol. 1, no. 1, p. 011307, 2014. [Online]. Available: <https://doi.org/10.1063/1.4863665> (Cited on pages 67 and 68.)

- [174] L. R. Ram-Mohan, K. H. Yoo, and J. Moussa, “The schrödinger–poisson self-consistency in layered quantum semiconductor structures,” *Journal of Applied Physics*, vol. 95, no. 6, pp. 3081–3092, 2004. [Online]. Available: <https://doi.org/10.1063/1.1649458> (Cited on page 67.)
- [175] E. Cassan, “On the reduction of direct tunneling leakage through ultrathin gate oxides by a one-dimensional schrödinger–poisson solver,” *Journal of Applied Physics*, vol. 87, no. 11, pp. 7931–7939, 2000. [Online]. Available: <https://doi.org/10.1063/1.373477> (Cited on page 67.)
- [176] Y. Ando and T. Itoh, “Calculation of transmission tunneling current across arbitrary potential barriers,” *Journal of Applied Physics*, vol. 61, no. 4, pp. 1497–1502, 1987. [Online]. Available: <https://doi.org/10.1063/1.338082> (Cited on page 67.)
- [177] V. D. Jovanović, D. Indjin, N. Vukmirović, Z. Ikonić, P. Harrison, E. H. Linfield, H. Page, X. Marcadet, C. Sirtori, C. Worrall, H. E. Beere, and D. A. Ritchie, “Mechanisms of dynamic range limitations in GaAs/AlGaAs quantum-cascade lasers: Influence of injector doping,” *Applied Physics Letters*, vol. 86, no. 21, p. 211117, 2005. [Online]. Available: <https://doi.org/10.1063/1.1937993> (Cited on page 68.)
- [178] A. Lastras-Martínez, R. E. Balderas-Navarro, L. F. Lastras-Martínez, and M. A. Vidal, “Model for the linear electro-optic reflectance-difference spectrum of gaas(001) around E_1 and $E_1 + \Delta_1$,” *Phys. Rev. B*, vol. 59, pp. 10 234–10 239, Apr 1999. [Online]. Available: <https://link.aps.org/doi/10.1103/PhysRevB.59.10234> (Cited on page 69.)
- [179] D. E. Aspnes and A. A. Studna, “Anisotropies in the above-band-gap optical spectra of cubic semiconductors,” *Phys. Rev. Lett.*, vol. 54, pp. 1956–1959, Apr 1985. [Online]. Available: <https://link.aps.org/doi/10.1103/PhysRevLett.54.1956> (Cited on page 70.)
- [180] D. E. Aspnes, “Above-bandgap optical anisotropies in cubic semiconductors: A visible–near ultraviolet probe of surfaces,” *Journal of Vacuum Science & Technology B: Microelectronics Processing and Phenomena*, vol. 3, no. 5, pp. 1498–1506, 1985. [Online]. Available: <https://avs.scitation.org/doi/abs/10.1116/1.582974> (Cited on page 70.)
- [181] S.-H. Wei and A. Zunger, “Theory of reflectance-difference spectroscopy in ordered iii-v semiconductor alloys,” *Phys. Rev. B*, vol. 51, pp. 14 110–14 114, May 1995. [Online]. Available: <https://link.aps.org/doi/10.1103/PhysRevB.51.14110> (Cited on page 70.)
- [182] L. F. Lastras-Martínez, A. Lastras-Martínez, and R. E. Balderas-Navarro, “A spectrometer for the measurement of reflectance-difference spectra,” *Review of Scientific Instruments*, vol. 64, no. 8, pp. 2147–2152, 1993. (Cited on page 70.)

- [183] “Nanophotonics iico’s repository group,” 2020. [Online]. Available: <https://github.com/NanophotonIICOs> (Cited on page 80.)